Copyright Warning & Restrictions

The copyright law of the United States (Title 17, United States Code) governs the making of photocopies or other reproductions of copyrighted material.

Under certain conditions specified in the law, libraries and archives are authorized to furnish a photocopy or other reproduction. One of these specified conditions is that the photocopy or reproduction is not to be "used for any purpose other than private study, scholarship, or research." If a, user makes a request for, or later uses, a photocopy or reproduction for purposes in excess of "fair use" that user may be liable for copyright infringement,

This institution reserves the right to refuse to accept a copying order if, in its judgment, fulfillment of the order would involve violation of copyright law.

Please Note: The author retains the copyright while the New Jersey Institute of Technology reserves the right to distribute this thesis or dissertation

Printing note: If you do not wish to print this page, then select "Pages from: first page # to: last page #" on the print dialog screen

ABSTRACT

MONITORING OF CEREBELLAR INJURY USING MICRO ECoG SIGNALS IN KETAMINE/XYLAZINE TREATED RATS

by
Gokhan Ordek

Much of the cerebellar research has been conducted in anesthetized animals, particularly using ketamine/xylazine combination in rats, and yet the absolute impact of the anesthesia on the neural circuit remains unanswered. In the current study, spontaneous electrical activity and sensory evoked potentials from the cerebellar surface with chronically implanted, flexible-substrate, multielectrode arrays in rats were collected and analyzed with the motor cortex signals. The power spectra and the intercontact coherence plots of the spontaneous activity in the awake-quiet animals extended up to 800 Hz in the cerebellum and only up to 200 Hz in the motor cortex. Ketamine/xylazine anesthesia suppressed most of the activity in the cerebellar cortex, which was in clear contrast to the motor cortex. In the awake cerebellum, large coherence values were observed between contact pairs as far apart as ~2 mm. Otherwise, there was not a discernable relation between the coherence and the intercontact distance. These results have suggested that the surface electrodes could provide much more detailed information about the state of neural circuits when they were used on the cerebellar cortex compared with the cerebral areas.

Findings in ketamine/xylazine treated rats by using micro ECoG signals extracted the baseline information in the cerebellum to investigate the altered electrophysiology in the damaged neural circuitry. The temporal course of excitability change in selected neural networks was used as a method to study traumatic brain injury (TBI). This

research demonstrated the use of cerebellar evoked potentials (EPs), which was characterized in the first phase of the study, for monitoring the injury progression in a rat model of fluid percussion injury (FPI). A mechanical tap on the dorsal hand was used as a stimulus, and EPs were recorded from the paramedian lobule (PML) of the posterior cerebellum via multi-electrode arrays (MEA). Evoked response amplitudes (EPAs) were analyzed immediate after the injury and on a daily basis for one week thereafter. This data indicated a trend of consistently decreasing EPAs in all nine animals, losing as much as 75% of baseline amplitudes measured before the injury. Notably, it was highlighted that there was two particular time windows; the first 24 hours of injury in the acute period and day-3 to day-7 in the delayed period where the largest drops (~40% and 30%) were observed in the EPAs. Immunohistochemical analysis supported electrophysiological findings that there was severity dependent Purkinje cell (PC) loss under the implant site. Current research has presented the evidences that sensory evoked potentials recorded from the cerebellar surface can be a useful technique to monitor the course of cerebellar injury and identify the phases of injury progression even at mild levels

MONITORING OF CEREBELLAR INJURY USING MICRO ECoG SIGNALS IN KETAMINE/XYLAZINE TREATED RATS

by
Gokhan Ordek

A Dissertation
Submitted to the Faculty of
New Jersey Institute of Technology and Rutgers-The State University of New Jersey
in Partial Fulfillment of the Requirements for the Degree of
Doctor of Philosophy in Biomedical Engineering

Department of Biomedical Engineering

January 2015

.

APPROVAL PAGE

MONITORING OF CEREBELLAR INJURY USING MICRO ECoG SIGNALS IN KETAMINE/XYLAZINE TREATED RATS

Gokhan Ordek

Dr. Mesut Sahin, Dissertation Advisor — Date
Associate Professor of Biomedical Engineering, NJIT

Dr. Bharat Biswal, Committee Member — Date
Professor of Biomedical Engineering, NJIT

Dr. Bryan J. Pfister, Committee Member — Date
Associate Professor of Biomedical Engineering, NJIT

Dr. Vijayalakshmi Santhakumar, Committee Member — Date
Assistant Professor of Dep. Neurology and Neurosciences, Rutgers B-H.S,

---

Dr. Kevin Pang, Committee Member — Date
Professor of Dep. Neurology and Neurosciences, Rutgers B-H.S

BIOGRAPHICAL SKETCH

Author: Gokhan Ordek

Degree: Doctor of Philosophy

Date: January 2015

Undergraduate and Graduate Education:

- Doctor of Philosophy in Biomedical Engineering, New Jersey Insitute of Technology, Newark, NJ, 07102

- Bachelor of Science in Electrical Engineering,
  Pamukkale University, Denizli, Turkey, 2007

Major: Biomedical Engineering

Presentations and Publications:

Ordek G., Proddutur, A., Santhakumar, V., Pfister, B.J., and Sahin, M. (October 2014). Electrophysiological Monitoring of Injury Progression In the Rat Cerebellar Cortex. Frontiers in Systems Neuroscience 8. doi: 10.3389/fnsys.2014.00197.

Ordek, G., Groth, J. & Sahin, M. (2013) "Differential effects of ketamine/xylazine anesthesia on the cerebral and cerebellar cortical activities in the rat. Journal of neurophysiology", 109, 1435-1443.

Ordek, G.,Sahin M.,(2014) " Spatial Patterns of High-Frequency Oscillations in the Rat Cerebellar Cortex" 35th Annual International Conference of the IEEE Engineering in Medicine and Biology Society (EMBC), Chicago IL.

Ordek, G., Groth, J., Pfister J.B. & Sahin, M. (2013) "Electrophysiological Monitoring of Cerebellar Evoked Potentials Following Fluid Percussion Injury" 6th International IEEE/EMBS Conference on Neural Engineering (NER), San Diego CA.

Ordek, G., Groth, J. & Sahin, M. (2012) "Effect of Anesthesia on Spontaneous Activity and Evoked Potentials of the Cerebellar Cortex" 34th Annual International Conference of the IEEE Engineering in Medicine and Biology Society, San Diego CA.

Ordek, G., Groth, J. & Sahin, M. (2012) "Effect of Anesthesia on Spontaneous Activity and Evoked Potentials of the Cerebellar Cortex" 34th Annual International Conference of the IEEE Engineering in Medicine and Biology Society, San Diego CA.

Ordek, G., Groth, J., Pfister J.B. & Sahin, M. (2013) "Intracranial Electrophysiology of Cerebellar Activity Alterations in Traumatic Injury Rats" Annual Meeting of Society for Neuroscience (SfN), San Diego CA.

Ordek, G., Groth, J. & Sahin, M. (2012) "Recording Surface Oscillations on the Rat Cerebellum via MicroECoG Multi-Channel Electrode Array" 40th Neural Interfaces Conference, Salt Lake City UT.

Ordek, G.Proddutur A., Santhakumar V., Pfister J.B. & Sahin M.,(2014) "Impact of brain injury on high frequency cerebellar oscillations in rat", Nanosymposium session at Annual Meeting of Society for Neuroscience, Washington DC.

Ordek, G.,Sahin M.,(2014) " Spatial Patterns of High-Frequency Oscillations in the Rat Cerebellar Cortex", Oral Session in Neural Signal Processing - 35th Annual International Conference of the IEEE Engineering in Medicine and Biology Society, Chicago IL.

Ordek, G.,Sahin M.,(2013)"Electrophysiological Monitoring of Cerebellar Evoked Potentials Following Fluid Percussion Injury", Annual North East Turkish Association (NETA) Meeting, Buffalo NY.

Ordek, G.,Sahin M.,(2012)"Recording Cerebellar Oscillations from resting animals via chronic MEA implants", Annual North East Turkish Association (NETA) Meeting, Boston MA.

Ordek, G.,Guruler H. (2011) "Sleep Apnea Diagnosis via Single Channel ECG Feature Selection" 37th Annual Northeast BioEngineering Conference (NEBEC), Philadelphia PA.

Sahin M., Groth Jonathan, Ordek Gokhan, (2011) "Cerebellar Activity Patterns Revealed by Micro-EcoG Technique" Minisymposium session at 33rd Annual International IEEE EMBS Conference, Boston MA.

I praise Allah for giving me strength and patience along my PhD journey.

To my parents, Ismail and Fatma Goksu Ordek, who dedicated their lives for their children and supported me with no condition. They always deserve the biggest credit from my success. I'm tremendously fortunate to have a brother like Hakan Ordek, who has shared this challenging path with me for the last six years. Without his support and encouragement, I wouldn't be able to complete my PhD. And I'm grateful to my sister, Neslihan Efe, for being a second mom to me and supporting my career in every step.

ACKNOWLEDGMENT

My sincere appreciation goes to Dr. Mesut Sahin, for being my advisor and more importantly being my mentor throughout this long journey. Without his guidance and encouragement, I wouldn't be in the same position today. He was not only a talented mentor for me, but also he has influenced me with his admirable personality. Thank you Dr. Mesut Sahin! I thank to Dr. Bryan J. Pfister and Dr.Vijiyalakshmi Santhakumar for the collaboration on my thesis with their helpful feedbacks as well as being in my committee. I also thank to Prof. Bharat B. Biswal and Prof. Kevin Pang to be in my committee with encouraging comments. I'm so grateful to meet with Prof. Biswal for giving me moral support in my last years of PhD.

I also thank to my colleagues and friends, Abhishek Prasad for being my surgery mentor, Ammar Abdo, Jonathan Groth and Ali Ersen for their laboratory experiences in my research. Special thanks go to Archana Proddutur and Matthew Long for their collaborations and inputs to my research. I appreciate the help from Eren Alay, John Binion and Sara Keller for their assistance in animal trainings and sterile surgeries. I also would like to include my sincere appreciation to Chair Assistant, Mrs. Candida Rocha for being our person in the department.

I am very fortunate to have a family; my parents (Ismail and Goksu Ordek), my sister (Neslihan Efe) for their moral support and especially to my brother (Hakan Ordek) for giving me any kind of support a brother and a friend can give. He was always there for me, thanks again. Lastly, I would like to thank my special friend, Vrajeshri Patel, who was with me in the last few years of this journey and helped me to get through the tough times.

TABLE OF CONTENTS

TABLE OF CONTENTS
(Continued)

Chapter **Page**

TABLE OF CONTENTS
(Continued)

TABLE OF CONTENTS
(Continued)

Chapter **Page**

LIST OF TABLES

Table **Page**

LIST OF FIGURES

LIST OF FIGURES
(Continued)

Figure **Page**

LIST OF FIGURES
(Continued)

Figure **Page**

LIST OF FIGURES
(Continued)

Figure **Page**

LIST OF FIGURES
(Continued)

Figure **Page**

LIST OF FIGURES
(Continued)

Figure **Page**

CHAPTER 1

INTRODUCTION

1.1 Problem Significance

There are about 2.5 million traumatic brain injury (TBI) cases every year in the United States according to the U.S. Center of Disease Control and Prevention. TBI is a leading cause of morbidity and mortality under the age of 35 years (Bruns and Hauser, 2003;Langlois et al., 2006). Recent reports have indicated a significant increase (from 0.023% to 0.051%) in concussion rate among young individuals involved in the sport-related accidents (Rosenthal et al., 2014). Despite the fact that the statistical rise may be explained by developing techniques such as helmet-sensors, point-of-care interventions and balance tests, there remains significant work to assess the extent of brain injuries.

TBI results from a direct or indirect force exerted on the head that leads to rapid sequela of changes in the brain such as mechanical tissue deformation, hemorrhage, and high intracranial pressure. Extensive cell death can be observed in different parts of the brain as early as 10 minutes and progresses over a month following injury (Conti et al., 1998;Sato et al., 2001a;Ai et al., 2007). While the initial injury is predominantly dependent on the severity of impact (trauma), subsequent reactions that can last days to months and involve a complex sequence of events (Thompson et al., 2005;Marklund et al., 2006;Bramlett and Dietrich, 2007). The latter is the main focus of the current research, especially in the under-diagnosed cases such as concussions, since it presents a broad window for cascaded injury events to take place.

1.2 Cerebellar Anatomy and Injury Relevance

The cerebellar cortex lays isolated from the other cortices and contains more nerve cells than rest of the brain (Herculano-Houzel et al., 2006;Herculano-Houzel, 2010) and their connections within in the circuitry, which promotes the morphological deformations in the injury context. In contrast to defined complexity by the numbers, cerebellar cortex encompasses rather a simple circuitry within a highly organized structure. It has only two major inputs; climbing (Cf) and mossy fibers (Mf), which project to co-modulate the purkinje cells (PCs) through separate pathways to generate the sole output for cerebellar cortex.

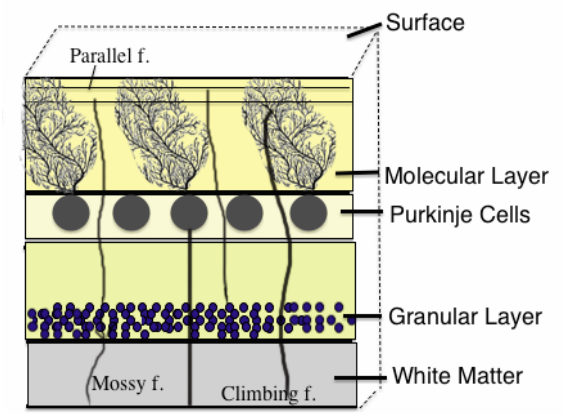

Figure 1.1 A sketch of simplified morphology in cerebellar cortex from a sagittal section.

Though the cerebellum is involved in motor function, it also receives a vast number of sensory inputs to modulate sensory-motor control (Bower and Woolston, 1983;Gao et al., 1996). The cerebellum has been confirmed as a brain site that can be affected even in mild injuries that is capable of progressing after the trauma incident. Studies of human TBI demonstrate that the cerebellum is affected even when the initial mechanical impact is directed to the cerebral cortex (Soto-Ares et al., 2001;Spanos et al., 2007), which suggested

the extensive axonal degenerations mediated through corticocerebellar pathways. Several TBI symptoms; such as ataxia, postural instability, tremor, impairments in balance and fine motor skills, and even cognitive deficits, can be attributed to cerebellar damage. Direct cerebellar injury is much less common than supratentorial trauma (Tsai et al., 1980b).

Animal models of indirect trauma to the cerebellum, including fluid percussion, controlled cortical impact, weight drop impact acceleration, and rotational acceleration injuries, as well as models that will induce direct trauma to the cerebellum were considered. In general, these models showed characteristics of cerebellar damage including regionally specific Purkinje cell injury or loss, activation of glia in a distinct spatial pattern, and traumatic axonal injury.

The cerebellum exhibits pathological changes including selective cell loss, altered metabolism, and white matter injury after focal and diffuse TBI. There are several clinical reports of cerebellar atrophy following TBI (Sato et al., 2001b;Gale et al., 2005a). Metabolic changes have also been documented in the cerebellum to cortical injury (Alavi et al., 1997;Niimura et al., 1999;Newberg et al., 2000). Loss of cerebellar gray matter after TBI has also been reported (Gale et al., 2005a).

1.3 Animal Models in TBI Studies

As an injury model, animal studies have become a promising approach to understand the temporal course of the human head injury. Increased temporal content of the post-injury such as an immediate epileptiform activity (Walker, 1994) , succeeded by suppression of cortical activity (Dixon et al., 1987a;Hayes et al., 1988) or observable behavioral (McIntosh et al., 1989;Rubovitch et al., 2011) and cognitive (Hamm et al., 1996) deficits following injury

induction, have manifested the animal models an ideal platform. For many decades, spontaneous oscillations and sensory evoked potentials have been investigated to understand the cellular originations of the cerebellar circuitry. Armstrong and Drew (Armstrong and Drew, 1980), and Eccles *et al*. (Eccles et al., 1967) have reported that cerebellar signals evoked by electrical stimulation of the snout contained characteristic volleys, including those from mossy and climbing fibers, that could be recorded with penetrating microelectrodes and surface ball electrodes in rats. While, Bosman *et al*. showed the Purkinje cell responses in mice with and without stimuli presence (Bosman et al., 2010). Cerebellum also generates highly rhythmic pattern of oscillatory activity, (Lehew and Nicolelis, 2008), which can be collected by the surface recordings (Ordek et al., 2013). This study proposes to identify the injury-induced changes in the neural circuitry, which may convey unique information about the development of cerebellar injury.

1.4 Research Motivation

Diagnosis of traumatic brain injuries, particularly in middle cases (mTBI), has challenged clinicians for many reasons. Consequences of mild brain injuries may be subtle and delayed (in weeks or months) or may not occur in many patients. Compared to other brain imaging techniques such as PET, MRI or CAT scan as well as behavioral/cognitive evaluations, EEG has been proposed to measure and localize brain injuries in a temporal pattern among individuals who have suffered from acute and chronic complications

Reports have indicated that symptoms of a mild injury can be presented as early as minutes to hours after incident (Kelly and Rosenberg, 1997), while it may last weeks to months for most patients (Levin and Eisenberg, 1978). The temporal course of a TBI has

been described in two major periods; acute and long-term effects. The acute period, also known as primary injury, is a direct result of mechanical forces involving tissue deformation, shearing and tearing blood vessels at the impact site. Delayed consequences of the injury (secondary mechanism) are believed to be initiated by the primary injury and cause prolonged deficits including metabolic, cellular and molecular events in the injured brain (Thompson et al., 2005;Marklund et al., 2006;Bramlett and Dietrich, 2007). To this purpose, investigation of the temporal course of a developing injury can yield significant outcomes to understand the on-going mechanism of a brain injury.

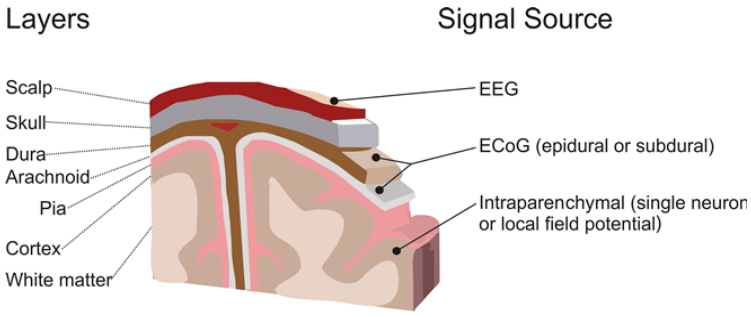

Figure 1.2 Methods for recording electric activity of brain tissue by depth. Source: Leuthardt, E.C., Schalk, G., Roland, J., Rouse, A., and Moran, D.W. (2009). Evolution of brain-computer interfaces: going beyond classic motor physiology. Neurosurg Focus 27, E4.

To understand the cascaded injury mechanisms, chronically implanted animals will serve to extract the time course information from electrophysiological recordings.

1.5 Choice of Electrode in ECoG Recordings

The electric field of a nerve cell (neuron) is defined by the electric potential generated in the cell with respect to recording distance. The magnitude of the electric potential on the recording electrode can be described by the source of a neuron or group of neurons. Electric

activity in a brain tissue can be picked up by two fundamental methods: intracellular (single cell) and extracellular recordings from a spine, dendrite, soma, axon, or any transmembrane current (Buzsáki et al., 2012) – and the cerebellum is not an exception to this. Single unit and extracellular – also known as local field potentials (LFPs) - activity of the cerebellum has been reported by many researchers over the decades (Dow, 1938;Adrian, 1944;Eccles et al., 1966;Oscarsson, 1968;Armstrong and Drew, 1980;Pellerin and Lamarre, 1997;Teune et al., 1998).

Electroencephalography (EEG) is one of the common clinical procedures to detect the severe alterations in the brain's electrical activity after a trauma incident. . EEG, also known as scalp electrophysiology, is a non-invasive technique that can serve to monitor alterations in the electric activity following of a head injury. Despite the advantageous features of EEG such as high-temporal resolution, low-cost and usability, it has also limitations; low-bandwidth and spatial resolution, which can limit the discerning subtle changes, particularly in mild injuries. Electrocorticography (ECoG) can overcome these shortcomings significantly by increasing the frequency content of neural activity coupled with a greater proximity of target brain area.

One of the common aims in all these studies is to identify the electrophysiological characteristics of cerebellar neurons and the communications within the network. While the first one requires analysis of single cells, the latter can be analyzed by recording subunits of neuron populations. Recent developments in electrode fabrications have improved LFP recordings, while minimizing the risk factors in the in vivo environment. Over the last decade, electric activity recordings with subdural implantations (ECoG) have become a promising technique in research, applications and clinical settings. ECoG or recording the

brain electric activity is conducted by placing recording electrodes underneath the skull on the cortical surface, see Figure 1.2 (Leuthardt et al., 2009). Leveraging the technical characteristics; increased bandwidth and signal to noise ratio (SNR) combined with multi-electrode array (MEA) technology, improving the spatial resolution to millimeter scale with (Bazhenov et al., 2011;Hill et al., 2012) a number of electrodes fabricated on an implantable substrate (electrode grid), ECoG can be highly selective and provide improved signal characteristics.

In the cerebral cortex, MEA implants have demonstrated reliable long-term (chronic) signal characteristics (up to months) in animal research (Yeager et al., 2008;Prasad and Sanchez, 2012) as well as in human subjects (Axmacher et al., 2008;Lalo et al., 2008). One of the first reports described the abnormal activity in cerebellar ECoG recordings from tumor and epilepsy patients (Foerster, 1935). More recent reports also showed that intracranial cerebellar recordings can be used for clinical diagnostics (Armstrong and Harvey, 1968;Chae et al., 2001;Delande et al., 2001;Mesiwala et al., 2002).

1.6 Electrophysiology of a TBI

Currently, neuroimaging techniques (CT, MRI, fMRI) are the widely accepted clinical methods to assess brain injury. Despite the emergent significance in the life threatening situations, neuroimaging techniques do not provide further information on the progression of the injury, particularly in the mild cases. Moreover, it is impossible to detect any cellular or molecular deficits with the selected assessment method. Diffusion tensor imaging (DTI), is different than the conventional neuroimaging techniques by showing advanced details in the white matter tracts, was proposed to improve the TBI detection. However, its lack of

information about the cellular network has remained as a question mark. Recording the electrical activity from the scalp is another diagnostic approach in the TBI cases. Although monitoring the electrophysiological changes (EEG, QEEG) in TBI patients has increased the significance of usage as a clinical/diagnostic technique in the recent decades, recording the electrical activity in the TBI patients is not a novel approach. Earlier studies in sport related head injuries showed abnormal EEG activities immediate after the insults (Larsson et al., 1954;Pampus and Grote, 1956). Similarly in animal models, immediate EEG recordings following the experimental head injury indicated seizure like high frequency discharges (Meyer et al., 1970;Katayama et al., 1988;Nilsson et al., 1994). EEG can utilize the recorded brain electrical activity in different frequency bands which can be associated with functional deficits. For instances, few of the common findings of EEG reports after brain injury is the attenuated alpha band activity in the posterior region (R., 1950) and increased theta waves in the temporal region (Schneider E, 1962;Courjon J, 1972).

Evoked potentials have also been used to assess the abnormalities after the brain injury. Several studies reported the pattern of changes in the visual evoked potentials (VEP) of TBI patients in the broader window (up to 24 months) of the post injury period (Gupta et al., 1986;Freed and Hellerstein, 1997). Additionally, similar abnormalities in the evoked response patterns were observed during task-related activities. Connolly et al. showed the VEP alterations during behavioral language tests, particularly the N400 responses, in TBI patients lesioned in the left-hemisphere (Connolly and D'Arcy, 2000;Knuepffer et al., 2012). Primary findings on the evoked response pattern changes in TBI patients were the suppression of one or several evoked components accompanied with prolonged latencies in the EP waveform. Similar evidences were also reported in animal studies. Pathological

reports indicated the reduction in the presynaptic volleys in the hippocampus (Reeves et al., 2000) and the cerebellar cortex (Ai and Baker, 2002). Despite the considerable contributions, electrophysiological techniques have remained as a secondary option to assess the TBI in clinical usage unless it is combined with other methods such as neuroimaging or neurological tests.

1.7 Objectives

The main objective of this study was to detect the injury induced alterations of the neural activity in the cerebellum by comparing the characterized oscillations and evoked potentials from the injured and un-injured animals. First, the spontaneous oscillations were recorded from the paramedian lobule (PML) of the cerebellum in multiple animals under anesthesia as well as in wakefulness. Then, sensory evoked potentials (SEPs) were utilized to build a somatotopy of the PML region on the cerebellar cortex in chronically MEA implanted animals.

In the second part of the study, characterized SEPs and spontaneous oscillations were analyzed to detect injury induced changes in this rat model of TBI. Monitoring cerebellar injury responses through the subdurally implanted MEAs constituted the foundation of the second aim. The main objective of this aim will serve the traumatic brain injury research by providing detailed information about the neuronal injury mechanisms.

The final aim was to quantify the cerebellar injuries with conventional methods. Immunohistological method was used to verify the severity of injury as it reveals the damages in the molecular and cellular structures of the cerebellar cortex.

1.7.1 Aim 1: Characterization of Cerebellar Oscillations in Anesthetized Rats

This aim was designed to investigate the consistency of sensory somatotopy via subdural surface recordings with multi-electrode arrays in anesthetized rats. Awake recordings of the spontaneous and evoked potentials were also included following the anesthesia trials. The signals were sampled at 16kHz in all 32-channels throughout all trials. Episodes of resting state lasted 10 seconds for both anesthesia and awake recordings. Evoked potentials were induced by single and repetitive air puffs (30psi, duration > 50ms, where the puff onset elicited the response) to the periphery, e.g. the left or right dorsal forearm, whiskers, face, and perioral areas. Multiple trials of 20 epochs were averaged to reduce background activity against the evoked signals. During recovery from anesthesia and in awake rats, investigator made sure that the animal did not move immediately before the air puff thereby avoiding large spontaneous activity that would contaminate the evoked potentials. All data analysis was performed in MATLAB.

Somatotopic organization of the PML was evaluated through amplitude and time analysis of evoked potentials in anesthetized animals. The amplitude and the arrival times of volleys in the evoked signals were measured for 3-4 weeks period following implantation of each animal. The sources of these volleys were linked to components of the cerebellar circuitry (mossy and climbing fibers, parallel fibers, Golgi cells and their synapses onto Purkinje cells, etc.). Characteristic features of the cerebellar evoked potentials demonstrated a signature EP waveform in response to each stimulation area. Functional organization of sensory feeds of each stimuli will be assessed based on their amplitude changes under anesthesia.

Next, cerebellar network oscillations were investigated in anesthetized and awake but resting animals. Frequency and correlation analysis was utilized to extract highly synchronized oscillations in the cerebellum and study the effect of anesthesia in this highly organized circuitry. Compared to other parts of the brain, the cerebellar cortex constitutes a highly organized homogeneous morphology within the structure. The aim was to leverage this special feature to study the cerebellar network activity. Electrode contacts on the implanted multi-electrode array were separated by 300μm and able to collect sub population activity from underlying neurons; primarily Purkinje cells. Episodes of 10-second spontaneous recordings were collected prior to each anesthesia on every data collection day. Real-time monitoring was coupled to each data set collection to ensure the animals were still at rest. Both data sets were stored for future analysis.

1.7.2 Aim 2: Electrophysiological Assessment of Cerebellar Injury with Micro ECoG

This aim involved the implementation of direct cerebellar injury in MEA-implanted animals to monitor the injury-related changes in the cerebellar electrophysiology. The current approach evaluated the subtle changes in the cerebellar neural signals that may not be visible through conventional techniques such as behavioral analysis. Similar to EEG, which is one of the clinical diagnostic techniques currently used, ECoG provides high-temporal contents about the neural signals, but with additional insights. All surgical and experimental methods applied in Aim-1 were repeated in this aim. Additionally, this aim required the fluid percussion injury induction in the anesthetized rats. On the next day of electrode implantation, baseline recordings of evoked potentials were made under anesthesia by

applying a mechanical tap on the forelimbs. Evoked potentials from forelimb area stimulation were selected for this aim to demonstrate a clear contrast with the control results.

Firstly, the amplitude and arrival times of the evoked responses in the injured animals were compared with the control measurements during the implant period (1-2 weeks). The evoked volleys that represent the structural elements of the cerebellar circuitry were the assessment parameters for this aim. The impact of the injury on these volleys was documented.

Secondly, the cumulative effect of repetitive near-threshold (10-15 psi) FPI was investigated to better demonstrate the sensitivity of the electrophysiological method. A small amplitude pressure wave was applied repeatedly at certain intervals while following the acute and long term effects of the injury after each application. The magnitude of the FPI induction was gradually increased; until the pressure level determined the injury threshold (i.e. severity enough to cause any changes in the evoked potentials acutely). Parameters of the evoked potentials such as the peak-to-peak magnitudes that start declining or increasing earliest were observed. The impact of the determined injury severity was independently investigated for the two input systems of the cerebellar cortex mossy and climbing fibers (or simple and complex spikes).

1.7.3 Aim 3: Immunohistochemical Validation of Fluid Percussion Injury in the Rat Cerebellum

The next aim was to assess the cerebellar injuries with the cellular loss at the end of survival periods. This aim was directly connected to the second aim, which was to verify the pathological alterations in the injured cerebellum. Immunohistological data also provided the

level of injury in the cerebellar structure after the seven-day injury period. Rats were perfused following recording period, which usually lasted one-week, and then the cerebellum tissue was dissected for immunostaining procedure. Double immunostaining procedure was applied to provide control (CalbindinD28k) and degeneration results. The location of injury site was marked from the surface and the underlying slices were sectioned. Sections processed for CalbindinD28k staining were mounted on gelatin-coated slides to perform FluoroJade C staining for degenerating neurons. Negative controls were routinely included in which primary antibody for CalbindinD28k was omitted. Representative images were obtained using Nikon A1R laser confocal microscope using 20X objective with identical camera settings. This aim was designed to investigate whether there was any damages occurred by the implantation of the MEA on the cerebellar surface.

1.7.4 Aim 4: Evaluation of Cerebellar Injury in Behaving Rats

The final aim investigated the behavioral deficits after cerebellar injuries in awake animals. Small lesions produce negligible or transient symptoms in the behavior that can be compensated by the other parts of the brain. It was expected that the electrophysiological method would detect injuries much earlier than behavioral manifestation. Nevertheless, disruption of the cerebellar network by the FPI model is likely to elicit the functional deficits such as lack of motor coordination that are associated with the structural morphology of the cerebellum.

The experimental paradigm tested skilled motor functions: walking, limb placement and co-ordinations, during ladder-rung crossing. The test evaluated the spontaneous walking patterns, which includes grasping, stepping, limb placement, and ongoing locomotion in the learning context. The cerebellum is a well-known brain region that is associated with motor

coordination and learning, thus the ladder-crossing paradigm was considered to be a valuable tool to assess the injury related changes in the behaviors. Following identification of the behavioral deficits, the relationship between the electrophysiological results and functional impairments was analyzed. Finding the injury induced behavioral markers in the electrophysiology was particularly important to answer a challenging question in the field of cerebellar neuroscience.

CHAPTER 2

THE CEREBELLUM

2.1 The Cerebellum Circuitry and Sensory Somatotopy

The cerebellum is considered as a primary center of motor learning, although there is sufficient evidence now showing that it is also involved in a number of cognitive tasks, such as the language processing (Hart, 2011), and it has also been implicated in several cognitive disorders including schizophrenia and autism (Fatemi et al., 2012;Villanueva, 2012). Accordingly, much research has been conducted to understand how the cerebellum processes the sensory-motor information. However, to date, there is no consensus on how the cerebellum integrates information and makes its contribution to the motor control of the body, the lack of which generates symptoms that are very familiar to the clinicians.

The cerebellum constitutes an ideal platform to study neural circuits in many respects. Many laboratories have used the cerebellar cortex as a template to understand the nervous system because of its well-defined network connectivity and relatively few types of cells involved. The cerebellar cortex has two main input pathways: The climbing fiber input which arises from the inferior olive and terminates on the Purkinje cells produces a complex spike with firing frequency of around 1-2Hz (Thach, 1968;Armstrong and Rawson, 1979). Each Purkinje cell receives a single climbing fiber input and the Purkinje cells innervated by the same climbing fiber forms a parasagitally oriented microzone in the cortex (Voogd and Glickstein, 1998). The mossy fibers constitute the other input that terminate on the granule cells which then send up axons to the surface forming parallel fibers that terminate on the Purkinje cells (Voogd and Glickstein, 1998). The parallel fiber inputs are responsible for

modulation of the simple spike activity of the Purkinje cells, with firing frequencies from 10 to 100Hz (Armstrong and Rawson, 1979;Cerminara et al., 2009).

There are two ways in which the cerebellum may potentially encode information. The first is rate coding in which the simple spike frequency is varied. It has been shown that the spike frequency is correlated with multiple kinematic and dynamic variables of the arm movement (Ebner et al., 2011;Hewitt et al., 2011). The second is spatiotemporal coding where the spike synchrony between multiple Purkinje cells is the mechanism for propagation of information. Spike synchrony occurs both with the complex and simple spikes (Wise et al., 2010;De Zeeuw et al., 2011).

Anesthetized animal preparations have commonly been used in electrophysiological experiments conducted in rats, although anesthesia undoubtedly affects the neuronal circuitry in the cerebellar cortex. One of the most popular anesthesia regimes used in electrophysiological experiments is the ketamine/xylazine combination. Ketamine is known to affect the N-methyl-D-aspartate (NMDA) receptors (Anis et al., 1983;Yamamura et al., 1990), nicotinic receptors (Scheller et al., 1996), muscarinic receptors (Hustveit et al., 1995), and opioid receptors (Smith et al., 1987). It has also been shown to affect the voltage gated sodium and potassium channels (Schnoebel et al., 2005).

2.1.1 Extracellular Electrical Activity in the Cerebellar Cortex

First reports on the recording electrical activity of the cerebellar cortex via microelectrode technique came out in early 1900s. Beck & Bickeles (1912), Foerster and Altenburger (1935), Adrian et al. (1935), Spiegel et al. (1937), Dow et al. (1938) were the pioneer observers r of spontaneous cerebellar oscillations in animals as well as in humans. Despite

the limitations of recordings techniques; for instance lack of modern oscilloscopes or computers, reports indicated that, cerebellar cortex was able to generate electric activities spontaneously as well as with the perturbations. Characterization of these electric activities believed to be correlated with functional outputs such as; sensori-motor coding, muscle tones, eye-movements, etc. that cerebellar cortex involved.

It has been reported that cerebellar dysfunctions are associated with number of diseases such as, epilepsy (Brice et al., 1983;Mukawa, 1985), muscle rigidity (Bremer et al., 1922), ataxia (Tolbert et al., 1995), tremor (Geraud et al., 1965;Stuart et al., 1965;Kelly, 1980). Thus, describing the electric activities in the cerebellar cortex can enlighten the functional deficits occurred by the impairments of the cerebellum. Early human studies showed that it was possible to detect changes in particular frequencies (delta and beta band) of electrical activity in human cerebellum (Niedermeyer et al., 1974). Despite the vast number of studies investigated the characterization of cerebellar electric activity in animals as well as in humans, the functional interpretation of these oscillations has remained largely unclaimed compared to the cerebral cortex. While non-invasive techniques such as EEG, PET, fMRI can access to cerebellar cortex, the underlying neural activity is very limited with these approaches. In contrast, recording extracellular activities with intracranial electrophysiology (ECoG) can reveal more temporal and spatial contents of cerebellar neural mechanism, which can reflect cerebellar related diseases.

2.1.2 Projections of Peripheral Inputs to Cerebellar Cortex

The structure of the vertebrate cerebellar cortex is highly organized and governed by a simple neural circuitry. Cerebellar cortex is divided into three layers containing just a few

kinds of cell types. Granule cells, which are the most numerous cell types in the entire human brain, are packed in the bottom of the cerebellar cortex. Purkinje cells (PCs) are the sole output of the cerebellar cortex that process the received inputs from various origins of sources and reside in the middle of the cerebellar cortex. These two neurons are the most dominant features of the cerebellar cortex, where they also constitute the majority of cerebellar electrophysiology.

Purkinje cells receive the information through only two distinctive pathways; Mossy fibers activate the PCs with an indirect path via granule cells-parallel fibers, while the climbing fiber activations are direct on the PC dendrites. Each of these inputs has a unique source to facilitate the PCs of the cerebellar cortex to generate the correct output. In the conventional theory, climbing fibers carry out the ascending signals that contain 'elemental movements' such as representation of limbs, fine movements, vestibular information, etc. to the cerebellar cortex. In contrast, mossy fiber system, which is mediated by granule cells and parallel fibers, relay the information from broader sources including the cerebral cortex. While it is plausible to identify these cerebellar features morphologically, they also exhibit the unique electrophysiological features, which are discernible via extracellular recording techniques. For instances, PCs firing rate at around 50 per/sec at rest, which is also called simple spike activity. Whereas, their firing rate is modulated to 1-3 per/sec during the onset of the climbing fiber activation. Cerebellar electric activity, also known as cerebellar potentials, can be characterized by the influencing dynamics on the network such as under anesthesia, by stimuli or injury.

2.2 Evoked Signals in the Cerebellum

Earlier studies indicated the peripherally evoked electric discharges, which are also called evoked potentials (EPs), could be detected in at different depths of the cerebellar cortex via microelectrodes. It has been reported that cerebellar evoked potentials, which is directly linked to underlying neuronal mechanisms, could be designated by the onset latencies in response to given stimulus. For instances, mossy fiber activations can be detected in the granular layer, where MFs synapse on granule cells, within the 5ms window after a stimulus. Whereas, CF-related responses can be noted with longer latencies (15-25ms) in the Purkinje layer to the same type of stimulus. Additionally, each of these evoked responses can also be detected on the surface of cerebellar cortex and linked to their neuronal sources.

Cerebellar evoked potentials in anesthetized animals exhibited reproducible characteristics (Eccles et al., 1966;Eccles et al., 1967;Oscarsson, 1968;Armstrong and Drew, 1980;Atkins and Apps, 1997a;Bengtsson and Jörntell, 2007;Roggeri et al., 2008;Ordek et al., 2013). However, cerebellar neural network is sensitive to parameters of the anesthesia such as injected dose, targeted neuroreceptors (NMDA, GABA, etc.) or the recovery duration, which also alters the dynamics of the neural circuitry. Thus, controlling the anesthesia regimen is one of the crucial elements in the evoked potential analysis.

2.2.1 Brief History of Cerebellar Evoked Potentials

Evoked potentials obtained from the cerebellar surface as a response to a stimulus in anesthetized animals have been analyzed to understand the neural signal flow in the cerebellar cortex. (Eccles et al., 1967;Oscarsson, 1968;Armstrong and Drew, 1980;Atkins and Apps, 1997a;Atkins and Apps, 1997b;Baker et al., 2001;Diwakar et al., 2011). Eccles et

al. used the juxtafastigial stimulation to identify subsequent MF mediated evoked volleys (i.e. P1, N1, P2, N2 and N3) with < 5 ms onset latencies in anesthetized cats (Eccles et al., 1967). Armstrong and colleagues observed volleys with similar onset latencies associated with MF activation to snout stimulation in surface recordings from the rat cerebellum (Armstrong and Drew, 1980). They also compared cerebellar evoked potentials from different depths and stated that all MF-mediated signal components were detectable from the surface using micro-electrodes. In a more recent study, although MF-activated evoked volleys in response to electric stimulations of the snout were substantially depressed in ketamine-xylazine treated rats, they were clearly detectable (Bengtsson and Jörntell, 2007).

Climbing fibers (CFs); one of the two afferents to the cerebellum, contribute significantly to sensory processing, and their evoked potentials can also be detected with surface recordings. In an earlier report, the CF related evoked potentials to a forelimb nerve stimulation was detected at 14-22 ms after the stimulus in the cerebellar surface potentials (Larson et al., 1969). Armstrong et al. reported observable CF-activation with the onset latencies of 16-22 ms and 20-25 ms in the vermis and ipsilateral hemisphere of the rat cerebellum, respectively. Apps et al. conducted a detailed characterization of CF mediated evoked potentials and concluded noticeable variations in the onset latencies of CF volleys within the same lobule of the rat cerebellum. The local field potentials (LFPs) contained CF activations with 10-15 ms onset latencies to forelimb stimulation in the central area of the PML, while CF response delays spread over to 16-26 ms in the lateral side of the PML with forelimb stimulation (Atkins and Apps, 1997a). All these reports agree that both MF- and CF-related evoked potentials are detectable from surface recordings. Furthermore, it is

convenient to be able to identify these two responses by their onset latencies where the MF-related volleys precede the CF-related potentials.

2.2.2 Effect of Anesthesia on the Cerebellar Potentials

Recording synchronous LFPs in the cerebellar cortex was documented in earlier reports in awake as well as anesthetized rats (de Solages et al., 2008a;Courtemanche et al., 2013;Ordek et al., 2013). Even though the anesthesia regimen depresses the frequency content of the cerebellar oscillations (Joynt, 1958;Ordek et al., 2013) signals have sufficient amplitudes to characterize oscillatory signals, particularly in low frequencies. Despite the fact all anesthesia regimens will affect the spontaneous and evoked potentials in the cerebellum, it has been proposed that: "A dramatic reduction in the field potentials does not necessarily imply that peripheral responsiveness is completely removed. The amplitudes of field potentials rely on a synchronous activation of afferent inputs." (Bengtsson and Jörntell, 2007).

The anesthesia effect on cerebellar oscillations and evoked potentials in ketamine-treated rats were exclusively reported (Ordek et al., 2013). It has been found that anesthesia regimen depresses the evoked potentials and spontaneous oscillations in the cerebellar cortex. It was also determined that the frequency content was diminished to 1-50Hz from a high-band width (up to 800Hz in awake animals) after anesthesia injection. However, the anesthesia effect can be controlled by maintaining the same anesthesia dose and the timings of the recordings after anesthesia injection.

The effect of anesthesia on spontaneous recordings as well as evoked potentials is a concern raised by a number of investigators in the past. Servais and Cheron (Servais et al.,

2005) compared differential effects of two different anesthesia regimens (ketamine and pentobarbitone) on local field potentials. They found that ketamine, an NMDA antagonist, depresses the LFP oscillations with PC desynchronization, while pentobarbitone, which targets the GABAa receptors, caused slight changes in PC synchrony. In the cerebellum, excitatory networks such as the MF-GC-PFs pathway use the NMDA receptors, whereas inhibitory signaling is mediated by GABAa receptors through the PCs and molecular layer interneurons. Therefore, using different anesthesia regimens could have different effects on the neural activity by selectively targeting different synaptic mechanisms. Another critical factor in anesthesia is the time delay allowed before data collection. Jorntell et al. (Bengtsson and Jörntell, 2007) reported that ketamine-xylazine (20:1) depressed both MF and CF responses significantly for 10 minutes after the injection. Similarly, LFP oscillations in the cerebellum exhibited sustained depressions for 5-10 minutes after anesthetic injection (Servais and Cheron, 2005). Although the recovery time was dose dependent, there was an observable delay that allowed between the injection and recordings can be used to control the anesthesia level in a reproducible manner, and thus obtain stable recordings.

CHAPTER 3

TRAUMATIC BRAIN INJURY (TBI)

Assessment of the development of a brain injury is crucial to understand underlying molecular, cellular and pathophysiological mechanisms for therapeutic interventions. However, there is not an accurate technique yet to detect brain injuries immediately and monitor its progression in time. Traumatic brain injury (TBI) is a leading cause of morbidity under age of 35 years (Bruns and Hauser, 2003;Langlois et al., 2006). In fact, recent reports indicate a rapid increase (0.051% from 0.023%) in concussion rate among young individuals involved in sport-related activities (Rosenthal et al., 2014). This may be explained by the developing technologies such as helmet-sensors, immediate blood samples and balance tests that can question the conventional methods' reliability.

TBI is defined by a direct or indirect external force applied to the head, which leads to rapid changes in the structure (mechanical tissue deformation, hemorrhage, intracranial pressure, etc.). Reports indicate that cell deaths could be observed extensively in different parts of the brain as early as 10 min to a month following injury (Conti et al., 1998;Sato et al., 2001a;Ai et al., 2007). While the initial injury is predominantly dependent on the severity of impact (trauma), subsequent reactions, which may last days to months, involve more complicated events (Thompson et al., 2005;Marklund et al., 2006;Bramlett and Dietrich, 2007). Latter is the main focus of research, since it manifests a broad window for cascaded injury progression in under-diagnosed cases such as concussions.

3.1.1 Overview of the Cerebellar Injury

Traumatic brain injury results from a direct or indirect force exerted on the head that quickly leads to a sequela of changes in the brain such as mechanical tissue deformation, hemorrhage, and an elevated level of intracranial pressure. Earlier reports indicated the delayed PC loss after midline and lateral FPI in the rat cerebellum (Mautes et al. 1996; Fukuda et al. 1996). Although the actual mechanism of indirect injuries to cerebellum is well understood, the primary injury occurs due to deceleration and inertial forces on the stationary skull. While the primary injury impacts are immediate throughout the cortices, secondary mechanism that involves cascaded metabolic events can last weeks to months. Indirect injuries to cerebellum in animal models demonstrated close relationship to human studies. Patients with cerebellar damages showed functional, complex nonmotor processing, and learning task deficits, which suggest a cerebrocerebellar involvement (Soto-Ares et al. 2001; Gale et al. 1995; Gorrie et al. 2002; Fiez JA et al. 1992). Cerebellar related deficits were reported in individuals within weeks to years following head injury (Iwadate et al., 1989;Louis et al., 1996b). Metabolic changes, which could be one of precursors of head injuries, have also been reported in the cerebellar injuries (Kushner et al., 1987;Niimura et al., 1999;Hattori et al., 2003). Extensive cell death can be observed in different parts of the brain as early as 10 minutes and progresses over a month following injury (Conti et al., 1998;Sato et al., 2001a;Ai et al., 2007). Ai et al. showed progressive PC loss after direct injury to the rat cerebellum (Ai et al., 2007), which may also be correlated with electrophysiological changes within the cerebellar circuitry (Ai and Baker, 2002;Ai and Baker, 2004). While the initial injury is predominantly dependent on the severity of the impact, subsequent reactions, which may last days to months, involve a complex sequence of

events (Thompson et al., 2005;Marklund et al., 2006;Bramlett and Dietrich, 2007). The latter is an emerging field of research, especially regarding under-diagnosed cases such as concussions since they present a broad window of cascaded injury events.

3.1.2 Underlying Mechanisms of the Cerebellar Injury

It has been suggested that progression of a brain injury involves molecular and cellular cascaded mechanisms, which may occur from minutes to months after trauma (Thompson et al., 2005; Marklund et al., 2006; Bramlett and Dietrich, 2007). Glutamate, the primary excitatory neurotransmitter in the CNS, is highly utilized in the cerebellum between different cell types; MFs – GCs, Parallel fibers – PCs and CFs –PCs (Ito, 2001; Nishiyama and Linden, 2007). One of the proposed mechanisms of brain injury involves excessive release of glutamate that leads to excitotoxicity (Gross, 2006). Elevation in the glutamate transmission is likely to disrupt the synaptic communication in the cerebellar cortex and compromise the cerebellar function. Ai et al. documented presynaptic hyperexcitation at the parallel fibers and the amplitude increase in the MF potentials on the days after the injury in the rat cerebellum (Ai and Baker, 2002; Ai and Baker, 2004). In FPI rats 7 days after injury, the same investigators also reported an amplitude decrease in the complex spike activity, which typically occurs by direct activation of the CFs on the PCs. (Ai et al., 2007).

3.1.3 Clinical Relevance of the Cerebellar Injury

Clinical reports have indicated that some of the neurological disorders, including ataxia, postural instability, tremor, lack of coordination and even cognitive impairments, are associated with the cerebellar damage (Louis et al., 1996a;Basford et al., 2003;Braga et al., 2007a). Though cerebellar related deficits could be diagnosed by variety of cases in

individuals, direct-cerebellar injuries are relatively a less common phenomena that was reported only <1% of entire TBI patients (Tsai et al., 1980a).

Similar to the adult, indirect supra tentorial trauma can lead to cerebellar damage in the brain-injured child. Sato-Ares et al. (Soto-Ares et al., 2001) studied cerebellar findings in brain-injured children an average of 16 months after moderate to severe TBI and demonstrated cerebellar atrophy in patients whose initial injury was to the frontal and temporal regions. In these children, injury-induced cerebellar atrophy was correlated with poor performance on standard intelligence quotient tests. Braga et al. (Braga et al., 2007b) investigated brain magnetic resonance findings and neuropsychological sequelae in a series of children who suffered severe TBI and showed an association between cerebellar lesions and deficits in visual recognition memory, arithmetic, object assembly, and overall intelligence quotient. Matschke et al. (Matschke et al., 2007) reported of a 4-year-old girl who had suffered mild TBI with an occipital skull fracture and expired 3 weeks later due to unrelated causes. At autopsy, they noted significant cerebellar atrophy with loss of Purkinje cells and activation of microglia. These finding correlate the cerebellar atrophy seen in radiological studies with vulnerability of Purkinje cells to TBI. Overall, these clinical reports show that the cerebellum is often affected in TBI, both directly and indirectly. However, the causes of cerebellar damage and the long term consequences are not completely understood (Potts et al., 2009).

3.1.4 Animal Models in the Brain Injury Research

Animal models propose a perfect platform to understand the development of brain injuries with repetitive and severity dependent injury models. Head injuries can produce varying

types and degrees of post syndromes lasting minutes to possible weeks or months in humans. Recovery duration could be improved by monitoring the post-traumatic symptoms, which would ultimately help the earlier interventions. "Though larger animals are closer to humans, rodents are mostly used in TBI research owing to their modest-cost, small size and standardized outcome measurements" (Xiong et al., 2013). To this purpose, various experimental models were implemented to examine reproducible TBI effects in the animal models. Most well-known are fluid percussion injury (Dixon et al., 1987b), controlled cortical injury (CCI) (Cernak, 2005), weight drop and rotational acceleration injuries (Goodman et al., 1994), and blast TBI models (Benzinger et al., 2009). The common hypothesis in all includes the replication of gradient dependent injuries in the animal models, and then assesses the correlations between pathophysiological results with behavioral/cognitive consequences. In the FPI models, an insult is induced by the fluid percussion produces a displacement and a deformation of the applied brain tissue, which can be rated by the magnitude of the fluid pressure. Deficits originated after the brain injury and association brain regions such as sensorimotor cortex, hippocampus, thalamus, cerebellum, etc. can be described by the functional tests such as beam walking, cylinder test, extremity force and precision tests. To this purpose, animal research can be used as an experimental model to explore possible parameters of the post-trauma syndromes such as neurobehavioral or cognitive deficits (Hamm, 2001;Morales et al., 2004), which are commonly observed in human TBI with the advantage of replication.

3.1.5 Current Diagnostic Techniques of a Brain Injury

Some of the current diagnostics of brain injury in humans include neuroimaging technics (MRI, CT or X-rays), neurological, neurophysiological examinations and (quantitative) EEG, which are usually not sufficient to diagnose the physical, behavioral and cognitive impairments, particularly in the mild injuries. A typical neurological evaluation includes checking the eye pupil reflexes, testing the hearing and visual impairments, muscle tone, coordination deficits and lose of upper body strength. While a neurophysiological examination requires list of cognitive tests to assess the individual's attention, memory, speed of thinking as well as reaction time. Though these examinations can be repeated in the chronic period of the injury, the actual outcomes are usually designed for the immediately after the trauma diagnosis. Neuroimaging assessments exhibit different advantages over each other for diagnosing the brain injury. For instance, CT scans are quick and widely available which makes them preferable in emergency cases. Whereas, MRI can extract more detailed images regarding the brain structure (deformation, white/gray matter changes, etc.), which can help to identify the deeper structural damages. Most of the neuroimaging techniques target to detect a brain lesion or hematoma occurred after the trauma incident. Additionally, pathological techniques (Immunohistochemical analysis) can also be used in vitro environments that can provide contents about the injury and underlying mechanism in more detail, however, this method cannot be applicable in human studies. Evaluation of the severity of a brain injury is necessary to take the proper care of the patient in the recovery period.

3.1.6 Limitations and problems with current TBI assessments

Currently, neuroimaging and neurophysiological techniques are commonly used diagnostic techniques for TBI evaluation in the clinics. While these methods allow the physicians to detect life-threatening conditions occurred following TBI, their detection reliability is very limited particularly in the mild cases. For instance, CT and MRI scans can detect signs of injury such as intracranial haemorrhage, haematoma or edema (Young and Destian, 2002). These conditions usually do not occur except the severe cases. Reports have shown that less than 10% of mild head injured patients indicate a positive injury sign (lesion, hemorrhage) in their CT scans, and only less than 1% of them require neurosurgical attention (Jeret et al., 1993). Moreover, the neuroimaging methods are not cost and time efficient (10-30 min/scan), and cannot provide detailed temporal information about the injury. Neurophysiological tests involve the patient's cooperation, which is not preferred due to intentional falsification, particularly in the acute phase of the trauma. Although neurophysiological assessment can provide injury related changes within the minutes of incident, it is challenging to link this information to the origin of injury source. The EEG technique is one of the latest implementations for the TBI diagnosis. It allows monitoring of the brain signals with a higher temporal resolution (< second). Although the EEG method has offered some valuable data such as the injury resulted changes in the neural network connectivity or the neuronal deformation in the injured areas (White-gray matter frequency spectrum alterations), the limitations of the application (low-bandwidth, low spatial resolution, etc.) have made it inefficient as a diagnostic technique (Leblanc, 1999). Overcoming the current drawbacks in the commonly used techniques can be challenging,

particularly in the mild TBI, which motivates the current research to develop novel methods for the assessment of the head injuries.

CHAPTER 4

HISTOPATHOLOGY OF THE CEREBELLAR INJURY

Fluid percussion injury causes a combination of focal and diffuse injuries that are characterized by pathological changes including cell degenerations, altered metabolism and axonal injury. Cerebellar atrophy is also one of the common phenomena occurred in the post-trauma period after the focal or diffuse TBI (Sato et al., 2001c;Gale et al., 2005b). Cerebellar atrophy, which can contribute to the origination of cerebellum related syndromes, was reported to be associated with Purkinje cell loss and activation of immune responses after the mild TBI cases in humans (Matschke et al., 2006). The FPI model implemented in this study allowed us to evaluate the electrophysiological changes and cell loss with the severity of impact. This model also showed the relationship between Purkinje cell loss and behavioral impairment in the forebrain injury (Floyd et al., 2002). Direct injury model, which limits the injury pathway in the studied brain area, may yield more consistent results to assess the temporal aspects of neuronal degenerations in the post trauma period. Purkinje cell losses were observed as early as within 24h of the trauma and in the following one month period (Sato et al., 2001a;Ai et al., 2007). In addition, different amounts of Purkinje cell losses were shown at different severities of the cerebellar injury (Ai et al., 2007), which suggests that the rate of the cell deaths can be exclusively related the severity of the injury..

4.1.1 Excitotoxicity in Cerebellar Injury

Underlying mechanisms of the brain injury is still under investigations in terms of primary and secondary components involved in the temporal course of the injury progression. While the primary phase involves mainly the mechanical damages as a result of the direct impact,

the second phase introduces a number of metabolic changes such as excessive release of excitatory neurotransmitters (i.e. glutamate, aspartate). Despite the lack of complete understanding in the underlying mechanisms of neuronal cell deaths in the cerebellum, excitotoxicity induced by the hyperexcitation can be one of the explanations (Sarna and Hawkes, 2003;Slemmer et al., 2004). Hyperexcitability in the cerebellum was reported by the earlier investigators indicating that the presynaptic level hyperexcitation can lead to cell losses in the mossy fiber and granule cell network (Ai and Baker, 2002). Neuronal cell deaths in the cerebellum were also shown after the hyperexcitation of climbing fibers in different brain injury models (Chen and Aston-Jones, 1994;O'Hearn and Molliver, 1997). Similar to other brain structures, injury in the cerebellum causes the release of excessive excitatory neurotransmitters that leads to cascaded events in the cellular and molecular levels such as calcium disturbance in the mitochondria and increased oxygen and nitrogen formations, which eventually results in cell damage and death.

4.1.2 Contribution of Neuronal Mechanisms

Cellular structure of the cerebellar cortex is highly sensitive to direct insults and the consequences can be assessed by the injury severity. In particular, organizational degeneration defined by the Purkinje neurons as “stripes” was indicated after the cerebellar injury (Sarna and Hawkes, 2003) and dose-dependent cell deaths following induced injury in the cerebellar cortex (Park et al., 2006; 2007). Although the mechanisms are not well understood, several studies suggest that this loss is due to cytotoxic injury (Immune cells involvement) to the neurons (Sarna and Hawkes, 2003;Slemmer et al., 2005). Each Purkinje cell receives inputs only from a single climbing fiber, but has an estimated 1,500 synaptic

connections with that climbing fiber. Almost 200,000 parallel fibers synapse with a single Purkinje cell. The anatomical connectivity of the cerebellum is defined by the two types of afferents, the climbing and mossy fibers, where mossy fibers create a patchy organization and the climbing fibers activate in the parasagittal direction. Differential findings between these inputs after the injury induction can help to localize the injury related damages in the spatial domain.

In addition, white matter degeneration (Matthews et al., 1998) and microglial activation (Fukuda et al., 1996;Mautes et al., 1996) is usually coupled with the Purkinje cell deaths in the prolonged window of injury effects (months). Strong microglial activation is a common inflammatory response observed following an injury to the cerebellum. Interestingly, this activation precedes the evidence of neuronal loss, suggesting that microglia may be the sensitive indicators of Purkinje cell injury serving as cellular scavengers to remove debris and promote healing (Kim and de Vellis, 2005), which can be the potential targets for therapeutic interventions in the recovery period.

Injury to cerebellar white matter (axonal injury) is another mechanism by which the functional consequences of TBI can be mediated. Several animal models of brain trauma have reported traumatic axonal injury (TAI) in the cerebellum (Hoshino et al., 2003). Current literature suggests that TAI is an evolving process, progressing from focal axonal damage at the time of injury to eventual complete disconnection (Buki and Povlishock, 2006). Extensive bilateral axonal degeneration is observed in the cerebellum as a result of the biomechanical forces during CCI injury (Lighthall et al., 1990;Hoshino et al., 2003). Although structural axonal degeneration following trauma is well established, the varying susceptibilities of myelinated (PC axons, climbing and mossy fibers) and demyelinated axon

(Parallel fibers) population in the cerebellum remain to be further investigated (Potts et al., 2009).

4.1.3 Indications of Immunochemistry Findings

Fluid percussion injury model typically introduces a combination of focal and diffuse injury. A direct mechanical injury causes cascaded pathophysiological changes including intraparenchymal and subarachnoid hemorrhage, followed by ionic abruptions in the cells, excitotoxic cell deaths, dendritic arborizations, axonal degenerations, etc. Immunohistological verification is an exclusive technique to assess the selective changes in the injured area such as the cerebellum. For instance, Calbindin is one of the two major calcium binding proteins, which is also widely used as a marker for naïve Purkinje cells in the cerebellum (Tolosa de Talamoni et al., 1993;Ai and Baker, 2004) to provide control results. Whereas, Fluro-Jade staining has been used for the delineation of irreversible cell deaths coupled with the progressive dendritic arborizations (Schmued et al., 1997). Progressive Purkinje cell deaths after the induced FPI in the cerebellum were reported in the rats. Furthermore, neuronal cell deaths were quantified with daily measurements after the FPI induction within the one week period. Statistical results compared with the healthy cells were observed in the naïve animals and Purkinje cell loss in the FPI animals (Ai et al., 2007). Interestingly, there was no measurable evidence of cell deaths anywhere in the structure of the cerebellum within hours of injury induction (Sato et al., 2001a;Ai et al., 2007).

Neuronal losses are not the only degeneration markers in the cerebellum. Noticeable axonal damage and related motor deficits were reported in cerebellar injury rats (Strahlendorf et al., 1998;Ding et al., 2000). Damages in the white matter were also noted

within the 24-48h period after the injury in the rat cerebellum (Hoshino et al., 2003). Another study determined the degenerations in the fiber tract of rat cerebellum after the 48h and 7 days of the FPI (Hallam et al., 2004). Immunohistology provides important insight information about the injury mechanism with pathological findings; however, the lack of in vivo monitoring in injury progression presents a significant obstacle in the assessment of the TBI.

CHAPTER 5

EXPERIMENTAL METHODOLOGY

5.1 Materials and Methods in Chronic Experiments

5.1.1 Flexible Multi-Electrode Array (flexMEA)

A custom-designed 32-channel multi-electrode array was implanted to obtain electrical activity of the cerebellum in this study (Figure 5.1). The design of the MEA was made by the investigator, and a company fabricated the MEAs (Neuronexus, MI).

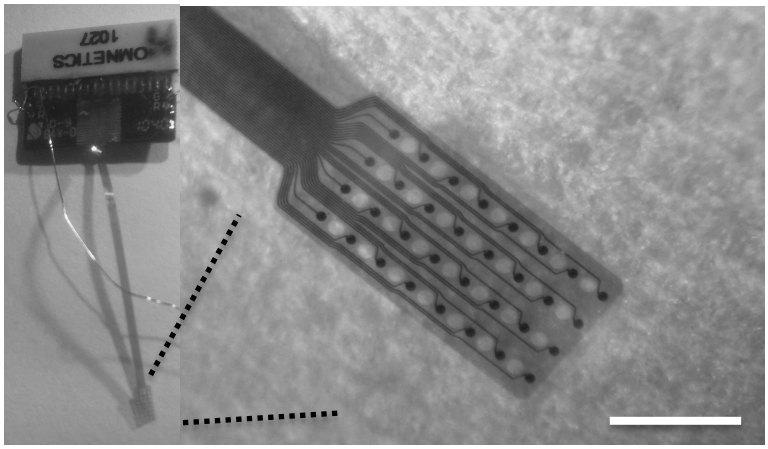

Figure 5.1 A custom made 32-Channel flexMEA (Right) connected to head micro-connector (Left, Neuronexus MI). Scale bar = 1mm.

The MEA substrate was made of a polymer (polyimide) to provide flexibility. Substrate was originally fabricated in 12µm thickness (8µm in the future experiments) and contained 32-electrode site contacts in the 4 by 8 configuration. Electrode contacts were 50µm diameter gold with 300µm inter-site distances (Figure 5.2). The array was connected to a micro-connector (Omnetics, MN) via 20mm ribbon cable made of the same material as

MEA substrate. Integrated circuit board and 32-electrode pathways were insulated and covered by the epoxy after the fabrication. The final design of the MEA with the connector side is shown in Figure.5.1 (Left).

Electrode impedance of the recording electrodes is a crucial parameter for the quality of neural signals.(Williams et al., 1999;Nicolelis et al., 2003;Prasad and Sanchez, 2012).

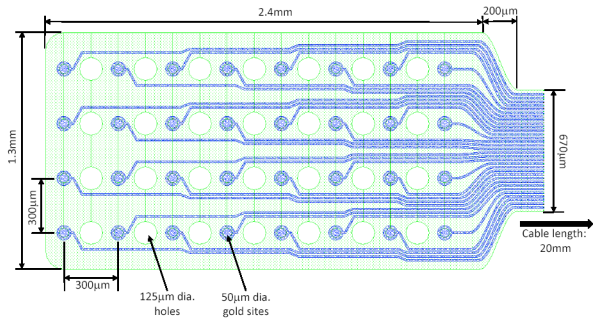

Figure 5.2 Scheme of the 32-site contacts on the MEA with inter-site distances.

Signal to noise ratio of the recorded neural activity is inversely proportional to √Z of the acquired channel. One of the common techniques to overcome this issue is to increase surface area through surface modifications. The material deposited on the electrodes must be corrosion resistant, highly conductive, and biocompatible to minimize the tissue host responses. Conductive polymers are organic materials with a high ability of electric conductivity and found to be improving the long-term recordings in the neural implants (Ludwig et al., 2011). In a similar fashion described by another investigator (Venkatraman et al. 2011), the electrode sites on the MEA were electrochemically coated with poly (3,4-ethylenedioxythiophene) or PEDOT prior to implantations. PEDOT surface modification was performed by delivering DC current through each electrode contacts in the prepared PEDOT solution (Figure 5.3). Following 1h-2h coating process, the surface impedances were

observed (typically gold turns to black under microscope) to decrease by one or two order of magnitude (<100k) after the polymer coating process.

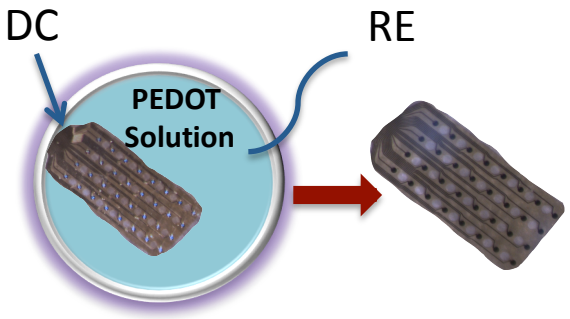

Figure 5.3 Experimental setup of PEDOT surface coating prior to implantation.

5.1.2 Surgical Procedure in Chronic Experiments

Sprague-Dawley or Long-Evans rats (300-350g, N>15) were anesthetized with IP injection of 80mg/kg ketamine and 12mg/kg xylazine cocktail. The animal was placed in a stereotaxic frame. Sodium pentobarbital (30 mg/kg, IP) was used to anesthetize the animals. Controlled anesthesia was maintained throughout the surgical procedure and additional doses of 0.1cc (IP) were administered as needed. Bupivacaine (0.1 ml, SC) was injected to the incision site for local anesthesia. Dexamethasone (0.1 mg/kg, IM) was used at the beginning of the surgery to prevent edema in the central nervous system and atropine (6mg/kg, IM) to improve respiratory function. The animal was placed on a heating pad equipped with a rectal probe to calibrate the body temperature at 36 ° ± 0.8°C (WPI). Surgical preparation and instruments are shown in detail (Figure 5.4).

F**igure 5.4** Surgical equipment and instruments are prepared in sterilized environment prior to chronic experiments.

After the initial anesthesia injection, animal's head was shaved from top to the neck line to provide clean surface during surgery. Animal was positioned to a stereotaxic frame with ear bars fixed into the auditor canal (Figure 5.5). The target and adjacent surgical area on the scalp was scrubbed with isopropyl alcohol and dried with sterilized wipes. Eye ointment was applied on both eyes to protect the dryness in the longer surgeries. A fine incision was made by #15 carbon steel sterile blade through the midline in the rostro-caudal direction. The opened scalp was pulled to the sideways and fixed by two hemostats. Next, the connective tissue and blood was cleaned on the bone surface by using the tip of a sterile cotton swab and disinfected with hydrogen peroxide.

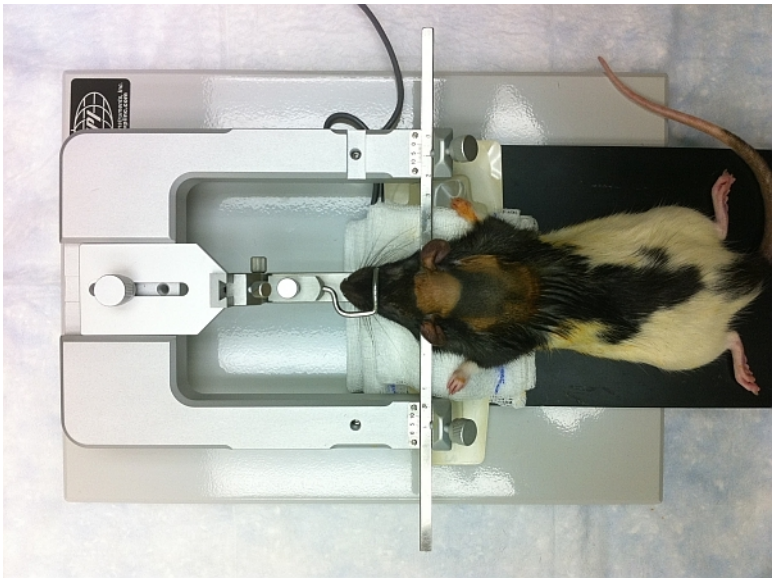

Figure 5.5 Animal's head fixed with the aid of stereotaxic ear bars for chronic experiments.

Six holes were drilled into the skull using a fine drill bit and metal screws (Plastics One Inc, VA, Figure 5.6A). A stainless steel or platinum wire as a ground connection was anchored to the skull with the aid of one screw on the frontal side. Incision was extended to the back down of the animal in order to reach the cerebellum. All connective tissues and muscles were separated using small scissor and scalpel's blunt tip (Figure 5.6B). A second craniotomy was drilled to the right lateral side from the midline of backbone. Once the craniotomy was large enough for microrongeurs, the cerebellar dura surface was exposed. Exposed dura surface was kept hydrated with saline or artificial CSF.

Following the bone extraction, the paramedian lobule on the cerebellar dura surface must be clearly noticeable under microscopic vision (arrowhead, Figure 5.6C). First, the PML surface was pierced by a needle tip (e.g., <30G) shaped into hook form. Subarachnoid space is vascularized, thus the puncture needed to be very gentle to minimize the potential threats caused by the hemorrhages. The MEA was slid under the dura by performing two

cuts at the medial and lateral side to yield the implantation (broken lines, Figure 5.6C). Once the MEA had been positioned on the desired region of the PML (~0.3mm lateral to the paravermal vein), biocompatible cyanoacrylate glue was applied on the four corners of the MEA to keep it in place (Figure 5.6D). A platinum wire was placed on the MEA implantation site with an aid of resected muscle pieces. Incisions were closed by suturing first muscles together with 5.0 absorbable sutures. The micro-head connector attached to the MEA was fixed to the skull with dental cement and made a robust head-cap. Skin on the opened scalp was closed by 4.0 non-absorbable sutures at the end. Buprenorphine (0.05mg/kg, IM) was used twice daily for 3 days post-operatively as an analgesic. Antibiotic ointment was applied when needed until the wounds healed completely.

Placement of the MEA on the PML surface of cerebellum could drastically effect on the recording characteristics and more importantly lead additional variations between the experimental animals. However, success of the MEA implantation was verified with surgical care and obtaining the signature waveform of evoked responses in the studied lobule, the PML. The width of the implanted electrode array had a perfect match (~1.2mm) in size with the width of the PML.

5.1.3 Recording Procedure

Recordings sessions started with the baseline measurements immediate after the animal recovery (~2-3 days). Initial recordings were acquired from the awake or behaving animal to ensure the quality of the neural data (Figure 5.7). Electrode impedances were also (Electrode Impedance Tester, Model IMP-1, BAK Technologies Inc., MD) noted to check if there was any electrode failure in the post-surgery period. After the full recovery (>3 days) evoked

potential responses in the anesthetized animals were coupled with recordings in the awake animals. Measurements were repeated every other day within one month of post-implantation.

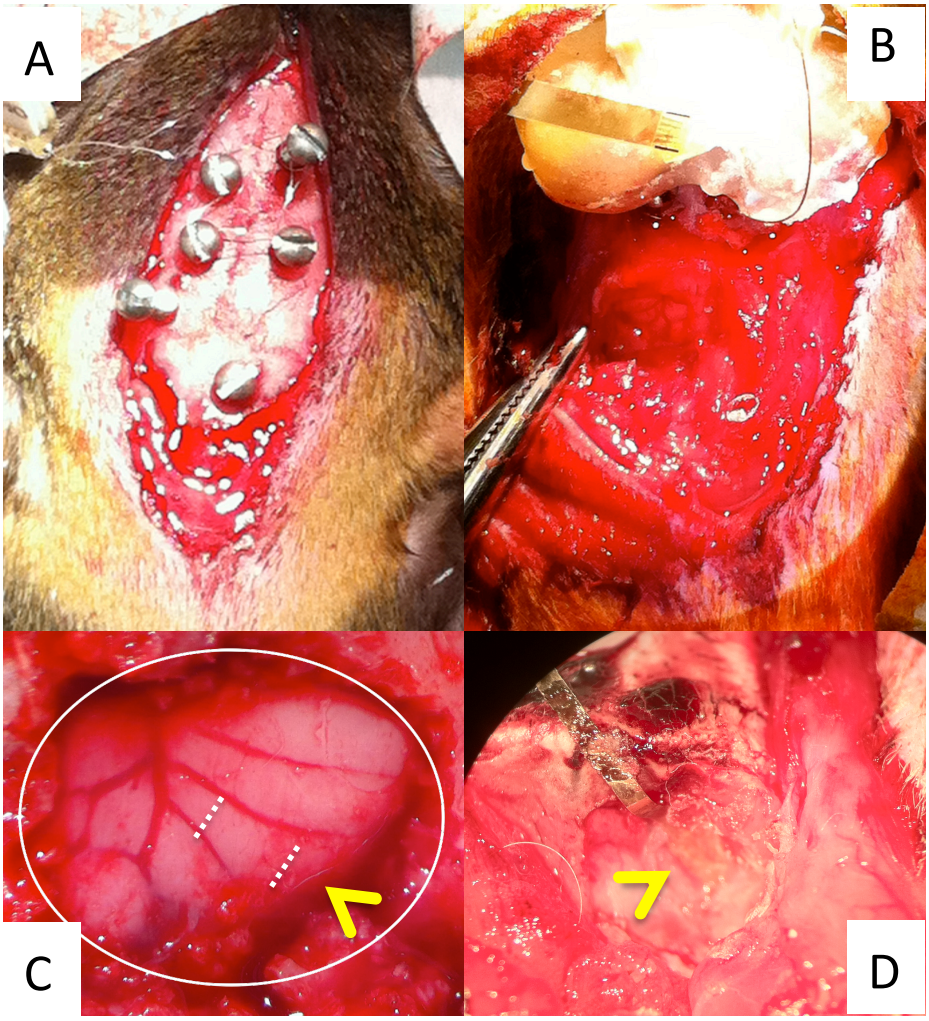

Figure 5.6 Main steps of the MEA implantation are shown (A-D). Skull on the cerebral cortex was used for the stability of the micro-head connector (A), while the cerebellum craniotomy was performed for the MEA implantation (D).

Anesthesia was induced in chronically implanted animals with a single intraperitoneal injection of 55 mg/kg ketamine and 12 mg/kg xylazine mixed and diluted in normal saline.

The recordings were performed in a large Faraday cage through a 34-channel head-stage amplifier (Gain 800, Band-Pass; 0.8 Hz – 3 kHz, Triangular Biosystems, NC) inserted into the micro connector on the rat's head, which was also interfaced with data acquisition card (National Instruments PCI 6259) and the computer. The signals were sampled at 16 kHz and collected in 10-s episodes before the anesthesia and also as the animals were recovering from anesthesia at regular intervals. Video images (Basler Inc., PA) were captured simultaneously with neural recordings to confirm retrospectively that the animals were not moving during data collection.

Table 5.1 Electrode Impedance Values Measured in a Sample MEA over a 45-day Period.

	Electrode Impedance (kOhms)			
Channels	**DAY-1**	**DAY-5**	**DAY-15**	**DAY-45**
1	60	270	180	145
2	155	85	180	155
3	45	70	180	130
4	55	40	180	120
5	60	40	90	70
6	35	250	150	130
7	45	70	190	120
8	65	125	330	140
9	50	160	440	135
10	50	90	280	130
11	40	110	330	130
12	50	90	360	140
13	75	80	360	195
14	55	50	280	165
15	45	75	500	305
16	35	125	300	220
17	140	100	90	70
18	65	110	80	60
19	60	95	230	110
20	40	100	200	170
21	55	65	170	170
22	70	150	150	160
23	115	145	190	145
24	140	100	160	150
25	30	100	450	150

26	50	110	170	170
27	20	40	170	95
28	15	100	150	90
29	30	100	450	90
30	30	260	300	330
31	45	175	100	120
32	35	50	100	90

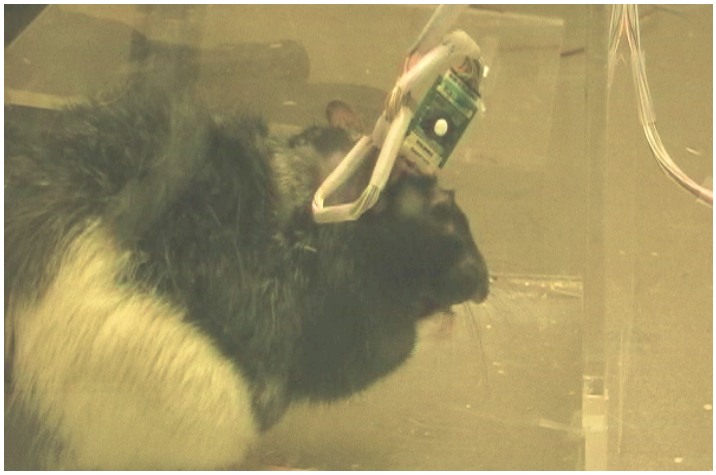

Figure 5.7 Picture of a chronically implanted rat while face cleaning, connected to a pre-amplifier via its skull- mounted percutaneous connector.

5.1.4 Stimulation Paradigm

Evoked potentials were induced by single or repetitive tactile stimulations in the anesthetized animals. Anesthesia depth was maintained at mild level (55 mg/kg ketamine and 12 mg/kg xylazine) to avoid depression of complete EP responses. As a stimulus, either air-puffs (30 psi, duration > 50ms) or the mechanical tap stimulations (1atm, 50μs) were applied to the periphery, e.g., ipsilateral forearm, whiskers, face, and perioral areas. Multiple trials were averaged to reduce background activity against the evoked signals. During recovery from anesthesia to wakefulness, rats were ensured not to move before the air puff thereby avoiding

large spontaneous activity that would contaminate the evoked potentials. All data analysis was performed in Matlab.

5.1.5 Coherence Analysis

Relationship between recorded signals across 32-channels was studied in the frequency domain. Signals from all recorded channels were filtered between 0.5Hz-3kHz. Cross-coherence values between each paired channels were calculated by using Welch's averaged modified periodogram method with pre-defined Hamming window. Magnitude squared coherence estimation ($C_{1,2}$) was varied between 0-1, which higher values indicating stronger relationship. Leveraging the MEA feature, this has 8 by 4 site configurations; cross-coherence values of paired channels were computed with respect to inter-site distances (300μm, 900μm) and averaged across multiple trials and animals (mean±s.d, Figure 6.10). Additional to distance selective analysis, coherence estimation was also computed for all 32-sites against each other, which represented the mean spatial coherences of all MEA channels in each trial (Figure 6.29).

5.2 Injury Methods

5.2.1 Fluid Percussion Injury (FPI) Setup

Lateral fluid percussion brain injury is one of the most commonly used and well-characterized experimental models of TBI, producing both focal and diffuse injury characteristics (Thompson et al., 2005;Cohen et al., 2007). It is often used to induce TBI in both rat and mouse models (Schwarzbach et al., 2006;Cohen et al., 2007). From experience working with the widely used animal model, Dr. Bryan Jim Pfister (BME, NJIT) has

developed a computer controlled fluid percussion injury (FPI) device to precisely control the characteristics of the pressure waveform of the fluid percussion (Abdul-Wahab R, 2011).

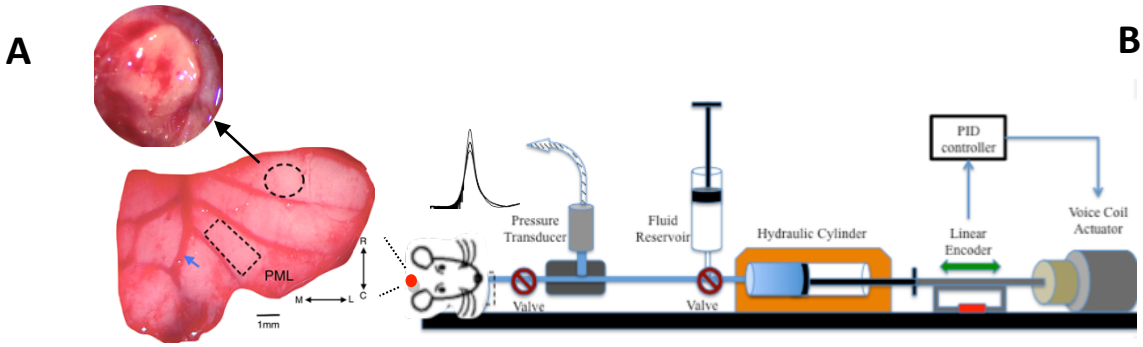

Figure 5.8 A, Position of the MEA (rectangle) and the injury hub placements (circle) on the actual sized cerebellum surface. Verification of the induced injury is shown immediate after the single fluid pulse (arrow). B, Programmable Fluid Percussion Injury system and the experimental setup.

This device utilizes a voice-coil actuator to generate a precise temporal forcing function under closed loop control with a proportional–integral–derivative motion controller and a linear encoder with a 1 μm resolution. The voice coil is coupled to a hydraulic cylinder that delivers the defined fluid percussion waveform. Model of experimental setup for the FPI is shown in detail (Figure 5.8B).

Adult rats were anesthetized using ketamine/xylazine and placed in a stereotaxic frame. The scalp was reflected with a single incision and a trephine with an outer diameter of 3mm creates a craniectomy. Only animals with dura intact were used. The needle was cut from a Luer-loc needle hub (3 mm diameter) and glued in place with cyanoacrylate adhesive. Dental acrylic was then applied to secure the connector. The animal was sutured and placed on a heating pad. Rats were attached to the voice coil activated FPI device, while they were still under anesthesia. The Luer-loc hub was filled with sterile saline, connected to the FPI device and injured. The approximate location of injury site with reference to electrode

placement (~1mm rostro and lateral) and a sample of injured area after FPI delivery are shown (Figure 5.8A). The animal was held on a heating pad and returned to the home cage when ambulatory.

5.2.2 Delivery of FPI and Injury Severity

Craniotomy for the FPI induction had been performed during the same electrode implantation surgery. A burr hole had been made into the skull 1 mm above the implanted electrode on the right hemisphere. A plastic tube had been firmly attached into the hole using dental acrylic mixed with cyno acrylate. Once the port had been placed and secured with tissue adhesive and dental acrylic mixture, animal was taken to recovery, which also yielded for 1-3 days to obtain baseline recordings prior to injury induction. There was always a gap ($\leq$3 days) between the surgical implantations and the time of the injury, which was utilized for the initial recordings from the un-injured animal. Typical steps of the surgical implantations and the electrophysiological recordings were highlighted in Figure 5.9. Then, the fluid percussion injury (FPI) device developed by Dr. Pfister in our group was connected to the plastic port. Dr. Bryan Pfister, who is a PI on a multi-investigator project from NJCBIR with Drs. Kevin Pang and Vijayalakshmi Santhakumar, had developed a custom fluid percussion injury device that was accurate in the lower pressure range necessary for producing mild brain injuries. It had the unique ability to independently control the rate, magnitude, and duration of the pressure wave (Figure 5.8B).

Following the baseline collection from the un-injured animal, a single pressure pulse with a peak of 5-15psi (0.35-1atm) and 5ms duration was applied through the port. The evoked potential recordings were repeated as described above to observe the immediate

changes (10 minutes) post-injury. It was important to collect the signals always at the same time window (10-20 minutes) from the time of anesthetic injection in order to standardize the anesthesia level. The timing of this window was the best way to control the anesthesia level, and even more effective than controlling the anesthesia dose itself in our experience.

In the first few animals, the threshold pressure needed to observe any changes (immediately or later) in the evoked potentials was determined. Preliminary experiments contained recordings from both anesthetized and awake animals. Anesthesia was instrumental to keep the evoked potentials free from any modulatory signals from the other brain sites, e.g. sensory motor cortex. The network activity was much higher once the animal recovers from anesthesia (de Solages et al., 2008b;Middleton et al., 2008;Ordek et al., 2013). The minimum intensity of FPI pressure to induce changes in the evoked potentials (amplitude or onset time) or the network connectivity (correlation and coherency) in the acute and chronic phase was determined by lowering the initial tested higher magnitudes (25-30 psi) to an optimum intensity; 10-15 psi. Quantitative injury results were included in this study were acquired from only the animals that were injured with optimum intensity (10-15 psi) by a single FPI induction. The time course of these measures was studied. The acute and chronic time course of the injury progression was monitored with daily recordings.

5.2.3 Monitoring the Baseline Electrical Activity in the Injured Animal

Experimental procedure of the FPI animals was initiated by the collection of baseline recordings following MEA implantation 1-3 days prior to injury. Once the baseline recordings were established, FPI was performed through the injury port, which was placed during the MEA implantation. Immediately after the FPI induction, electrophysiology of

each animal was monitored for acute and longer time courses (Acute – one week). Typical timeline of the experiments is shown in figure.5.9.

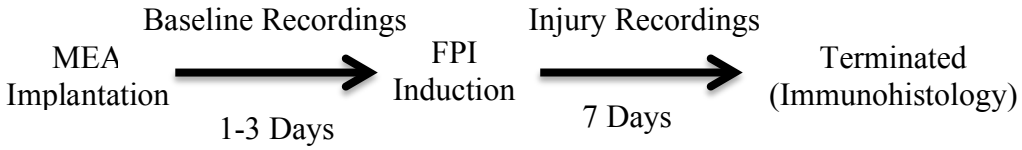

Figure 5.9 Experimental procedure is described with respect to time course. Each experiment lasted 7-10 days including 1-3 days pre-injury monitoring.

Prior to FPI induction, each animal was anesthetized again with ketamine/xylazine. First, a baseline evoked potential recording was made via bilateral MEAs before the injury. The cerebellar evoked potentials were recorded for a number of (N=20) mechanical stimuli had been delivered at 1Hz and averaged to remove the uncorrelated noise components from the signals. Mechanical stimulations were performed bilaterally on the peripheral areas (dorsal arm, whisker or hind limb) that were studied in the preliminary work. Components of the cerebellar evoked responses (MF or CF originated, Figure.6.1) were measured in amplitude and delay times on the computer retrospectively.

Three quantitative measures were extracted from the neural signals and followed over time: Firstly, the amplitudes and arrival times of the volleys related to the mossy fiber activity in the evoked potentials under anesthesia. Secondly, the amplitudes and arrival times of the volleys related to the climbing fiber activity in the evoked potentials under anesthesia. Finally, the average correlation and coherence values between all the contacts of the MEAs were recorded in quietly resting but awake animals.

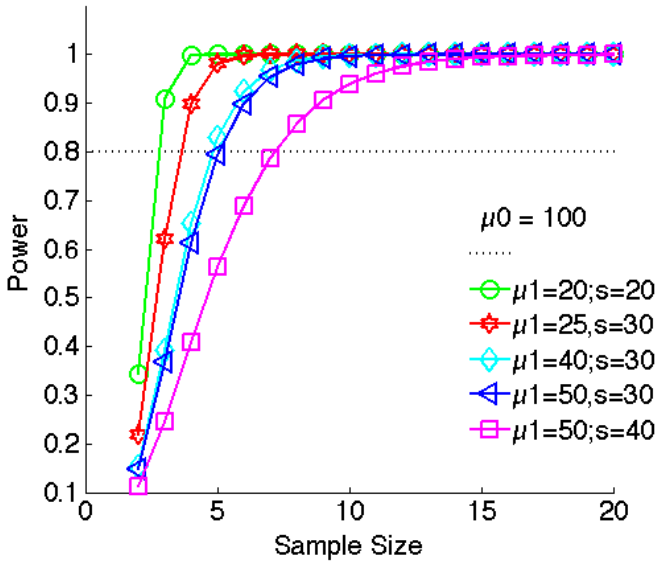

Figure 5.10 Analysis of statistical power was computed with observed EP amplitude changes in the preliminary data. Statistical power is computed with respect to normalized mean (μ1) ± s.d. (s) EPAs.

5.2.4 Determination of Population Size (Power Analysis)

Injury consequences were observed through the EPA changes in the FPI animals. The quantifications in electrophysiological changes were made by comparing the mean ± s.d. of normalized evoked potential amplitudes for pre-injury and 7-day post-injury values in each injured animal. In order to determine the required group size for the FPI experiments, the preliminary data including the minimum and maximum changes were utilized. Analysis of statistical power of sample size from expected changes in normalized EPAs is shown (Figure 5.10). As a reference, at least seven animals were required to indicate similar EPA changes in the FPI experiments in order to meet 80% of statistical significance power with the projected minimum values (50%±40%, violet line). In the current study, the group size was determined as nine animals (FPI experiments), which highlights >99% of statistical power

(red line, 25%±30%; Figure 5.10) with the proposed changed values in the EPAs after the 7 days of injury.

5.3 Immunohistochemical Procedure

Injury to the cerebellar cortex was confirmed with histological evaluations of the explanted tissue in collaboration with Dr. Vijayalakshmi Santhakumar, Neuroscience Department, NJ Medical School, Rutgers-Newark.

In this study, double immunostaining technique was performed. FluoroJade C stained the irreversible cell damages and axonal degenerations, while CalbindinD28k marker was used to provide negative controls staining all types of cells, particularly PCs. Age matched naïve controls (n=5) and FPI-injured rats (n=5) were anesthetized and perfused with 4% paraformaldehyde to harvest whole brains. All injured animals were survived 7 days after the FPI induction. The location of FPI on the cerebellum surface was marked with respect to the MEA implantation site, which was easily discernable after perfusion. The cerebellum was cut in half and then sliced in the lateral to medial direction in 50 μm parasagittal sections. The slices that contained the injury and electrode implantation regions were used for staining. Sliced sections were washed with 0.1M phosphate buffered saline (PBS), and blocked using 10% normal goat serum in 0.3% triton in 0.1M PBS. Then, sections were incubated overnight at room temperature with anti-CalbindinD28k antibody (MAB300, 1:1000, mouse monoclonal; Millipore) in 0.3% triton and 3% normal goat serum in PBS. Sections were reacted overnight at 4˚C with Alexa 594-conjugated goat anti-mouse secondary antibody (1:500, Invitrogen) to reveal staining. Sections processed for CalbindinD28k staining were mounted on gelatin-coated slides to perform FluoroJade C

staining to mark degenerating neurons [58]. Sections were stained with 0.0001% FluoroJade C solution for 1 hour at 4˚C and cover slipped with DPX mounting media. Negative controls were routinely included in which primary antibody for CalbindinD28k was omitted. Representative images were obtained using Nikon A1R laser confocal microscope using 20X objective with identical camera settings.

CHAPTER 6

DATA ANALYSIS AND RESULTS

All data analysis and illustrations were prepared using MATLAB (Mathworks, MA). Statistical results were conducted through SPSS (SPSS Inc., IL) and R (Bell Laboratories, NJ) in addition to MATLAB. The signals were acquired as 32-channels or 64-channels (Two MEA implants) in a non-referenced single-ended (NRSE) specification with respect to Pt wire positioned nearby the recording MEA in the animal's head. Data acquisitions were performed either at 16kHz or 20kHz sampling resolutions with two NI-daqmx cards (PCI-6255, National Instruments, TX). An anti-aliasing filter (0.1Hz – 3kHz) with a gain of 800 (Gain = 100, in earlier recordings) was applied at the input stage of signal recordings. Additionally a band-pass filter (5-400Hz) was added to time series analysis. Data typically were obtained 1sec, 5sec or 20sec lengths of windows for signal analysis. Spike-(or stimulus) triggered averaging (STA) was performed over multiple epochs of stimulations (T=20sec, f=1Hz).STA improved the SNR value of the evoked potentials proportional to square root of the stimulus repetition ($\sqrt{20}$). 0.5Hz-3kHz pre-conditioned signals were additionally filtered between 5-400Hz (4^{th} order, Butterworth) to eliminate any noise components in the evoked signals. In order to investigate the spatial relationship between 32 electrode channels that recorded different neural activity, correlation analysis (Pearson and Spearman) was included. Frequency domain was studied through cross-coherence analysis by using Pwelch windowing. Measurable data was analyzed and reported by the (non-) parametric statistical methods; student's t-test, rmANOVA, Mann-Whitney, post-hoc tests.

6.1 Characterization of Cerebellar Potentials

6.1.1 Evoked Potential Analysis

Cerebellar evoked potentials were characterized in terms of their temporal and waveform patterns with a given stimulation (Figure 6.1). A typical evoked potential waveform contained relatively lower magnitude deflections within the first 10ms of stimulus arrival, which was followed by larger positive wave(s) at 10-30ms after the stimulation. Initial volleys were described as the mossy fiber related potentials confirming the earlier reports, where the MF responses were faster and typically observed within the 5ms of stimuli-evoked response window (Figure 6.1, Left).

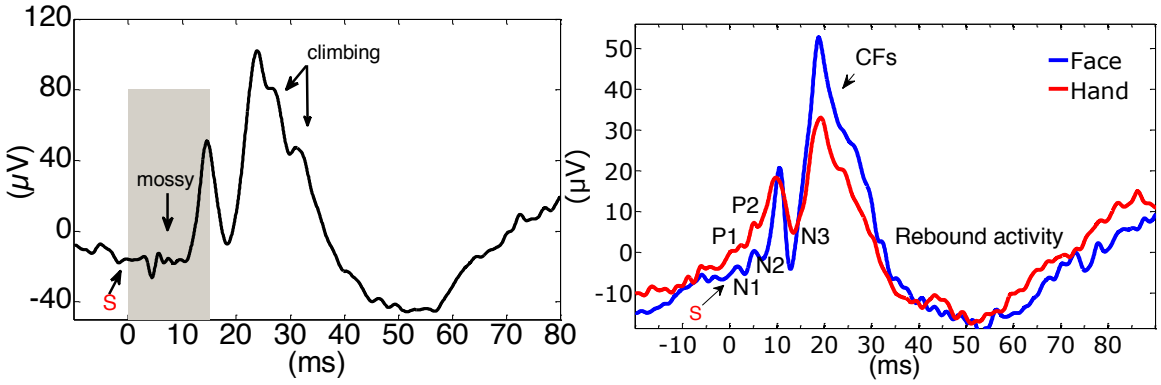

Figure 6.1 Typical evoked potential waveforms within the temporal course of the stimulation arrival (s). Mossy fiber and climbing fiber responses were labeled with respect to onset latencies of deflections to a mechanical tap (Left) and air-puff stimulations (Right). Evoked potentials in cerebellum exhibit characteristic responses to different stimulation areas (Face and hand, Right). Onsets of the EP arrivals for MF responses were labeled with respect to positive (P) and negative (N) polarities.

Identified evoked potentials in response to peripheral stimulations (air-puff) from STAs epochs (20 repetitions, 1Hz) are shown in detail for anesthetized animal (Figure 6.1, Right). The peripherally evoked signals obtained from both stimulations resembled signature

volleys allocated to mossy fibers (MF) and climbing fibers (CF), subsequently. In both stimulations, MF related volleys were denoted within the 10ms after the stimulation arrival, while CF responses showed longer latencies >10ms.

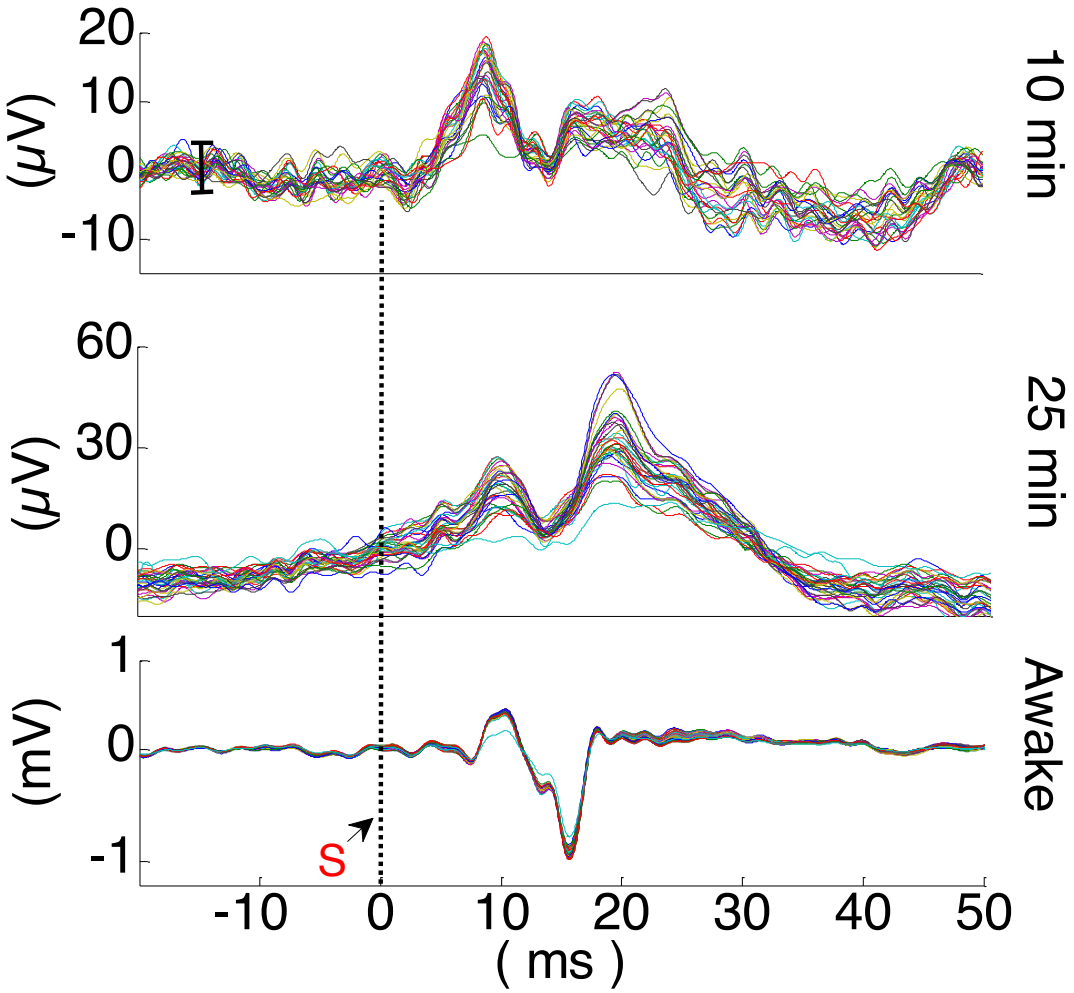

Figure 6.2 ECoG signal characteristics in the anesthetized animals for 32 MEA channels. The amplitude and synchrony between recorded channels were drastically improved as the anesthesia worn off from the system.

The mossy fiber signal arrived approximately 1.4ms after stimulation. The evoked potentials showed the P1, N1, P2, N2, N3, and N4 components of the field potentials that

closely resembled the surface recordings made by Armstrong & Drew (1980). The mossy (P1-N3) and climbing fiber potentials to hand and perioral face stimulations showed similarities to previous reports with additional delays in the order of millisecond range. This variation was likely dependent on the stimulation paradigm where mechanical stimulations may cause additional onset delays compared to electrical stimulations.

6.1.2 Quality of ECoG signals during Anesthesia Wakefulness Recovery

Cerebellar oscillations contained evoked responses were collected via subdural MEA recordings from multiple animals.

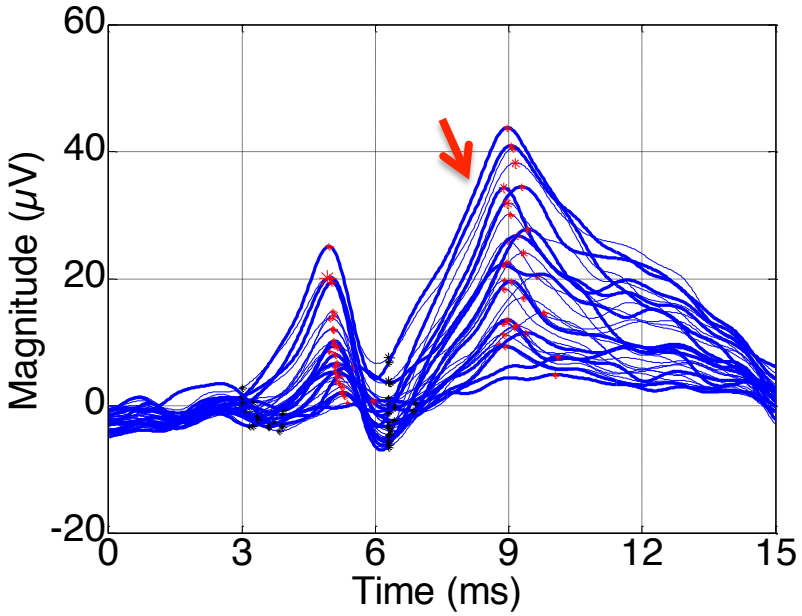

Figure 6.3 A sample of amplitude measurement from two evoked potentials in response to hand stimulation. Evoked amplitudes were calculated from absolute magnitude differences between the beginning (black starts) and the peak point (red stars) of each deflections for 32-channels.

ECoG signals recorded through the subdural implantation contained the local field potential signals (LFPs) which are defined by the summation of extracellular fields such as synaptic

activity, transmembrane currents, and dendritic activity from multiple sources. Despite the fact that LFPs ideally represent larger neuronal populations, synchronous action potentials from many neurons can contribute the high frequency components of the ECoG signals.

Anesthesia regimen depresses the evoked signals and desynchronizes the oscillations substantially at the initial phase after the injection. Depending on the dosage of anesthesia, full recovery of the cerebellar network signals may vary.

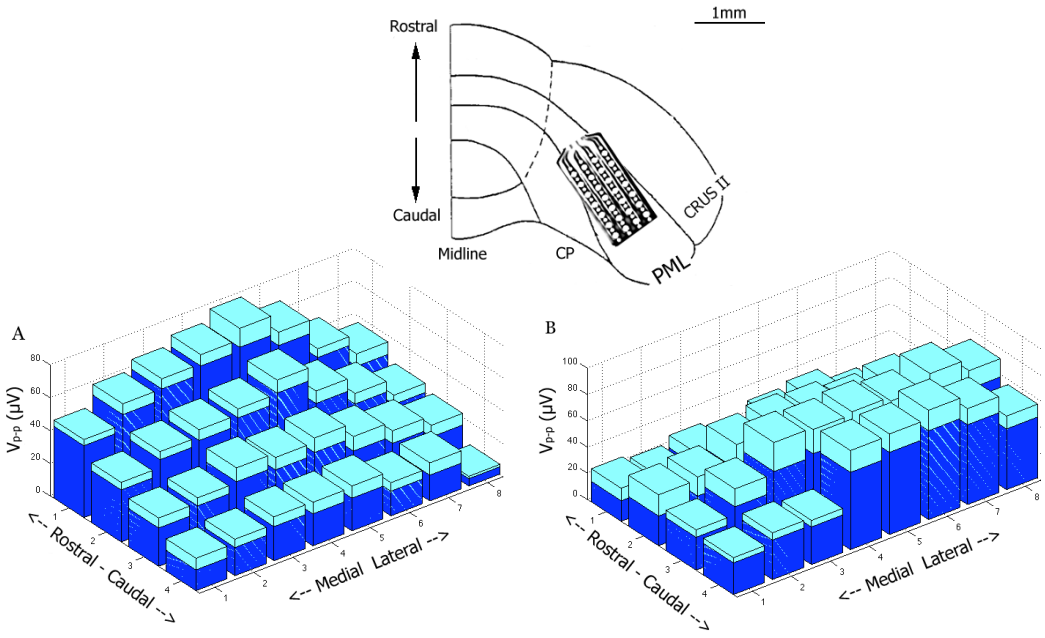

Figure 6.4 Somatotopic mapping of the PML area studied with peripherally evoked potentials under anesthesia. Climbing fiber response (arrow, Figure 6.3) was referenced for the somatotopical analysis. Placement of the electrode array (4 × 8) corresponding to the bar results are shown at the top panel. Towers indicate the amplitude mean ± s.d. (dark and light blue parts) of signal deflection that arrived at 6-10ms after the stimulus arrival. Multiple air puffs were applied (n = 20) in each acquisition, either to the dorsal arm (A) or to the wisher free face area (B).

The current study focused on the recordings obtained in anesthetized animals, thus the stability of the anesthesia was determined at the beginning of the recording

characteristics a relative high dosage of ketamine xylazine mixture (80mg/kg and 15mg/kg, respectively) was administered and taken to the recordings chamber for continuous monitoring. The cerebellum recordings in response to mechanical hand stimulations were shown in the temporal course of the anesthesia recovery within the 1h period (Figure 6.2).

The evoked potentials were obtained within the first 10 min after the anesthesia induction exhibited sustain low-amplitude (V_{p-p} = 5-20μV, top panel, Figure 6.2) and de-synchronized pattern across recorded 32-channels. After 10 min, there was a dramatic change in the evoked potentials as well as oscillations that was most likely due to the anesthesia wearing off. The evoked response amplitudes were increased by 3-4 fold (V_{p-p} = 20-60μV, center panel, Figure 6.2) in the following 25 min of anesthesia injection. Amplitudes of evoked potentials were in the millivolt range (V_{p-p} > 1mV, bottom panel, Figure 6.2) as the animal started to wake up from anesthesia. Wakefulness also re-synchronized the oscillations drastically that the recordings from all 32-channels resembled nearly a single channel.

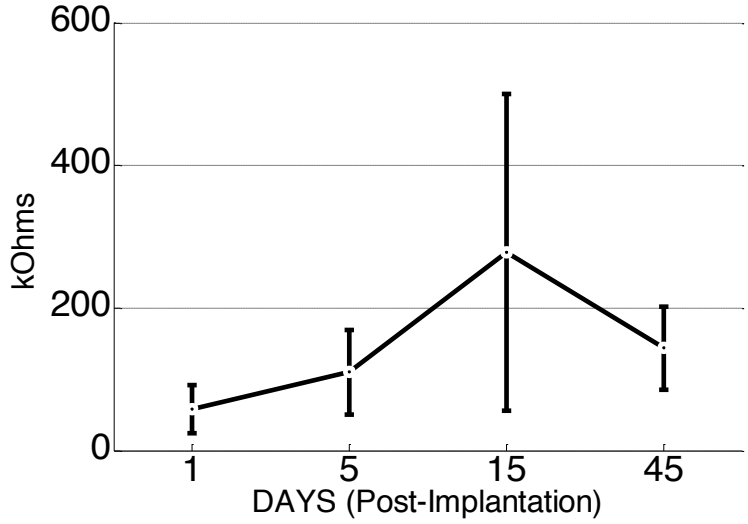

Figure 6.5 Impedance changes in mean ± s.d. values of 32-channels are shown for the 45-day implant period. Impedances showed an increase and regression period after two weeks of the implantation.

Additionally, subdural ECoG recordings demonstrated a high signal to noise ratio in the chronically implanted animals. The amplitudes of evoked responses were as great as >1mV in the awake recordings, while the background noise activity fluctuated ~2-3μV (scale bar, top panel, Figure 6.2).

6.1.3 Somotatopy Investigation in the Cerebellum with Surface MEA Recordings

Evoked potentials collected in response to different peripheral area stimulations were investigated whether there was a selectivity across 32-channel aligned on the two dimensional plane of the PML surface (Figure 5.6C). Multiple repetitions of the evoked response amplitudes were calculated for each stimulation epoch and then averaged for 20 times. The amplitude calculations of EPs are shown in an anesthetized animal recording (Figure 6.3). Averaged evoked responses consistently produced larger amplitudes on the

caudal aspect of the array when the dorsal arm was stimulated, whereas the face stimulation generated larger potentials on the rostral side of the array (Bottom panels, Figure 6.4). The bar plots represent the approximate locations of the implanted zones on the PML surface (Top panel, Figure 6.4) leveraging the MEA design.

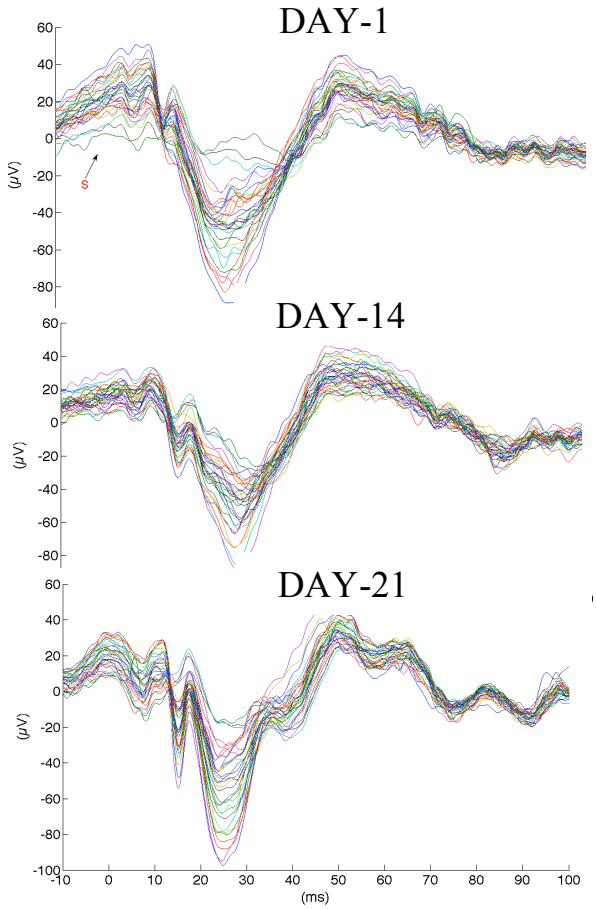

Figure 6.6 Evoked potentials demonstrated a long-term stability in amplitude and waveform characteristics over the 3 weeks period. Signal to noise ratio remained at the lowest level as the evoked potentials resembled the same waveforms in response to 3-week whisker stimulations. There was also polarity reversal in the evoked waveform.

These plots clearly demonstrated that evoked potential amplitudes expressed a somatotopic mapping in the PML area of the cerebellum in anesthetized animals, which is a well-known phenomenon from earlier reports. However, it wasn't possible to reproduce this

map in the unrestricted and awake animals because of the high neural background activity and movement related signals that overlapped the evoked waveform.

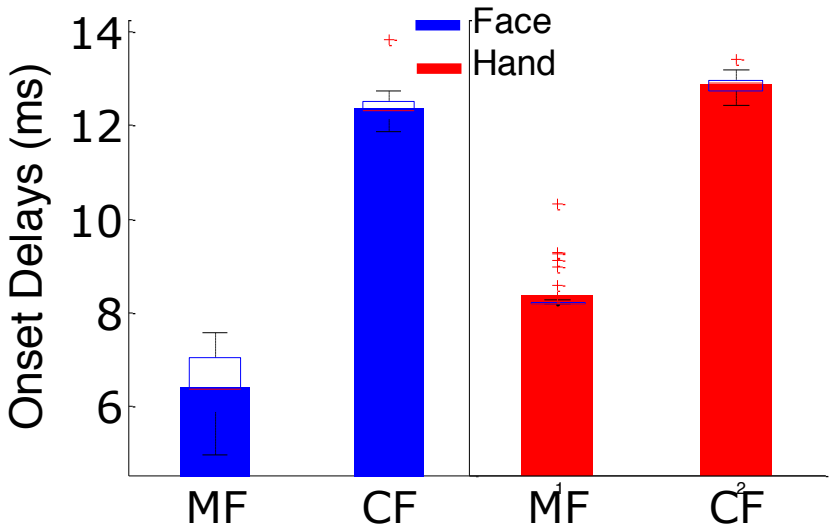

Figure 6.7 Onset latencies of mossy and climbing fiber network responses to given face and arm stimulations. Arrival latencies indicated strong reproducibility across multiple animal and day recordings (N = 6 rats, n > 20 trials). Evoked volleys in response to hand stimulation demonstrated longer latencies (1-3ms) with respect to face stimulations.

6.1.4 Longevity of the Chronic ECoG recordings by using Evoked Potentials

One of the biggest drawbacks in the neural recordings is the reliability of the signal quality. In the current study, flexible MEA fabricated on polymer substrate was utilized which minimizes the electrode breakages due to the mechanical stress in the chronic recordings, however, the immune response and the encapsulation was still a problem.

In order to monitor these issues, two principals; periodic impedance measurements with monitoring the signal to noise ratio, was taken into account. Impedance changes for 32-channels were shown over the 45-day recordings periods (Figure 6.5). Mean impedances were increased to 500-600kΩ from 50-100kΩ range within the two weeks period. Electrode

impedances across 32-channels indicated an initial incline trend within the first week of implantation, and then stabilized after the second week.

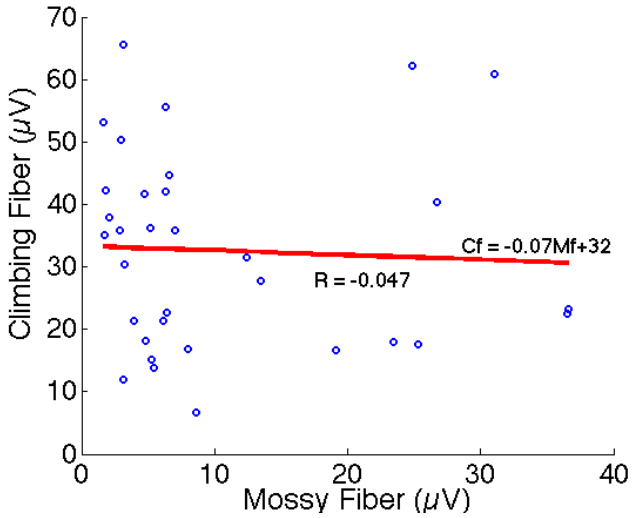

Figure 6.8 Relationship of mossy and climbing fiber originated evoked responses. EPAs were obtained from multiple animals and trials (N = 8 rats, n = 33 trials). Variations in individual EPAs show no correlation between two evoked responses, indicating two different sources are responsible generating these sequential waves; R =- 0.047. The linear fit is Cf = -0.07Mf + 32.

Furthermore, evoked potentials were analyzed in the temporal course of three weeks period (Figure 6.6). It has been verified that the ECoG electrodes on the cerebellar surface could collect reliable signals in the 50-100μV amplitude range in the weeks following the implantation. Polarity reversal in the evoked waveform was also noted in these ECoG recordings. This could be dependent on the placement of the reference electrode and/or the main contributor dipole sources along the somatodendritic axis.

6.1.5 Identification of Neuronal Mechanisms of Cerebellar Evoked Responses

The evoked deflections in the cerebellar circuitry were generated by the internal neural mechanisms in response to given stimulations. Most distinctive feature of the mossy and

climbing fiber responses was the onset latencies of the volleys with respect to stimulus arrival. Typically, early responses within the 5-10ms window after the stimulus were linked to mossy fiber related networks. Whereas, the latter responses were activated by the climbing fiber inputs on the Purkinje cell synapses. The arrival latencies of these identified evoked potentials were very reproducible in multiple animals under anesthesia recordings (n>20 trials, N = 6 rats, Figure 6.7). In addition, the onset latencies of these potentials were similar in time regardless of the face and hand stimulations.

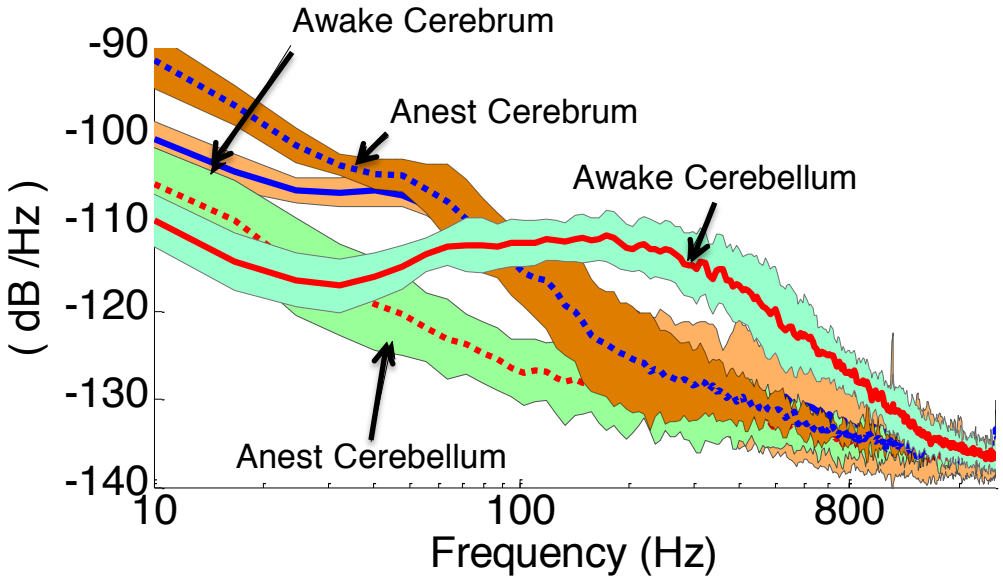

Figure 6.9 Power spectra of micro-ECoG recordings from the cerebellar and the motor cortices in anesthetized and awake-quiet animals. First, all 32 channels of recording were combined into one power spectrum as a representative spectrum of all the channels and then the spectra from multiple epochs (N=20) were averaged (Welch's method) for a robust measure of frequency content. The lines and shaded areas indicate mean±s.d. The power spectrum of the cerebellar cortex in the awake animal extends almost up to 1kHz. The effect of anesthesia is much more prominent on the cerebellum than it is on the motor cortex.

While the face stimulations elicited the MF and CF related responses at 6.23±1.45ms and 12.23±2.3ms, respectively (blue bars, Figure 6.7), the same latencies were delayed to 8.15±1.56 ms and 13.56±2.36ms in the hand stimulations (red bars, Figure 6.7).

Similarity in the onset latencies of MF and CF related evoked potentials had intrigued us to investigate whether there was a direct relationship between the two sub-networks. This time, the one to one amplitudes of evoked potentials to given any random stimulation were measured. Multiple trials of face and hand stimulations demonstrated almost zero correlation; r = -0.0469, between the two input amplitudes (Figure 6.8). The regression line had a declining slope, where the CF amplitudes were always the greatest in magnitude (CF =-0.07MF +32).

6.1.6 Spectral Analysis of Cerebellar Activity in the Anesthetized and Awake Animals

Cerebellar activity recorded in quietly resting, awake animals had frequency components up to 1kHz, which was in clear contrast with the signals from the cerebral cortex, in particular motor cortex (Figure 6.9). Interestingly, the spectrum of awake cerebellar activity had a dip around 20-60Hz (Red solid line, green shading; Figure 6.9), roughly covering the high beta and the gamma band. Ketamine/xylazine anesthesia strongly reduced all the high frequency components in the cerebellum except below ~30Hz. In fact, these lower frequency components were larger under anesthesia ($F = 1.83$, $p = 0.09$ for <30Hz, n=20 trials, N=9 animals). The motor cortex signal amplitudes declined by frequency and they were observable only up to ~200Hz above the noise level (Blue solid line, brown shading, Figure 6.9). The motor cortex spectrum was virtually not affected by the anesthesia at the high frequencies, however the signal power was significantly less at the lower end of the spectrum

in the beta band and below ($p<0.01$). These spectra demonstrate a clear difference between the frequency components in the spontaneous activities recorded from the motor and PML cortices with micro-ECoG electrodes and a drastic contrast in the way that the two cortices are affected by ketamine/xylazine anesthesia.

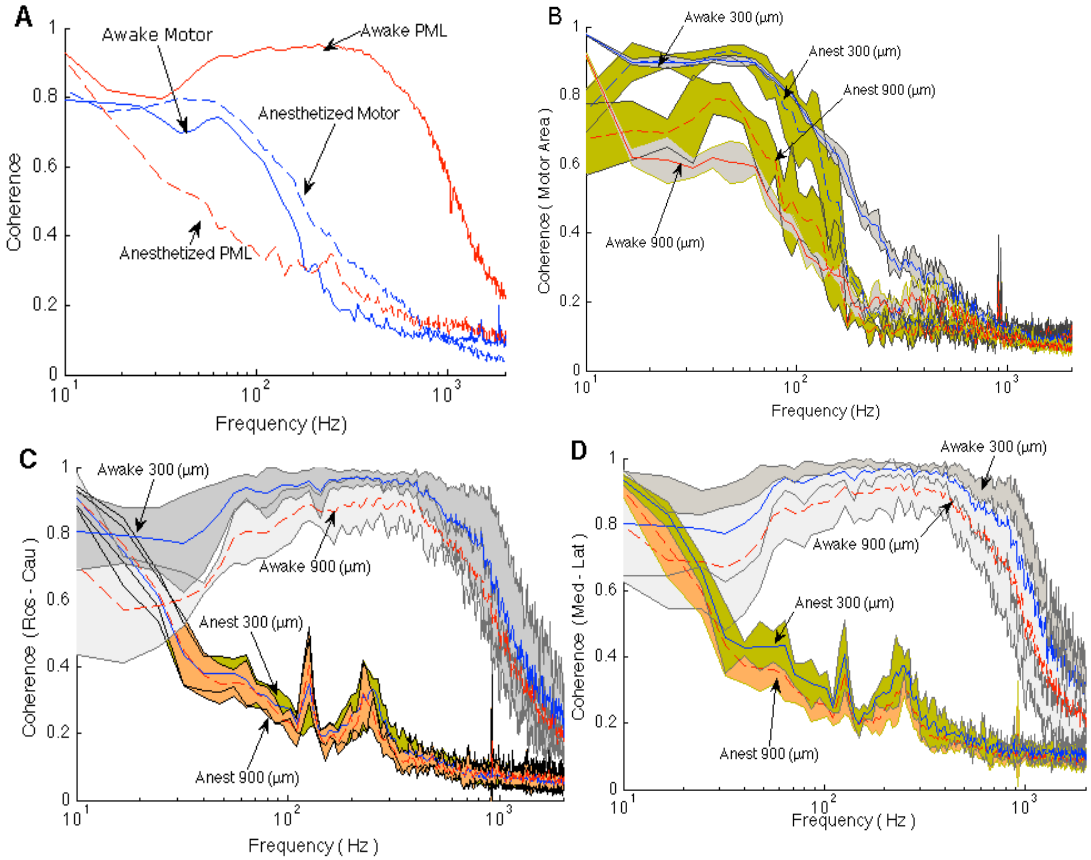

Figure 6.10 Coherence between electrode channels from the cerebellar and the motor cortices in anesthetized and awake-quiet animals. A. Average coherence between all adjacent channel pairs (300μm in medio-lateral or rostro-caudal direction) in anesthetized and awake-quiet animals. B. Average motor cortex coherences between all electrode contact pairs that are 300μm and 900μm apart (in either orientation), showing the decline of coherence by distance and anesthesia. C and D. Average cerebellar coherence between all electrode contact pairs that are 300μm and 900μm apart in rostro-caudal (C) and medio-lateral (D) directions with and without anesthesia.

6.1.7 Coherence Analysis over the Cerebellar Surface

Spatial relationships between recorded MEA channels placed on the 2-D surface of the cerebellum were investigated in the frequency domain. The difference between the two cortices was evident also in the coherence spectra (Figure 6.10A). In the cerebellum, the average coherence calculated between all adjacent contacts pairs (300µm center-to-center distance) were above 0.6 (to pick an arbitrary value for comparison) for all frequencies below 1kHz. A drop in the coherence plot was consistently observed in the beta and gamma bands similar to the one in the power spectrum.

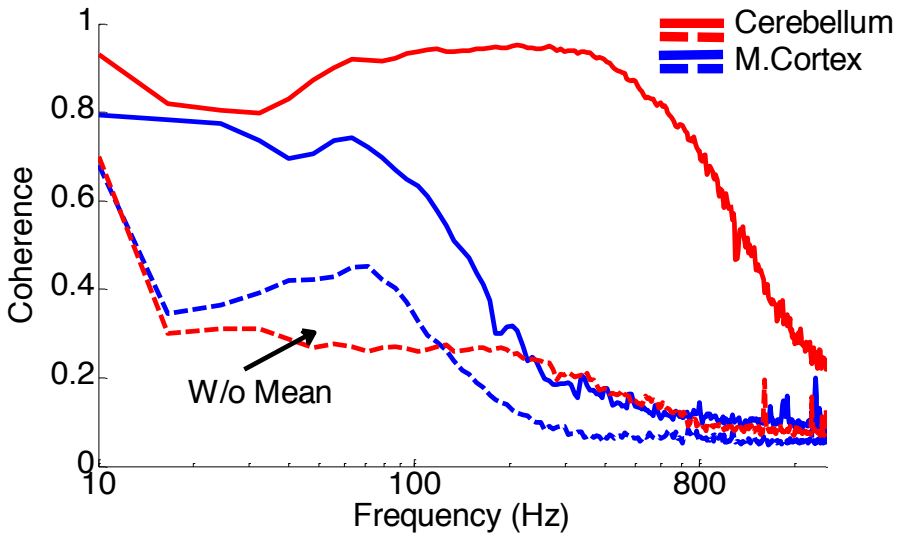

Figure 6.11 Average coherence between all adjacent channel pairs (300µm inter-site distance) in both cortices with and without the mean taken out. Changes in coherence values, particularly in cerebellum awake data indicated a substantial common mode signal in the cerebellar cortex.

Anesthesia induced a drastic decrease in the coherence at all frequencies across the spectrum that only the values below 30Hz were above 0.6. In contrast, the cerebral coherence between adjacent contacts was above 0.6 for frequencies only below 100Hz in the awake animal, and it was only slightly affected by anesthesia across the spectrum. Coherence in

cerebrum was higher during anesthesia and this was substantial in the adjacent electrodes (300μm).

Overall, the awake state coherence values were lower in the motor cortex than the PML at all frequencies. Figures 6.10B –D show the effect of electrode separation on the coherence plots from the motor cortex and the PML respectively.

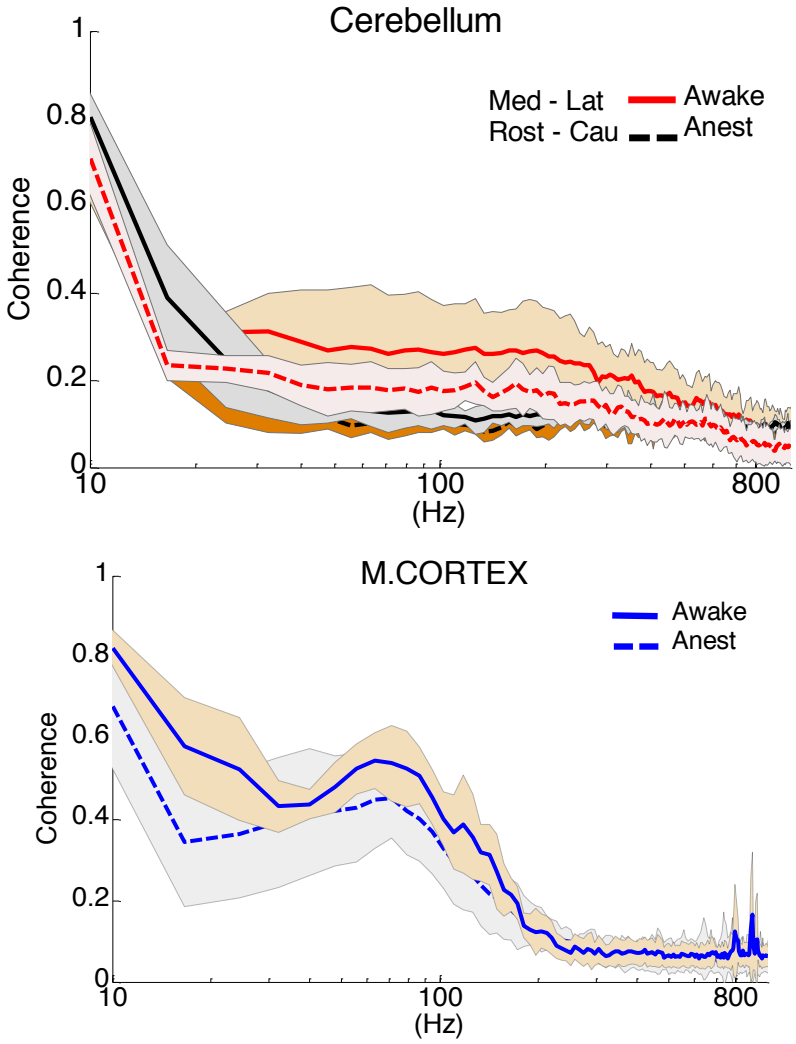

Figure 6.12 Average coherences with subtracted mean value between all adjacent electrode contact pairs in awake-quiet and anesthetized rats in the cerebellum in the medio-lateral and rostro-caudal directions clustered (Top panel), and in the motor cortex in both directions (Bottom panel).

The average coherence for 900μm electrode separation is much lower compared to that of the adjacent electrodes at all frequencies in the motor cortex.

This effect of electrode separation is more evident in awake recordings (Figure 6.10B). The effect of anesthesia is appreciable only above 150Hz at 300μm separation.

6.1.8 Common Mode Signal in the Cerebellar Cortex

The difference between the two cortices was evident also by the coherence analysis (Figure 6.11). In the cerebellum, the average coherence calculated between all adjacent contact pairs (300m center-to-center) was ~0.6 (to pick an arbitrary value for comparison) for all frequencies <1 kHz before the common mode signal was taken out. A drop in the coherence plot was observed at 30 Hz similar to the power spectrum. The coherence values decreased <0.3 when the common-mode signal was cancelled by subtracting the spatial average of the contacts in the cerebellum. The motor cortex coherence was higher in general but extending only up to 200 Hz. The cerebellum coherence plot was reaching up to 800 Hz, hence, clearly contrasting with the motor cortex. Both cortices had large coherence at the lower end of the spectrum even after the mean was taken out (0.7 at 10 Hz). At this point, the results argued that the common-mode signal in the cerebellar recordings could be originated from the distance source or sources that were not interested in the cerebellum. Thus, only the signals without mean were used in the rest of the analysis.

The cerebellar coherence (without mean) was higher between adjacent contact pairs oriented in the medio-lateral direction than the ones in the rostro-caudal direction (Figure 6.12; Top panel). Anesthesia induced a significant decrease in the cerebellar coherence at all frequencies in both directions (red vs. yellow lines in Figure 6.12B; Bottom panel).

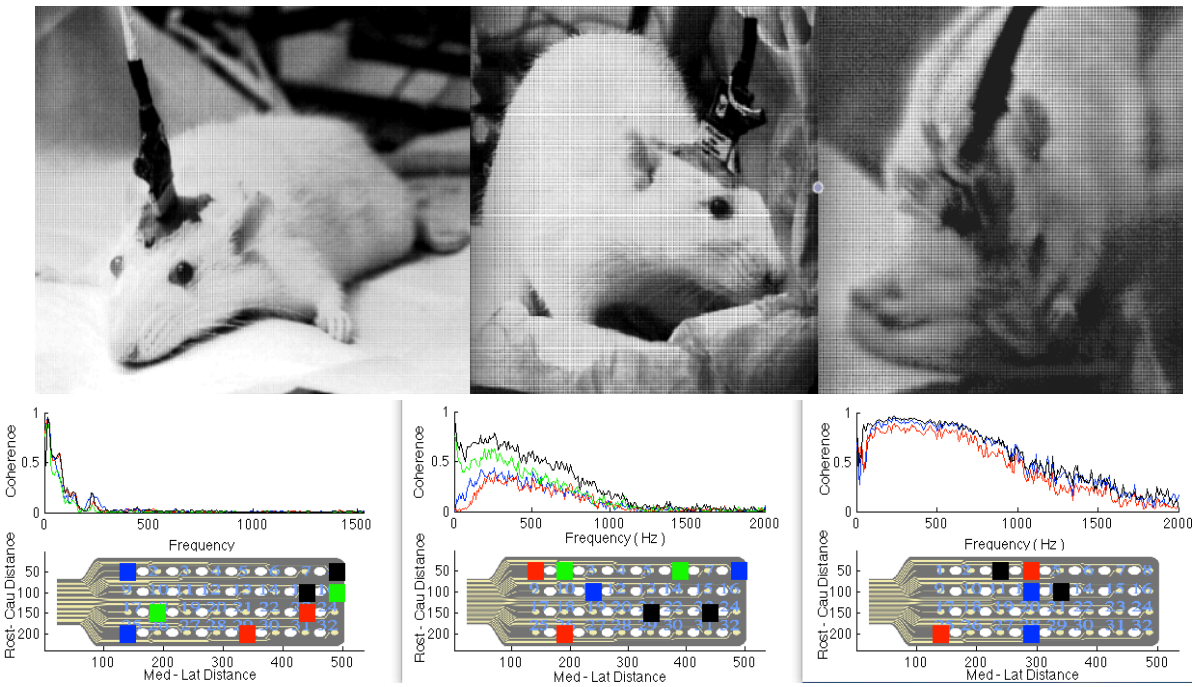

Figure 6.13 Cross-coherence across selected electrode pairs were analyzed in anesthetized and behaving animals. During anesthesia, coherence was limited in the low frequency band (1-100Hz) any of the selected electrode pairs (Left). Coherence was dramatically increased up to 1kHz in the awake states (Right).

A small bump was frequently observed in the anesthetized plots between 200 and 300 Hz as the rat was arousing from anesthesia (not shown in this plot). The motor cortex coherence (without mean) slightly decreased by anesthesia across the spectrum, although the effect was not as strong as that of the cerebellum, and it was limited to the frequencies <200 Hz (Figure 6.12; Bottom panel). In general, the impact of anesthesia was better demonstrated by the coherence analysis than the power spectra in both cortices.

6.1.9 Spatio-Spectral Analysis in Behaving Animals

Cerebellar circuitry is capable of synchronizing in larger populations to generate functional output signals. MEA was utilized to investigate these characteristics by looking at the cross-

coherences across different inter-site distant electrodes at the 0.5Hz-1kHz frequency band (Figure 6.13). Coherence between electrode channels was increased in the awake states. Face cleaning behavior maximizes the all LFP strength even across larger distances (>1mm, right panel).

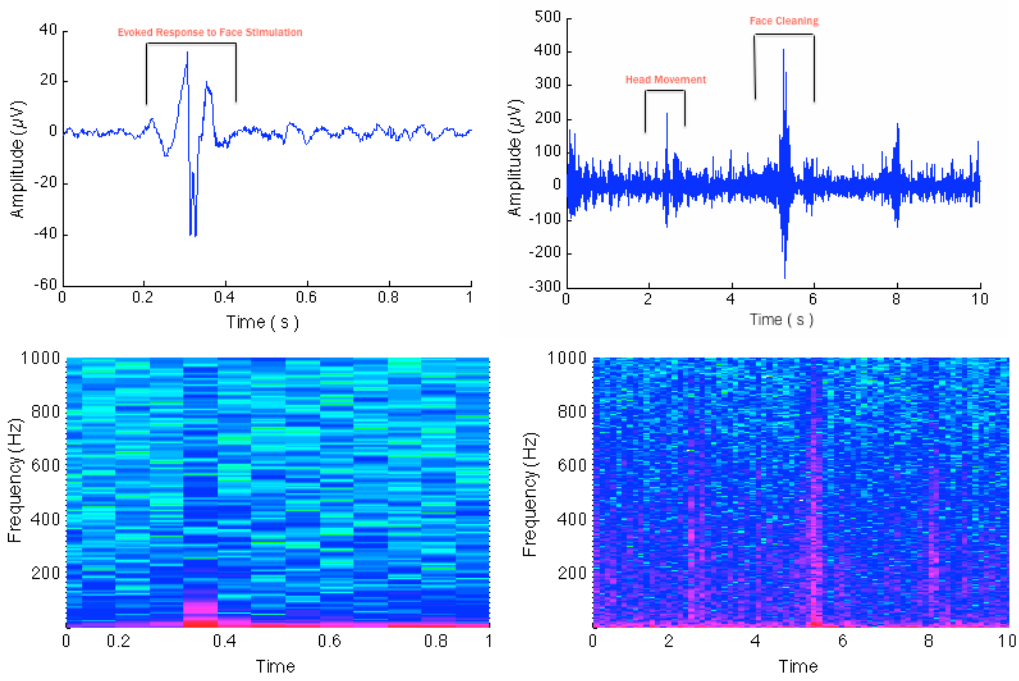

Figure 6.14 Spectral density variation in time was studied in a behavioral context. Raw signals (0.5-3kHz) averaged over 32-channels in anesthetized and awake animal are plotted (Top panel). Corresponding spectrogram plots are shown for each trial (Bottom panel).

During attentive resting (center), cerebellar LFPs were strongly coherent with measurable differences between close distant and far distant paired electrodes. Results indicated the network strength in the cerebellum during wakefulness. In addition to anesthesia-wakefulness comparison, cross-spectral analysis also showed the distance dependent coherences between paired electrode contacts (Figure 6.13, center).

6.1.10 Frequency Analysis in Freely Behaving Rats

Cerebellar LFPs demonstrate very dynamic changes in the frequency context during sensory as well as motor behaviors. The spectral analysis (Figure 6.14, bottom panels) was conducted, as the animal was able to freely walking in the recording chamber for 10 seconds (Figure 6.14, right panel).

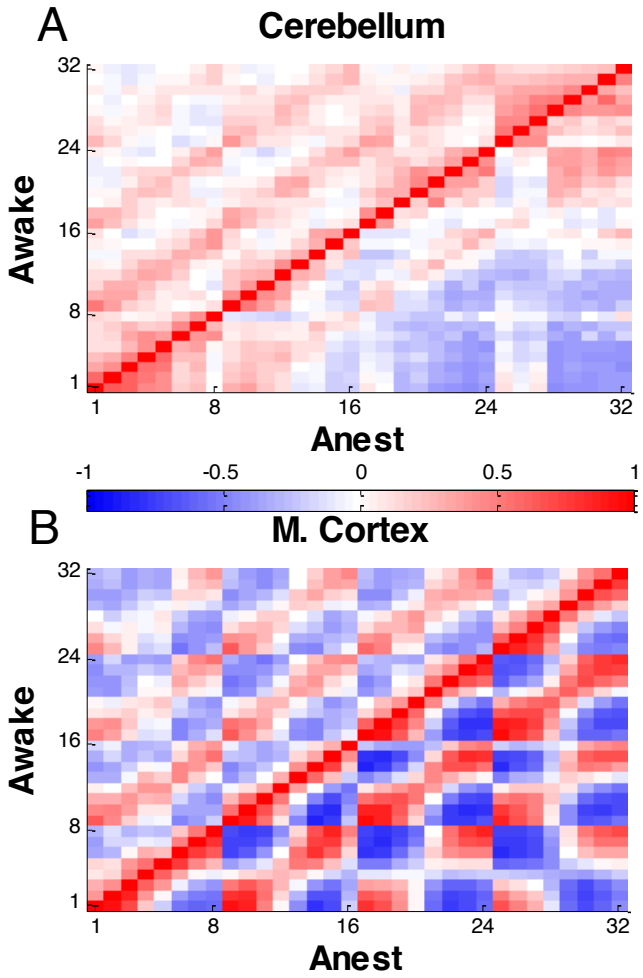

Figure 6.15 Correlation matrixes between all 32 channels of recordings for the cerebellum (A) and the motor cortex (B). Top triangles in A and B represent the awake data, and bottom triangles indicate the anesthetized data collected in different days and animals. Positive and negative Pearson correlation values are indicated by different shades of red and blue, respectively

MEA channels recorded only the low-frequency contents (< 100Hz) during no-movement episodes. In contrast, the power in LFPs was increased up to ~800Hz as the animal attempts for head movement or face cleaning behaviors. In anesthesia recordings, cerebellar LFPs were only strong in the very low frequencies <10Hz, except the evoked response period (Figure 6.14, left panel).

6.1.11 Correlation Strength in LFPs of Cerebellar vs. Motor Cortex

The difference between the two recording sites and the effect of anesthesia was further investigated with correlation analysis (Figure 6.15). The signals were filtered with a wide band-pass, Pearson's correlation coefficient was calculated between all electrode pairs in the arrays using 5-s long time signals, and correlation values were averaged from multiple acquisitions (N > 10 animals, n > 25 trials). The checker-board pattern in the matrixes indicates that the contacts that are nearby have higher correlations than the distant ones (dark red) between adjacent electrodes both in the horizontal and vertical directions in the motor cortex, and it shifts to negative numbers steadily as the separation increases. The correlations are clearly stronger, and the relation between the correlation values and the contact separation is more evident in the awake motor cortex than the awake cerebellum (compare top triangles from each matrix in Figure 6.15).

With anesthesia, the motor cortex signals become more correlated to each other and the effect of contact separation becomes clearer (compare top and bottom triangles in Figure 6.15B). In the cerebellum, however, the correlation values shift to negatives after anesthesia and the effect of contact separation is almost lost completely (Figure 6.15A). These results seem to contradict with the coherence analysis where neither cortices showed a clear effect

of contact separation. Dependency of correlation on contact separation, especially in the motor cortex, may be due to the inclusion of low frequencies in this analysis.

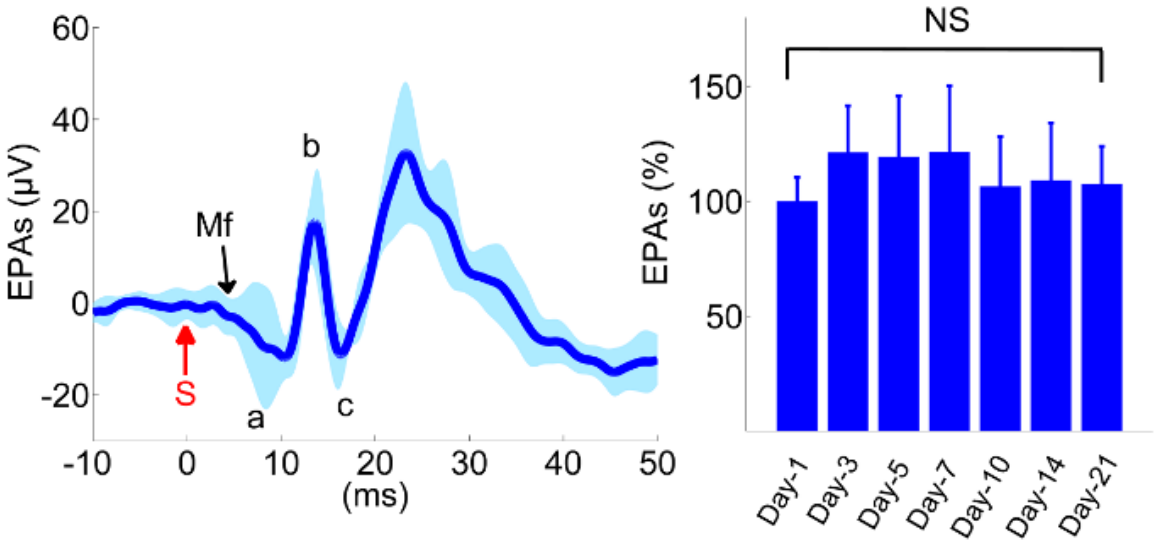

Figure 6.16 Analysis of evoked potentials in the control animals (n=6). Left; Evoked potential (EP) waveforms show sustained amplitudes over a 3-week period. Waveforms from ten different recording days were superimposed from all animals. Evoked potential amplitudes (EPAs) of MF-mediated volleys were calculated by averaging the triphasic volley amplitudes using the equation $\frac{|a-b|+|b-c|}{2}$. None of the days were statistically different than the others ($F_{(6,59)}$ = 1.41, rmANOVA, repeated measures of 6 rats,1-2 trials from each animal, 8-11 trials per day from all animals). NS: not significant.

6.2 Electrophysiological Alterations in the Cerebellar Injured Rats

6.2.1 Pre-Injury Evoked Potentials

The evoked activities under ketamine/xylazine anesthesia demonstrated reproducible and consistent characteristics collected in the 3 weeks period after the electrode implantation (Figure 6.16). A set of animals (n=6) served to provide control results in uninjured animals comparing periodic recordings after the electrode implantation. Evoked volley waveform and

EP amplitudes for the selected (a-c volley) collected from six animals were analyzed with different day recordings.

In both control vs. injured (N = 6 and 9 rats, respectively) analyses, evoked response (a-c, Figure 6.16) was selected and investigated across all animals. This evoked volley demonstrated the most consistency across multiple trials and animals in the control recordings (s.d$V_{p\text{-}p.}$ = ±5%) under the controlled anesthesia recordings. EP amplitude for the selected volley was analyzed during the 3-week survival period (right panel, Figure 6.16, n=6 rats, 8-11 trials per day). None of the days was statistically different in EP amplitudes in the recording period (Repeated measures of ANOVA, F(6,59) = 1.41), though the largest variations were observed during the first few days, e.g. ~21% on day-3 (Mann-Whitney; n = 9 trials, p = 0.06). The recordings in uninjured animals show that the signal amplitudes and arrival times are stable over a period of at least 21 days and thus the implantation of the MEA itself does not cause a significant trauma to the cerebellar cortex.

6.2.2 Post-Injury Evoked Potentials (Minutes – One week)

Multi-channel evoked responses recorded in a mild FPI animal is shown in Figure 6.17. The FPI pressure amplitude was 5psi (0.35 atm) and the wave duration was 5ms. The injury was applied one to three days after the electrode implanted through a fluid port placed about 1mm lateral to the electrode site (see Figure 5.8A). Possible electrode failure after the FPI delivery was eliminated with the control experiments (Injury preceded the MEA implantation) and ensuring the MEA extraction from the implanted PML surface after the survival period. The signals decreased in amplitude immediately after injury (5 min) and continued to decrease over a period of seven days. Both mossy fiber (0-10ms) and climbing

fiber (10-30ms) activities were affected by the injury. At day seven, most channels showed only minimal activity and the hyperpolarization phase was completely suppressed. Interestingly, there was a high frequency oscillations emerging after 80ms, which was consistently observed in other FPI animals as well.

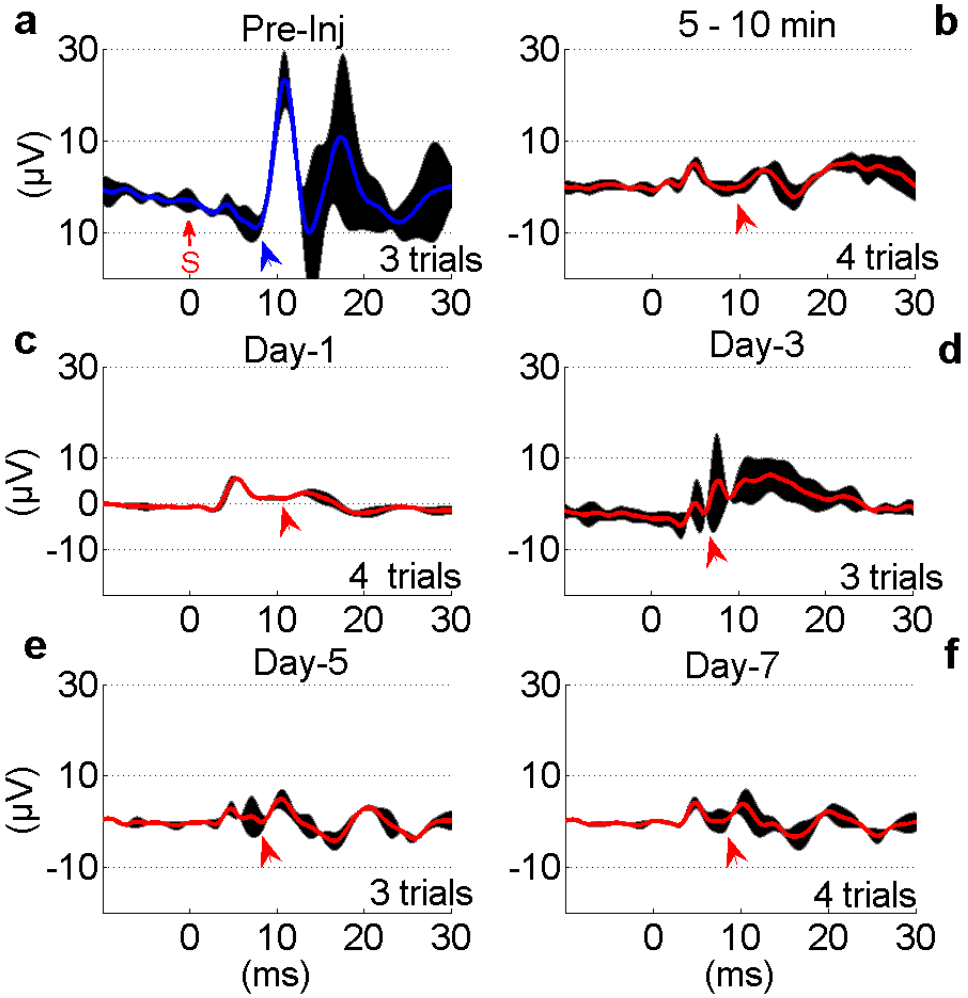

Figure 6.17 EP waveform progression in a sample animal from the time of injury (A-F). Each trace represents the average of multiple trials (gray traces), and each trial is the stimulus (S, t=0) trigger-average of 20 EPs. The pre-injury recordings were obtained 5-10 minutes before the application of FPI (A). Time of recording after anesthesia was ~ 5 min (A,C-F) and 5-10 min after FPI induction (B). All injury-day recordings showed great depression in the EP waveform and amplitudes. Day-3 EPs demonstrated larger amplitude variations; 5±5 μV (D)

The amplitude of the MF-mediated responses declined drastically to 5 ± 2 µV (arrowhead, Figure 6.17b) within 10 min of injury induction from the baseline of 40±5 µV (a-c, Figure 6.16). There was no additional anesthesia injection at this period. Amplitude of MF-mediated volleys were diminished by ~ 8 fold to a value barely above the background neural activity (2 µVrms), while the arrival latency was preserved (10-11ms) in these early acute responses. On the following day after injury (~20 hours), similar waveform characteristics were observed in the EP signals (Figure 6.17c).

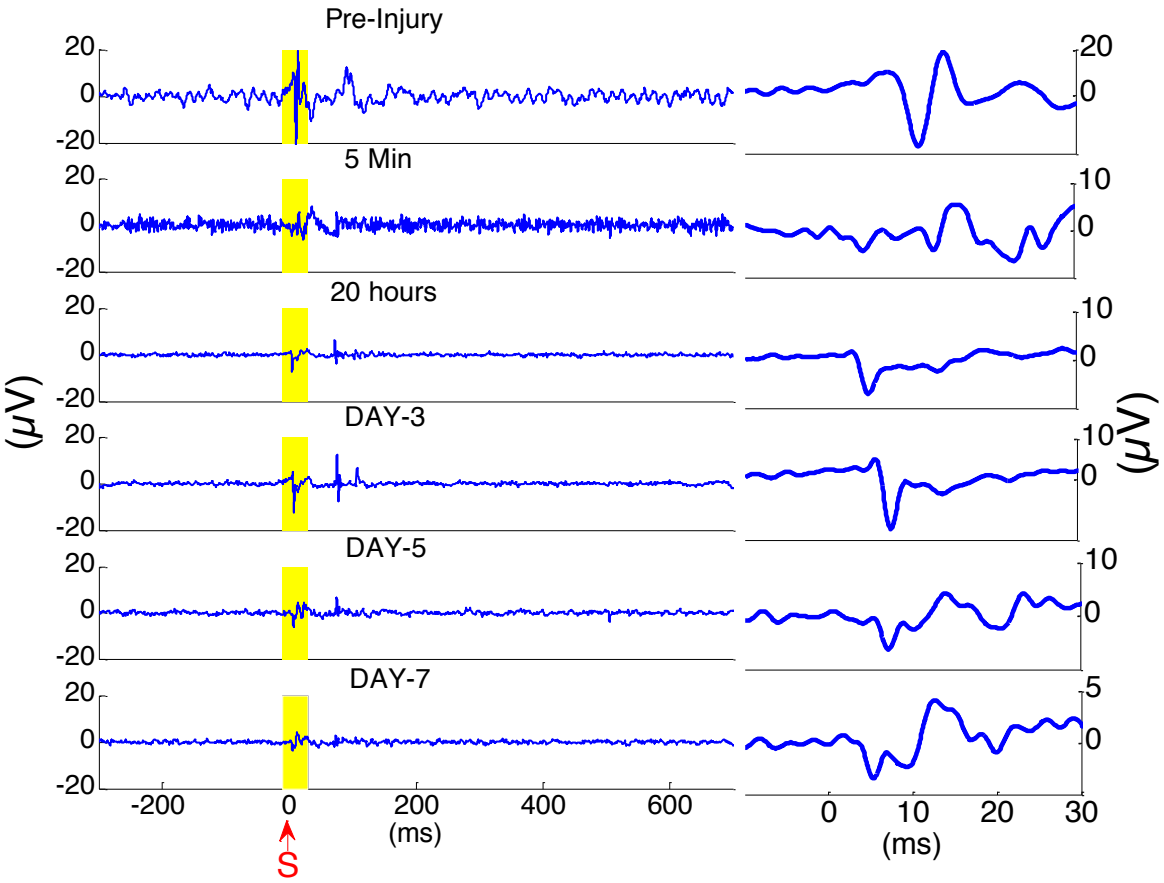

Figure 6.18 Magnitude of evoked potential decreases with respect to injury induction. Traces represent sensory triggered average of 20 repetitions obtained periodically for pre-/post injury period. Vertical scale is fixed to ±20 µV for all traces (Left) and adjusted to ±5-20 µV (Right).

Multiple trials indicated detectable EPAs but reduced by 8-10 times from the baseline level. Three days post-injury, EPs were regressed to about ±10 μV range (gridlines, Figure 6.17d). Day-3 was noted as a recession point in the EPA trend, which was consistent across all injured animals. At the end of the survival period, the EPA reductions were as large as 90% of the baseline, fluctuating around ± 3-5 μV (Figure 6.17e-f).

The evoked potential changes were coupled with the elevated rhythmic activity in the spontaneous oscillations after the injury induction. The changes in the electric acitivty of the cerebellum was shown in larger window (~1 sec) and for the duration of evoked response window (Figure 6.18). Pre-/post stimulus (S) period included background neural activity was shown for 1-second window (Figure 6.18, left panel) and zoomed in yellow (Figure 6.18, right panel). Evoked volleys dropped to background oscillation magnitude range (± 5μV) in the immediate recordings; 5 min. On the next days of injury (Day 1-3), sensory stimulation evoked greater deflections; Vp-p~ 10μV but failed to recover back to original magnitudes at the end of survival period (Day-7).

6.2.3 Amplitude Changes in the Grouped Data

The Mf-mediated EPAs from all injured animals (n = 9) are grouped in Figure 6.19. Each dot in the scatter plot is the mean volley amplitude calculated from the stimulus-trigger-averaged signals between 2-3 trials from each rat on the given day (top panel). There was a clear decline in the EPAs as indicated by the negative slope; $V_{EPA} = -4.2d + 37$ (d; days, Figure 6.19). Amplitude drops were found to be significant for each day (Day 1, 3 and 7, bottom plot) of the post-injury period against the pre-injury values. (20 trials per day, n = 9

rats, rmANOVA, $F(3,76) = 43.25$, $p<0.001$). Post-hoc analysis indicated the sharpest drop (40%) on day-1 of injury (Bonferroni correction, $p = 0.006$).

Relatively subtle amplitude changes were seen from day-1 to day-3. The EPA losses reached to 45%of the baseline level on average on day-3, however, not statistically different from day-1 measurements (Bonferroni correction, $p = 0.33$).

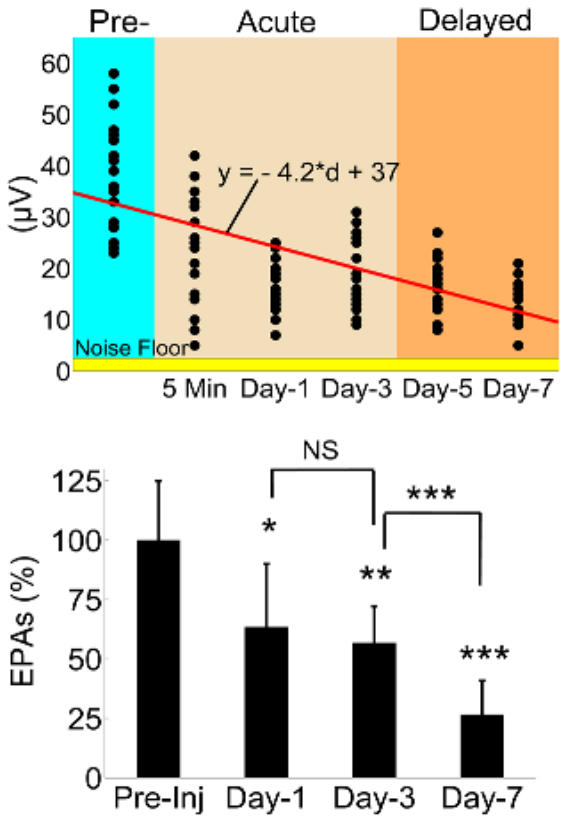

Figure 6.19 Monitoring injury progression by Mf-mediated volley amplitudes (arrowheads in Figure 6.17) on group data. Top; All animals as a group demonstrated nearly a linear decreasing trend by the number of days (d) after injury (R^2=0.48). Each dot in the scatter plot shows the mean of EPAs in a trial from a rat (n=9 rats, 2-3 trials per animal on a given day). Bottom; Data shown are the mean ± std of normalized EPAs for the pre-injury and three selected days of the post-injury period. Other significances shown were calculated using repeated measures of ANOVA followed by Bonferroni correction. *P <0.05, ** P <0.005, *** P <0.001.

Prolonged recordings revealed that the loss in EPAs reached the maximum at the end of the survival period; Day-7 post-injury EPA was equal to ~26% of the pre-injury EPA (n = 9 animals; Bonferroni correction, $p < 0.0001$).

6.2.4 Differentiation of the Affected Neuronal Mechanism in the Cerebellar Cortex

Cerebellar circuitry generates the evoked responses to a given sensory stimulation by using two main pathways. Mossy fibers and climbing fibers are the main components of these two segregated pathways, which can be identified by their onset latencies (see Figure. 6.1, 7).

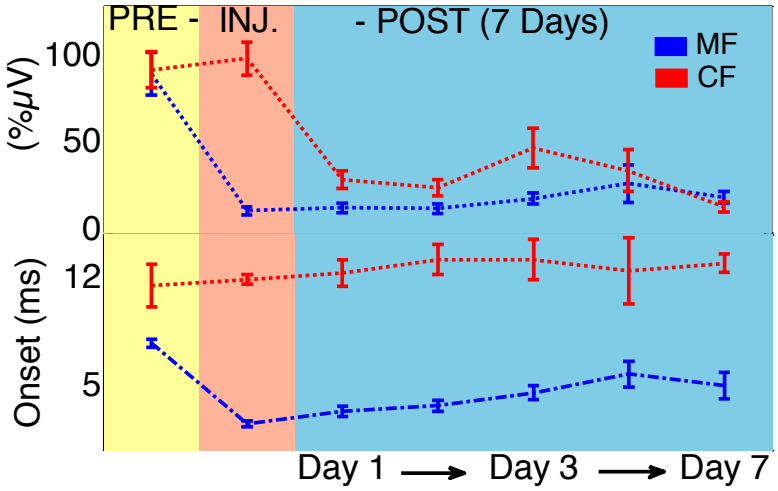

Figure 6.20 Normalized amplitudes and the onset latencies of the MF and CF related potentials were analyzed in the temporal trend of the injury period. Amplitudes dropped ~80-90% in both response types immediate after the injury induction (orange shading). There was a recovery phase; 30-40%, in the post injury period for the EPAs in both responses (blue shading).

In two sample injured animals (All nine animals were not included to avoid redundancy), the amplitude and the onset latencies of EPs for MF (blue) and CF (red) related responses were compared in the injury context (Figure 6.20).

Despite the drastic drops in the amplitudes of both responses, the arrival latencies were remained similar in the pre- and post-injury period, particularly in CF potentials.

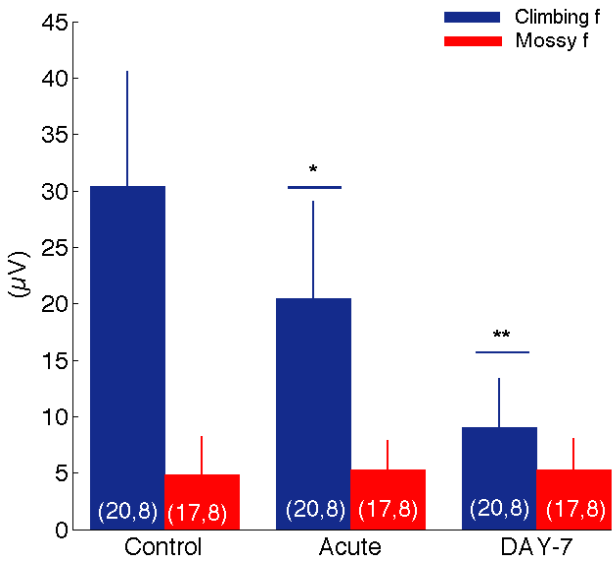

Figure 6.21 EPAs were analyzed in terms of two main input sources of cerebellar cortex; mossy and climbing fibers. Numbers on bars indicate the recordings and animals, respectively. (Two-tailed paired t-test *; P≤0.05, **; P≤0.005)

The amplitudes of MF and CF evoked responses were analyzed individually for pre- and post-injury period (Figure 6.21, N = 8 rats, n = 17-20 trials). Two different time points of injury progression, acute (minutes to day-1) and day-7, were included from injury-applied eight animals. Cf-originated evoked potentials (blue bars) were significantly reduced in all injured animals starting day-1. Decreasing trend of EPAs were continued in the next days and reached ~ 3 times the mean baseline amplitude at the end of the survival period. Mf related evoked potentials (red bars, Figure 6.21) did not demonstrate any significant changes with respect to injury induction for all animals (N=8). In fact, there was a subtle increase in the mean amplitudes of evoked responses.

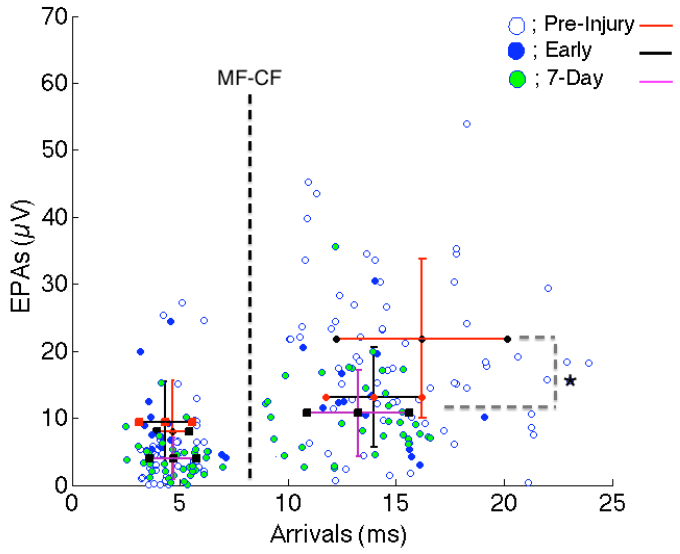

Figure 6.22 Arrivals of cerebellar EP volleys are characterized with respect to injury induced amplitude changes (N=8,7,8 and n=28,26,29). Mossy (Left to broken line) and climbing fiber related responses (Right to broken line) were identified by the onsets of pre-injury recordings.

Onset latencies of the cerebellar inputs for the pre-/post-injury period were compared on the scatter plot across multiple injured animals (Figure 6.22). Mean onset arrivals were reduced to 14 and 13 ms corresponding acute and 7-day periods from ~16.5 ms pre-injury values (paired t-test; $p<0.05$ and $p<0.01$ (N=8, n=28), respectively). There was a large variation in the climbing fiber response during pre-post injury responses. Variation is also significantly diminished for injury day recordings (~2 folds). In contrast, no drastic changes were noted for Mf arrival latencies. Variation and mean alterations were in the order of milliseconds (~1-2 ms). Arrival latencies of evoked volleys were directly related to conduction velocity of the mediated pathways for the mossy and climbing fiber responses. Damage to either pathways would introduce a disruption in the associated evoked responses.

6.2.5 Disruptions in the Cerebellar Network after FPI induction

In order to evaluate the effect of injury on synchrony across the cerebellar cortex, cross-correlations between all contact pairs were investigated during evoked and spontaneous activity (not-evoked) before and after injury (Figure 6.23A-C). Neural signals collected for pre-and post-injury period including the evoked potential window (center panel, Figure 6.23) and the cross-correlation values across recorded channel (right panels, Figure 6.23) are shown for a single animal. The EPs were large in amplitude and highly similar in waveform and timing across all 31-channels in the pre-injury trials (Figure 6.23A, left panel). Pearson correlation was as high as $r \geq 0.8$ between some channel pairs of EP waveforms, while it varied between $0.2 \leq r \leq 0.6$ during spontaneous oscillations (Figure 6.23A, right panel). After the injury, overall correlation for all channel pairs decreased by ~2-fold (Figure 6.23C, right panel), i.e., to ~0.2-0.3 and 0.3-0.4, respectively for spontaneous and evoked windows. Those channels that showed stronger correlations in the pre-injury trials (red squares in top panel) were also diminished to mean values of $r = 0.3$-0.4. Disruption of synchrony in evoked LFPs was clearly noticeable in the spike-trigger averaged plots of single channels (Figure 6.23C, left panel).

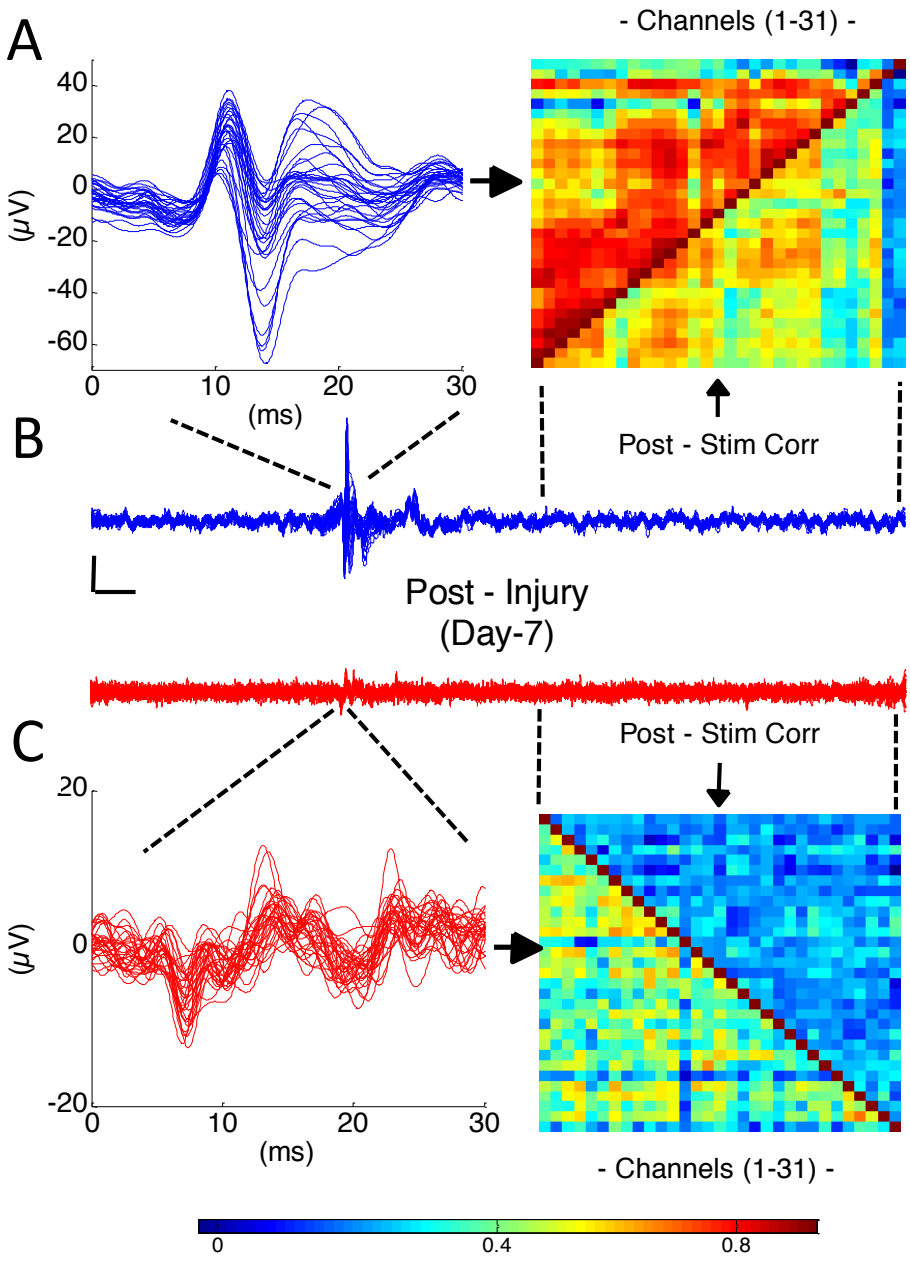

Figure 6.23 Injury disrupted the synchrony across cerebellar cortex in the studied region (PML) during the evoked and not evoked (no stimulus) as demonstrated in this sample recording. Left; traces (Blue and red; before and after injury, respectively) illustrate EP volleys for all 31-channels. High synchronization (Top) was lost after the injury (7-day FPI; bottom). Right; cross-correlations between all contact pairs for pre- and post-injury signals during EPs and nEPs periods. Prior to injury, inter-channel correlations varied within R=0.5-0.8 and 0.3-0.6 during EPs and nEPs recordings, respectively (Top). Cross-correlation values diminished drastically in both EPs (R=0.2-0.5) and nEPs periods (R=0.2-0.4) by day-7 of injury (Bottom). EPs, evoked potentials;

6.2.6 Spatially Disorganized Cerebellar Oscillations

Cerebellar network contains multiple level functional subunits that can be synchronized exclusively during sensori-motor process as well as at rest. The MEA on the surface of the cerebellar cortex searched the disrupted organizations in the injured cerebellar signals (Figure 6.24).

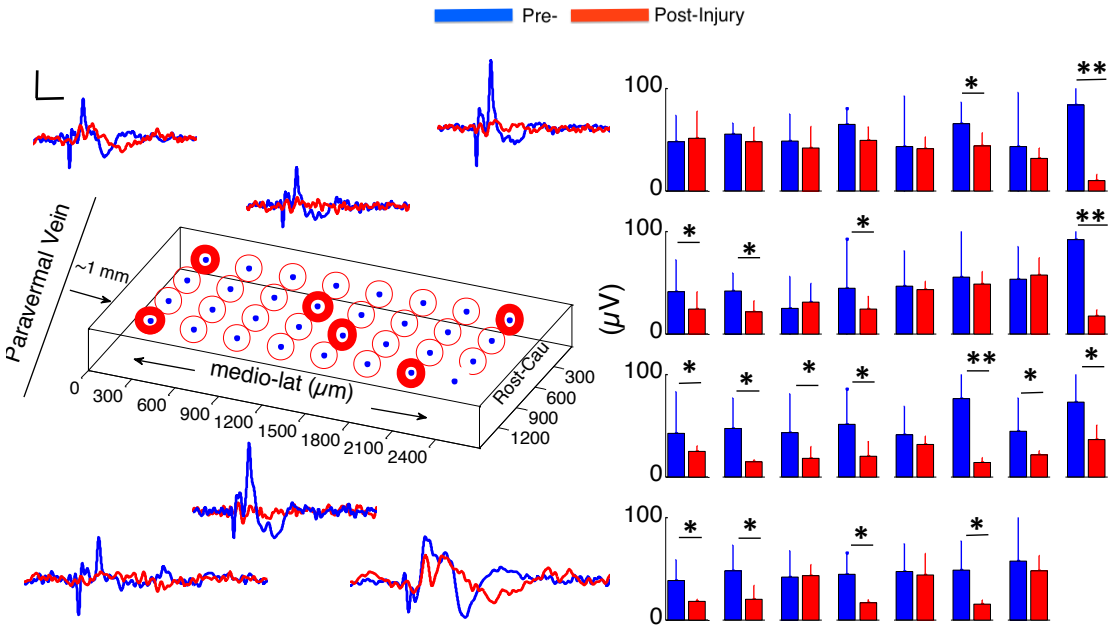

Figure 6.24 Spatial investigation of pre-/post (Blue and red traces or bars, respectively) injury evoked potential changes. On the left; Averaged EPs from selected 6-single channels are plotted with respect to electrode position on the surface of cerebellum. Multi-electrode array orientation on the PML surface and inter-channel distances are shown in the center. Three paired recordings from pre- and at day-7 of injury recordings were calculated. While some of the channels did not indicate any significant changes with the injury, in some channels the changes were drastic (Paired t-test *; P≤0.05, **; P≤0.005).

Cerebellar surface potentials can be collected differentially by equally spaced (~300μm) 32-channel MEA (Top left, Figure 6.24). Sample recordings (Blue traces, #ch = 6) of EPs, particularly CFs, showed different amplitudes (±10-20μV) and onset delays (±

500µs) in response to same peripheral stimulation. This feature was lost following injury induction by diminishing the EPs differentially in the recorded channels amplitudes (Red traces). In some channels the amplitude decline reached to ~30-40µV, while this was limited to ~5-10µV in others. Changes were significant in both sagittal and transverse planar electrodes calculated among 31-channels in averaged EPs (Right, # trials and size with P values).

The correlation change in seven animals in terms of high-frequency coherency with respect to injury induction was calculated in the 2-D space (Figure 6.25). Two animals were discarded from this analysis due to high common mode signal across all channels.

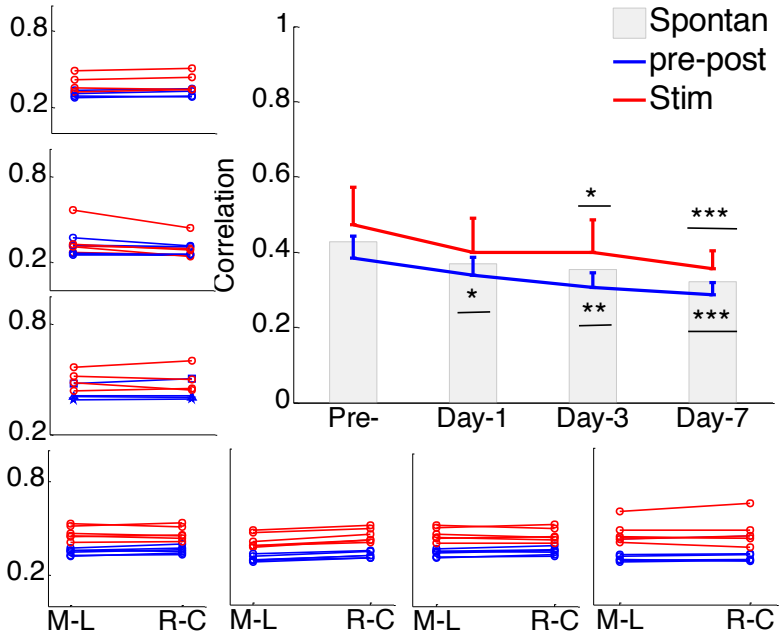

Figure 6.25 Cross-correlation decreases during injury progression. Correlation values were calculated and averaged between electrode groups aligned in 2-D dimension shown in Figure 6.23. Left-bottom; Spontaneous neural activity (blue) and stimulation period (red) correlation changes were shown for each animal medio-lateral (M-D) and rostro-caudal (R-C) plane. Data shown as mean ± s.d. (upper limits only, red and blue). P values from measures of Wilcoxon signed-rank test. *P≤0.05, **P≤0.005, ***P≤0.001.

Loss of synchrony was consistent in all seven animals for both spontaneous activity and stimulation period values (r = 0.1-0.2 and 0.3-0.4, respectively). Direction selective activity (red lines, M-L vs. R-C) was also diminished in individuals (I-II and VII) with the induction of injury. Right top; Pre-injury (baseline) vs. post-injury values was compared in subsequent three time points. Quiet recordings absent of stimulation period were also included in the same analysis (Gray bars). In each case, greatest drops were noted at the end of survival period; day-7.

6.2.7 Injury Induced De-Synchronizations in the Cerebellar Circuitry

Functional outputs of cerebellar signals can be associated with well-defined frequency bands such as 80-200Hz. This specific frequency content was searched by looking at the temporal correlational changes by using a moving window (20ms) in the pre-/post injury recordings (Figure 6.26). Pre-Injury correlation values drastically increased ($r \geq 0.8$) with given stimulus (S) for all channel groups (Figure 6.26A). Additionally, long lasting (~300 ms) rhythmicity was observed in the post-stimulation period, particularly in one electrode group aligned in sagittal direction (Blue dot; middle panel). Cross-correlation values were also greater ($r = \sim 0.1\text{-}0.2$) for post-stimulation period compare to pre stimulus. Same analysis were collected in the next day of injury induction (Figure 6.26B). Both baseline (pre-/post stimulus) and stimulation periods were absent of any increased correlated activity ($r \leq 0.4$). Evoked potential pattern was also substantially abolished in the recorded frequency band (Blue traces). At day-3 of injury, neural activity still lack of synchrony in the baseline periods (Figure 6.26C). However, there was noticeable recovery in the stimulation-induced

oscillations ($r \geq 0.7$), which ceased rapidly. Loss of synchrony in the recorded LFP oscillations reached the maximum values at the end of survival period, day-7 (Figure 6.26D).

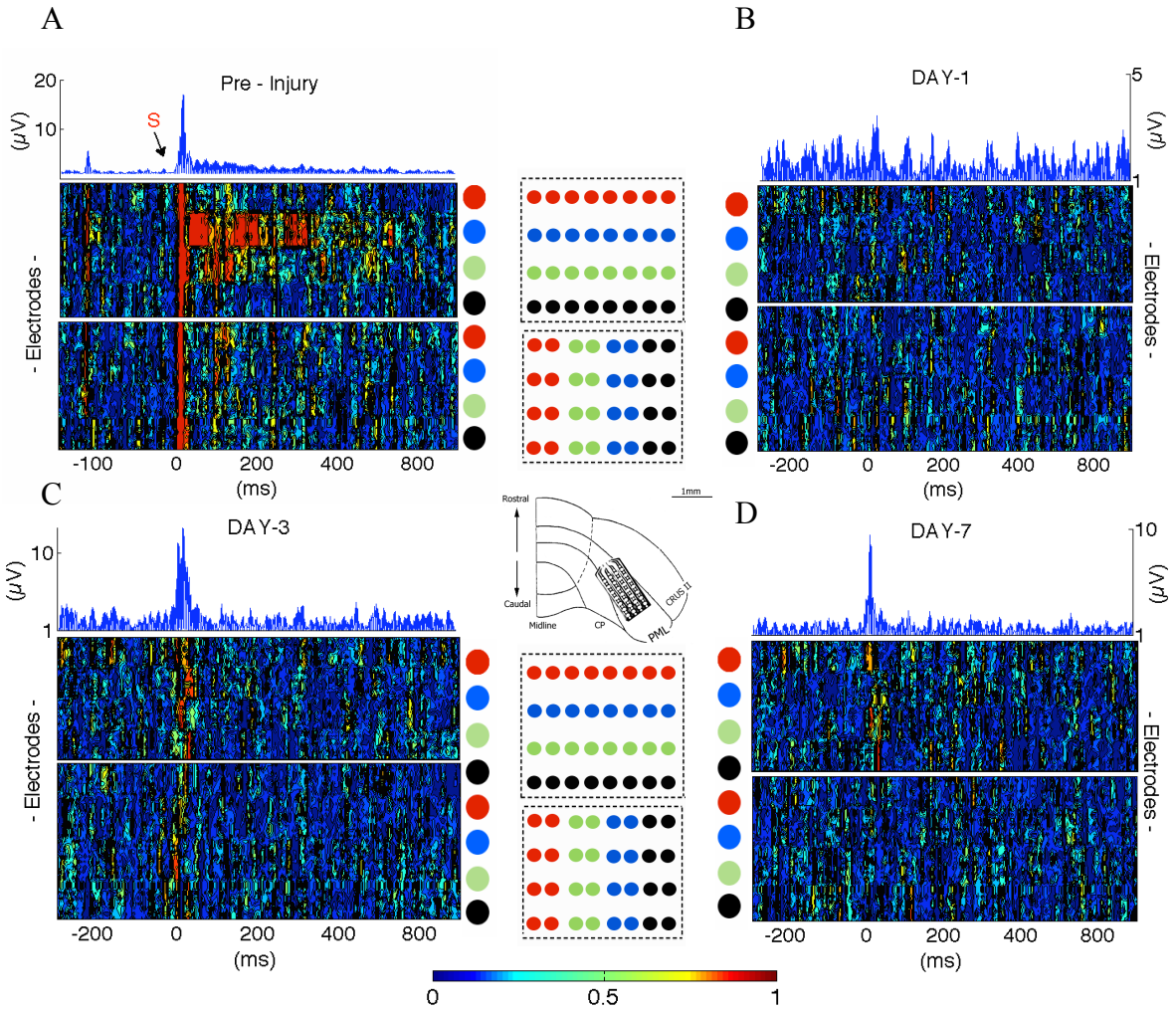

Figure 6.26 A-D Example of synchrony changes with respect to progression of injury. Mean cross-correlation values of high frequency oscillations (80-200Hz) are calculated across selected planar electrode configuration; transversely (middle) and sagittally (bottom panels) for Temporal resolution was selected as 20 ms for pre/post (~900 ms) and onset of stimulation period (~10-100 ms) and averaged over 20 repetitions.). Rectified-averaged filtered signals (80 - 200Hz) are coupled to indicate the time and magnitude of the recorded field potentials (Blue traces; Top). Investigated electrode couples on the MEA marked with the same color dots on the **time-correlation** plots. Estimation of electrode placement on the PML surface of cerebellum and MEA orientation is shown in center panel.

Overall reductions were noted across all grouped channels including pre-/post and stimulation periods. Only electrode groups aligned in sagittal directions, which were highly active to induced-stimulations for pre-injury trials, were able to sustain a brief activity ($r \geq 0.5$, dt = ~10 ms) in the stimulation period (blue traces).

6.2.8 Synchrony Changes in the Different Frequency Bands

This study also questioned if there was a differential effect of injury in different frequency bands. The signals were band-pass filtered and divided into four main frequency bands (5-30Hz, 30-50Hz, 50-100Hz and 100-300Hz) for each day of recordings (Figure 6.27).

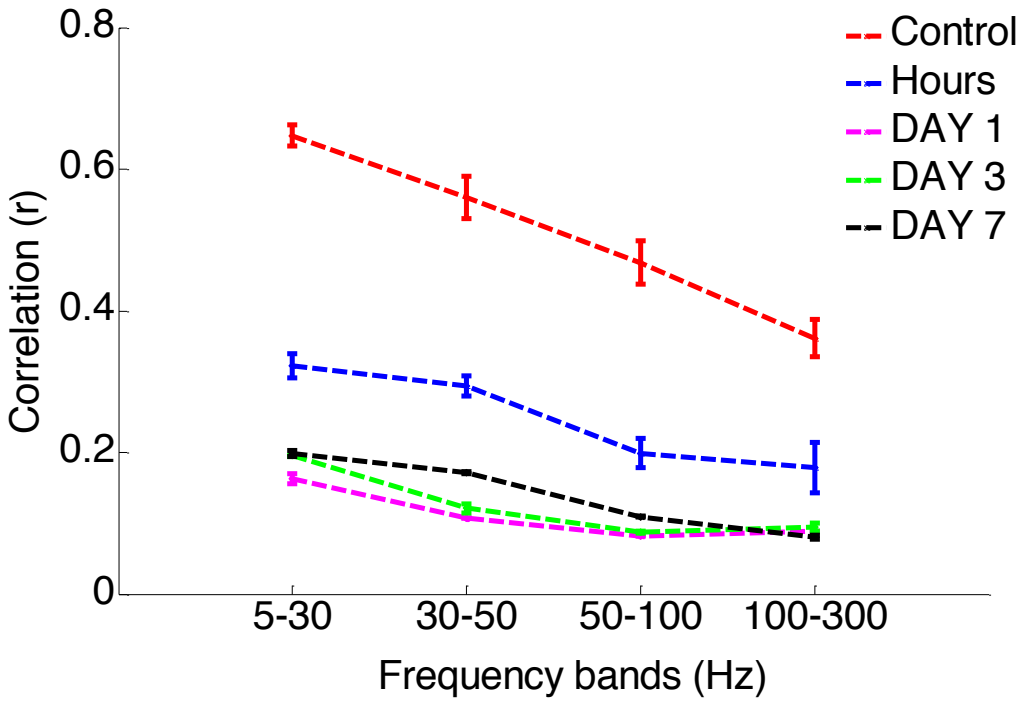

Figure 6.27 Correlation changes across 31-electrode contacts are shown as mean ±SEM in selected frequency bands. Pre-Injury values are taken as control and post-injury results are evaluated at four time points from a few hours to seven days. Same number of recordings (n=10) were taken from five animals and averaged. Injury significantly reduced the mean correlation between the electrode sites in all studied frequencies ($p < .001$, N=5 rats).

Correlation coefficients were calculated from control and post-injury recordings in 5 rats with multiple recording episodes (n=20). Linear decrease of correlation values with respect to frequency bands was observed for all recordings.

In the lower frequencies (5-50Hz), the drops were greater considering anesthesia recordings that typically demonstrate stronger correlations ($r = 0.5 \pm 0.23$) at lower frequencies in the control animals. Synchronous changes were most noticeable in the acute period (1-3 hours) indicating $r = 0.37 \pm 0.05$ ($r = 0.56 \pm 0.045$; pre-injury) in 5-30Hz band and $r = 0.16 \pm 0.03$ ($r = 0.29 \pm 0.02$; pre-injury) in 100-300Hz. While the reduction in correlation was significantly large from control to the first day of injury ($p < .001$), further changes were less significant in later days ($p < .05$).

6.2.9 Coherent Activity in the Cerebellar Injured Animal

Cerebellar network generates high frequency coherent activities up to 1kHz range in the awake animal. Coherence between paired electrodes (four selected pair groups) was calculated and compared for pre-/post-injury day trials (Figure 6.28). Cerebellar network was highly coherent; C = 0.8-0.9, particularly between 100-800Hz in the pre-injured animal, however the strength of coherency in the recorded electrode pairs decreased to C = 0.5-0.6 with the inter-electrode distances (300-2100μm), (Left panel, Figure 6.28).

The same electrode pairs on the MEA were searched for the same coherent activity at rest after the cerebellar injury (Right panel, Figure 6.28). It was indicated that the coherence between all electrode groups but one diminished drastically. The greatest drop (C = 0.8-0.9, pre-injury to C = 0.1-0.2, post-injury) was noted in the adjacent pair in the medio-lateral direction (black dots).In contrast, the coherence decline was subtle across the electrode

groups aligned in the rostro-caudal direction (blue dots, inter-site; 900µm). Moreover, the drops also degraded the coherence dependency of the electrode pairs with respect to inter-site distances.

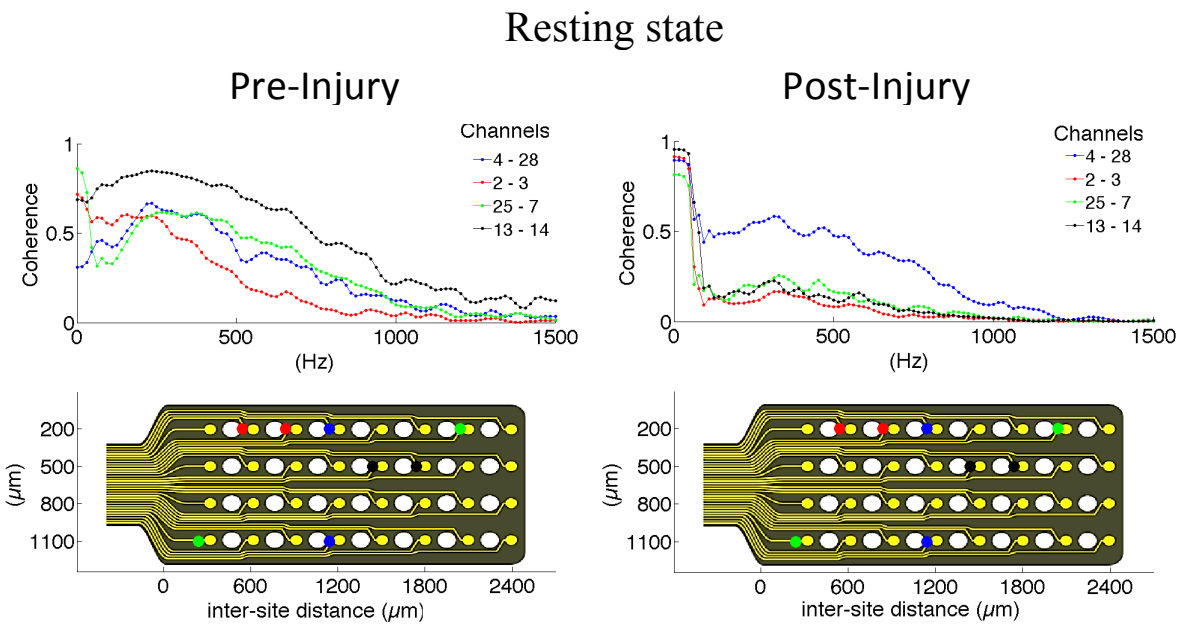

Figure 6.28 Cross coherence values were computed in the awake animal at resting and compared for pre-injury vs. post-injury trials. The analyzed channels marked (bottom) and plotted for the 0.1Hz - 1.5 kHz frequencies in the matching color order (Top). Coherence was as high as ~0.9 up to 800Hz band in the pre-injury recordings (Left). Cerebellar injury lowered the coherences across paired channels substantially without directional selectivity (Right).

The coherency was also compared in actively moving animals for pre-/post-injury period (Figure 6.29). In the averaged coherences across all recorded channels showed a persistent highly coherent activity in the high frequencies (30-1000Hz). However, the injury affected the low-frequencies (0.1-30Hz) indicating a drastic drop in the coherences (C_{drop} ~ 0.8) between recorded channels (red trace, Figure 6.29).

6.3 Immunohistochemical Analysis of the Cerebellar Injury

The current study addressed the development of the brain injury within the cerebellum structure by monitoring the electrophysiological changes in the multi-electrode implanted animals. To verify the presence of injury in the cerebellar neural circuitry, the immunohistological analysis was also included for control (un-injured) vs. injured for the matching day survival periods (7 days).

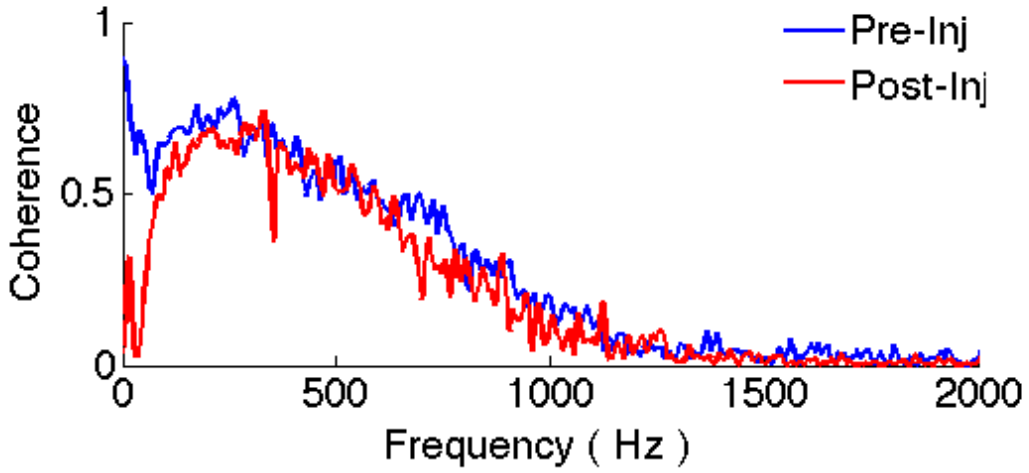

Figure 6.29 Mean coherence changes across 31-electrodes for pre- vs. post-injury days in freely moving animal. While the coherence drops were affected the low frequency (0.1-30Hz) contents in the LFPs, the higher frequencies seemed to sustain their highly coherency oscillations (30Hz-1kHz).

Purkinje cells are the most noticeable neuron type of the cerebellum and its unique organizational morphology, domino-like alignment, was indicated by the CalbindinD28k staining in multiple lobules of the naïve animals' cerebellum (Figure 6.30 top image). Calbindin labeling showed the induced disorganization in the Purkinje layer by indicating the increased gaps between cells and organizational abruptions in the cell lines (Figure 6.30 top image).

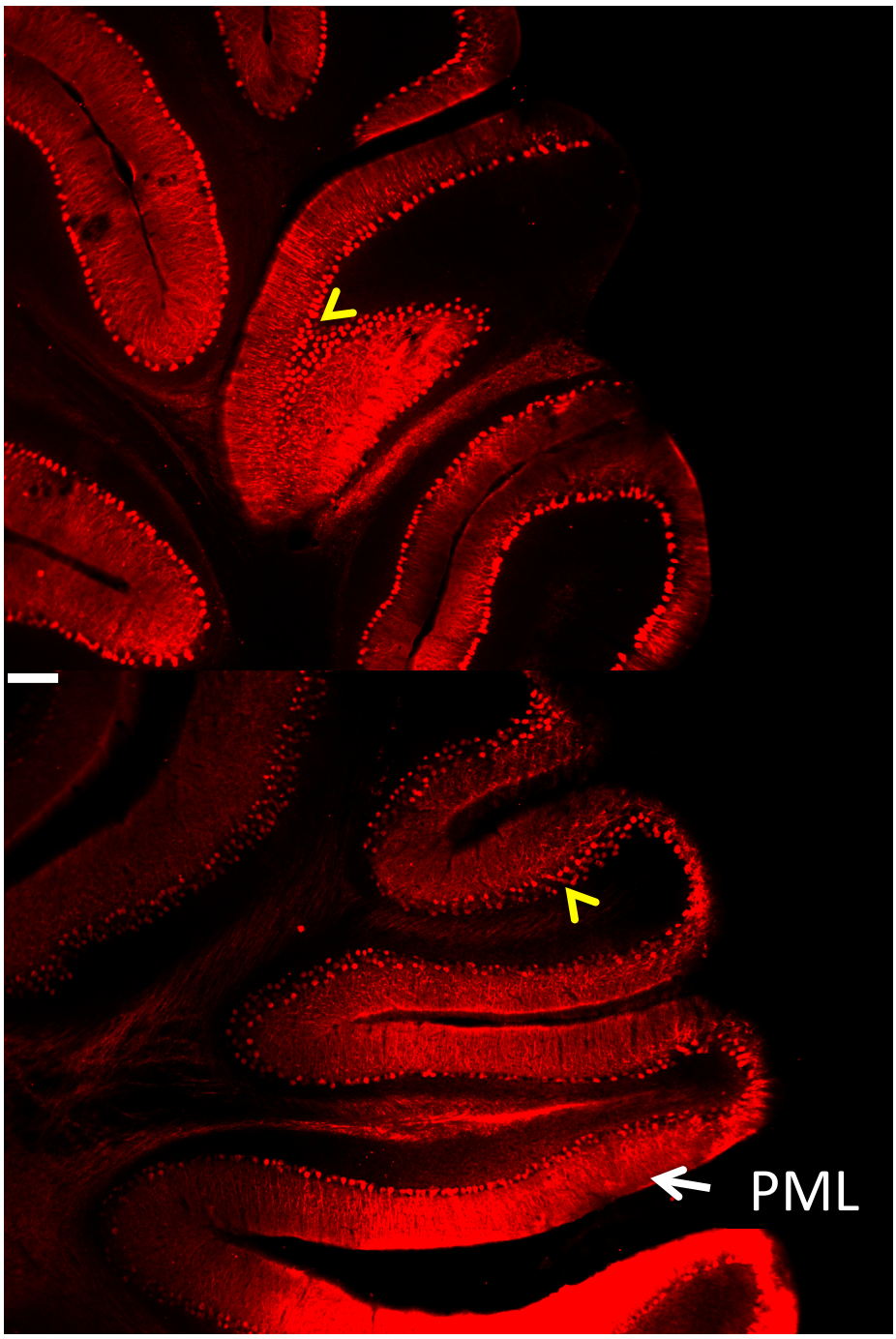

Figure 6.30 Purkinje cells are the principal cell types in the cerebellar cortex. CalbindinD28k staining showed the perfect alignment of the PCs in the un-injured cerebellum (Arrowhead, top) in multiple lobules, while this crystalline morphology was abolished after the fluid percussion injury (Arrowhead, bottom); Day 7. Scale bar

To determine the extent of cellular loss underlying the observed electrophysiological effects of injury, double immunostaining of the cerebellar tissue was performed to extract at

the end of the physiological studies for expression of CalbindinD28k, a marker for PCs and FluoroJadeC.

Different grades of FPI (15 and 25 psi) cerebellums were compared with a naïve control. As expected, naïve animals showed a layer of CalbindinD28k-positive PCs (Figure 6.32A-C, n=15 sections from 3 rats) with no FluoroJadeC labeling demonstrating the lack of neurodegeneration. There was a modest PC degeneration, as indicated by co-labeling of CalbindinD28k with FluoroJadeC labeled neuronal profiles in mildly injured rats (15 psi; Figure 6.32D-F, n=6 sections from 2 rats). There was more CalbindinD28k expressing

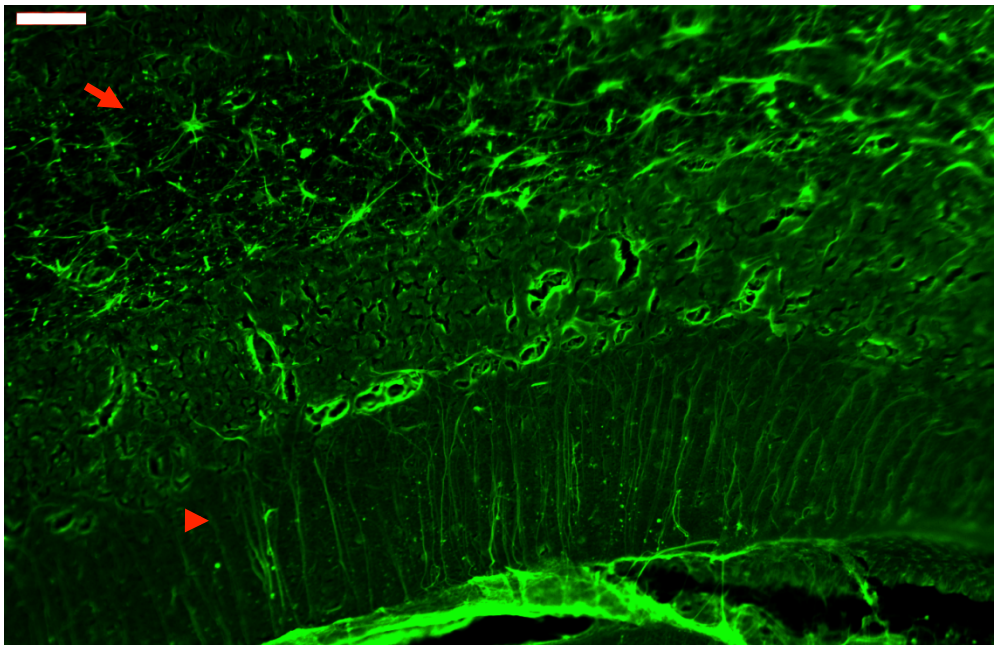

Figure 6.31 FluoroJade C staining indicated extensive cell degenerations coupled with glial response (arrow) in the longer survival period of injury (1 month). Purkinje cell dendrites (arrowhead) were also labeled in multiple layer of the cerebellar cortex. Scale bar: 100μm.

PCs co-labeled with FluoroJadeC in cerebellar sections from the rats injured at larger peak pressures, indicating more extensive PC degeneration (Figure 6.32G-I, n = 6 sections from one rat) than those with smaller peak pressure (Figure 6.32D-F).

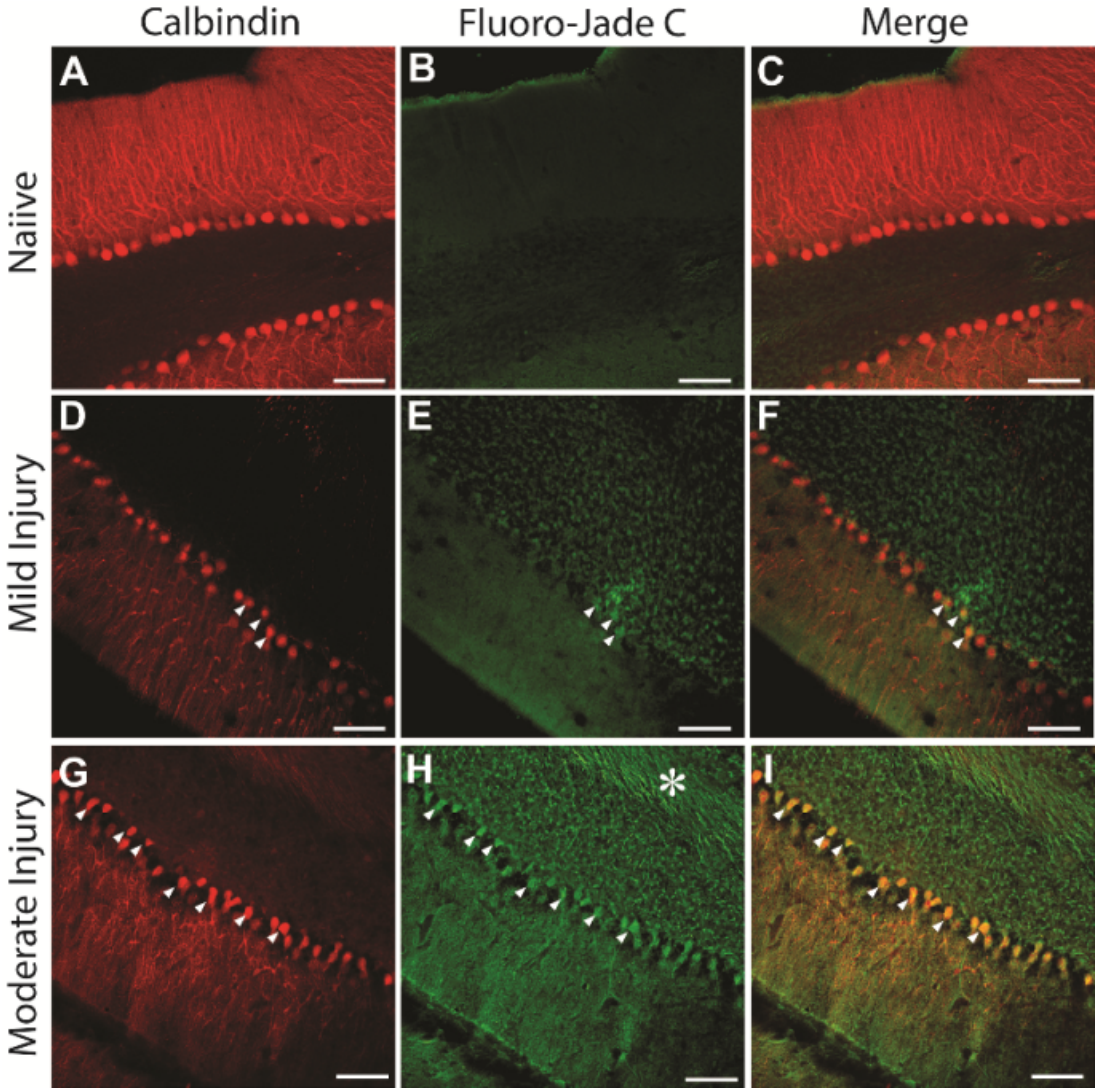

Figure 6.32 Purkinje cell degeneration at mild and moderate levels of severity of cerebellar injury (15 psi and 25psi). A-C. Representative confocal images show CalbindinD28k labeled PCs (A) and the absence of FluoroJade C staining (B) in the same section from a naïve rat. D-F. Images of a section from a rat 1 week after mild injury (15psi) shows CalbindinD28k positive PCs(D) and the presence of a few FluoroJade C labeled cellular profiles (arrowheads in E). Merged image (F) shows that CalbindinD28k positive PCs are co-labeled with FluoroJade C (arrowheads). G-I. Representative section from a rat 1 week after injury (25psi) shows CalbindinD28k positive Purkinje cells (G) and cellular (arrowheads) and axonal (asterisk) FluoroJade C labeling (H). Merged image (I) shows numerous CalbindinD28k positive PCs labeled with FluoroJade C (arrowheads). Scale bar: 100µm.

presence of FluorojadeC positive neurons in all FPI animals indicates ongoing neuronal degeneration at one week.

Remarkably, the domino-like alignment of PCs observed in naïve animals was degraded following injury at higher pressures (~ 25 psi). PCs showed the severity dependent loss in injured cerebellums indicating more degenerations at higher grade of the FPI compare to experimental severity (10-15 psi) that was quantified in the electrophysiological analyses.

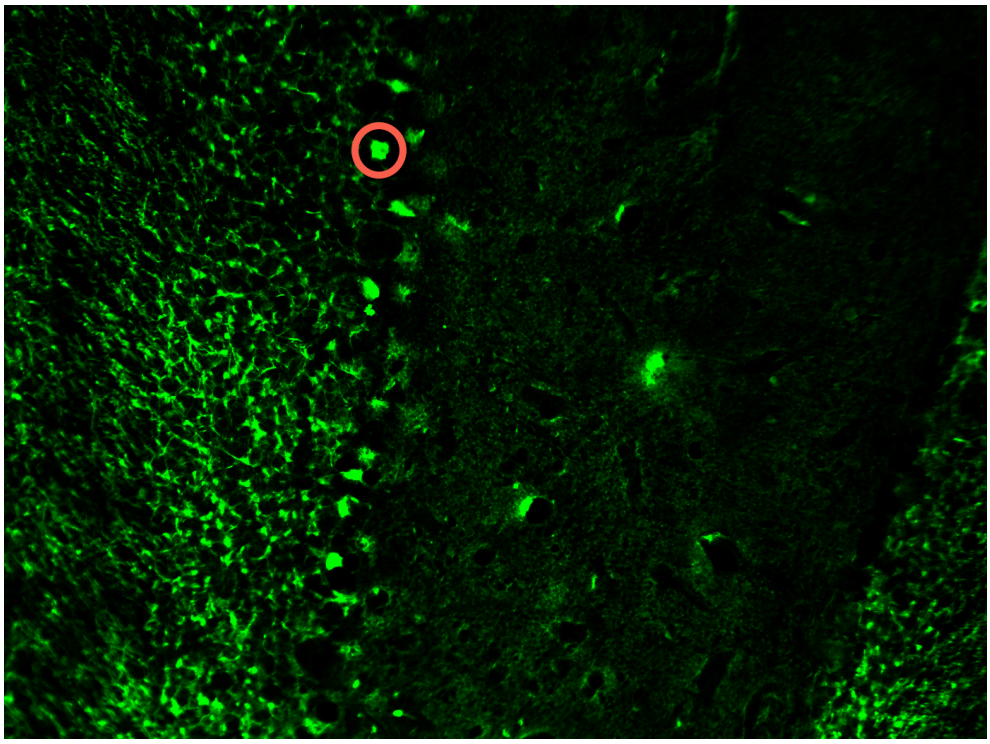

Figure 6.33 FluoroJade labeled the PCs in the contralateral side of the injury site in the FPI animals. Cell deaths were not exclusive to ipsilateral side of the cerebellum.

In addition to cell loss, sections from the rats subjected to injuries at higher peak pressures showed FluoroJadeC staining in the white matter tracks (asterisk in Figure 6.32H) suggesting the possibility of PC axonal degeneration. FluoroJade staining shows the

irreversible damages including cell deaths, dendritic degeneration and glial responses. FluoroJadeC staining also indicated the PC dendrites were damaged in the molecular layer after the injury (arrowhead, Figure 6.31).

PC degeneration was extensively observed throughout the cerebellar cortex in the 7-day perfused animals. It was also noted that the FluoroJade stained in the contralateral cortex of the cerebellum (Figure 6.33). Although the quantitative measurements were not performed in this study, the neuronal degeneration was observable in throughout the cerebellar cortex and extended in both side of the cerebellum.

CHAPTER 7

DISCUSSION

This study proposed a novel approach for the identification of a brain injury in the cerebellum by using the electrophysiological measurements with implanted micro-electrode array in the rats. The first part of the project involved the extraction of cerebellar signals with MEAs in the anesthetized animals and characterizing the somatotopy of the cerebellar surface on the PML. Current study established the reliable and consistent electrical activity recorded from the cerebellar surface with chronic recordings (weeks - months) in the multiple animals. These results also demonstrated the second objective of the study where it was identified the consequences of the brain trauma in the cerebellar structure after the fluid percussion injury. Alterations in the electrophysiological properties of the cerebellar network were determined by the evoked potential analyses, which was associated with the underlying neural mechanism of the cerebellar cortex. In the third aim, the immunohistological analysis indicated the severity dependent cell degenerations in the injured cerebellum after 7-day survival period.

The local field potential is the net potential of all the voltage sources in a volume conductor. In the neural tissue, field potentials arise from multiple sources. The large low frequency oscillations are mostly due to the postsynaptic potentials (Avitan et al. 2009; Mitzdorf 1985). The higher frequency components, however, have been shown to correlate better with the population spiking of the neurons (de Solages et al. 2008; Ray and Maunsell 2011). In the cerebellum, the source of the high-frequency oscillations was suggested as the synchrony of the Purkinje cells, which is produced by the inhibitory network of PC axonal collaterals (de Solages et al. 2008).

In the chronic recordings, the electrode array was implanted on the cerebellar surface subdurally. Thus the recordings must predominantly contain field potentials from the molecular layer, which primarily includes signals from ascending axons of the granular cells and parallel fibers as well as the postsynaptic potentials of parallel fibers on Purkinje cell dendrites and other inhibitory cells to Purkinje cells. Secondary to the molecular layer, Purkinje cell simple and complex spike activities and the granular cells might make weaker contributions to the recorded signals due to their distance from the pial surface. Armstrong and Drew (1980) electrically stimulated the cutaneous afferents to the snout in decerebrated rats and showed that the characteristic components of the extracellular field potentials generated within the cerebellar cortex by the mossy fiber inputs were detectable with surface ball electrodes. The field potential volleys shown in Figure 6.1 were in good agreement with their surface recordings, except that the arrival times are delayed by a few milliseconds in our signals. This may be attributed to the usage of air puff as a stimulus on the skin, as opposed to direct electrical stimulation of the snout sensory nerves, which may increase the delay and the variation in evoked potential arrival times and thus spread the signals out in time.

Bengtsson and Jörntell (2007) reported that mossy fiber activity (P1-N1) recorded in the granular cell layer was reduced only marginally by intravenous injection of ketamine/ xylazine combination or either one of them separately. In our evoked potential recordings from the pial surface, the P1-N1 volley is much smaller than the one in the awake animal. This may be due to the difference in the strength and route of anesthesia (33/1.7 mg/kg of ketamine/xylazine IV in their case and 55/12 mg/kg IP in our case). Bengtsson and Jörntell also reported that the N3 field potential, which was interpreted as the excitatory postsynaptic

potentials of parallel fibers on the Purkinje cell dendrites, was greatly reduced as well as the climbing fiber activity at the given dose above. The N3 potential in Figure 6.2 was not observable. The time duration and the shape of the long volley at the end rather fits the definition of a long-lasting negative field potential due to a reduction in simple spike activity triggered by a complex spike. This component became relatively insignificant compared with a much larger and shorter negative volley that emerges in the awake animal. This new component was most likely the N3 potential from the parallel fiber synapses as suggested by its arrival time and duration. This confirmed the report by Bengtsson and Jörntell that synaptic activity from parallel fiber-to-Purkinje cells was greatly reduced by ketamine/ xylazine anesthesia. Our recordings did not show the mechanism by which this anesthesia regime affects the cerebellar cortical networks. These evoked potential results, however, confirmed previous results and further show that the effects of ketamine/xylazine anesthesia on the granular and molecular layer activities (P1-N1, N2 and N3; Figure 6.1) of the cortex could be detected with MEAs from the cortical surface. This supported our motivation for using spontaneously generated surface potentials as a method of assessing the effects of anesthesia at the larger network level in the cerebellum. With the spontaneous signals, the fact that the intercontact correlation is so high in the awake animal suggests that the source of the common-mode components are away from the cortical surface, most likely generated by the distant cells that are deep in the sulci on both sides of the paramedian lobule. The common-mode and the differential signal power spectra look similar and both extend into very high frequencies up to 1 kHz, including the harmonics. These high frequency components were most likely to be generated in the molecular layer either by the parallel fiber's and/or the inhibitory neuron's post-synaptic activations on the Purkinje cell dendrites

or the PC axon collaterals in the recurrent network. One of the defining features observed in our results was that both the spectral power and spectral coherence analysis showed a large reduction in the amplitude of the high-frequency components under ketamine/xylazine. Bosman et al. (2010) reported that the ketamine caused a 20–25% decrease in the firing rate of Purkinje cell simple spikes. These numbers did not explain the marked decrease that was observed in the power spectra of the signals before the common-mode signal is taken out . If it cannot be explained by the simple spike power itself, a potential explanation for the drastic change in the power and coherence plots could be that the simple spike synchrony among the Purkinje cells may have been disrupted by the anesthesia regime. Because the local field potentials were recorded from the surface, desynchronized activity of Purkinje cell networks from regions of the cortex inside the sulci can appear as no activity in the signals averaged across the medium.

The power spectrum of the signals recorded with tetrodes in the Purkinje cell layer in unanesthetized rats had a sharp peak 254 Hz (de Solages et al. 2008). This study convincingly argued that network oscillations of simple spike activity is due to inhibitory recurrent collaterals of the Purkinje cells and that these oscillations of the Purkinje cell networks are independent of the firing frequency of the individual Purkinje neurons. The broad spectral elevation in higher frequencies in our case can be the average of signals from multiple networks of Purkinje cells oscillating at different frequencies in the awake animal. The narrower spectral peaks between 150 and 300 Hz observed sometimes in our rats recovering from anesthesia (not shown) may be the signature of a few oscillating networks that were awakening as the anesthesia wears off.

Current study in general agreed with the previous report's findings that ketamine/xylazine anesthesia substantially reduces the spontaneous and evoked signals in the cerebellar cortex (Bengtsson and Jörntell 2007). Despite the reports suggesting marginal effect of ketamine on the Purkinje cell activity, the studies investigating the network activity in large areas of the cerebellar cortex may better be conducted in unanesthetized animal models. There was a clear contrast between the spatial patterns of the spontaneous activity of the motor and PML cortices and the way they were influenced by the ketamine/ xylazine anesthesia. On the methodology side, this clearly demonstrated the need for electrode technology that could record the cerebellar activity in behaving animals to better understand the cerebellar function at the network level. Despite the decades of investigation on cerebellar function, multielectrode recordings in unanesthetized animals are very rare in the literature. Due to the proximity of the Purkinje cells and their dendrites to the cortical surface, nonpenetrating electrodes can record field potentials with large amplitudes and high-frequency components with subdural implantation. Through the use of MEAs, this study was able to analyze multichannel signals from a large area of the cerebellar cortex simultaneously, which was not possible with single microelectrode implants. This can provide a powerful tool to study cerebellar function in behaving animals trained for various tasks.

In the injury experiments at first, evoked potentials have been investigated for assessment of severity in traumatic brain injuries. Visual (Lachapelle et al., 2004), brainstem auditory (Soustiel et al., 1995), and sensory (Fossi et al., 2006;Amantini et al., 2009) evoked potentials in EEG signals were proposed previously for detection of head injuries. The current study demonstrated prolonged reductions in the cerebellar evoked potentials to hand

stimulations during the 7-day period following the injury in a rat model of FPI. Characteristics (onset latencies and amplitudes) of MF- and CF-mediated cerebellar evoked potentials were well documented by other investigators with highly reproducible results (Eccles et al., 1966a;Eccles et al., 1967;Armstrong and Harvey, 1968;Armstrong and Drew, 1980;Atkins and Apps, 1997a;Jorntell et al., 2000;Ordek et al., 2012). In the control animals identification of MF and CF related responses were shown by the evoked LFPs (Figure 6.14), which was also confirmed the reports indicating characteristic EPs containing mossy fiber (Brihaye et al., 1964;Eccles et al., 1967;Armstrong and Drew, 1980)) and climbing-fiber mediated responses (Eccles et al., 1967;Armstrong and Drew, 1980;Atkins and Apps, 1997b) differentiated by their onset latencies.

Various components of surface recorded evoked potentials were identified by the source localization in earlier reports. (Eccles et al., 1967;Oscarsson, 1968;Armstrong and Drew, 1980;Atkins and Apps, 1997a;Atkins and Apps, 1997b;Baker et al., 2001;Diwakar et al., 2011). Eccles et al. reported MF-mediated responses (MF – Granule cells – Parallel fibers - PCs) to have less than 5 ms onset latencies and denoted various deflections as P1, N1 – N3, N4 (Eccles et al., 1967). Armstrong and colleagues also identified similar MF-mediated volleys within the same arrival latencies in response to peripheral electric stimulation in rats (Armstrong and Drew, 1980). In agreement to both, our control recordings indicated that the earliest noticeable evoked deflection was at ~3-5ms following the stimulus (Figure 6.14-15), which was relatively a weak response with a negative polarity and probably a direct recording from the MFs (P1-N1). The rising edge of the subsequent volley was detected at 8-11 ms in our recordings. This volley was triphasic with a positive polarity, succeeded by excitation of parallel fibers (b-c, Figure 6.14), and it was attributed to MF

activation in the granular layer (a-b, Figure 6.14). These subsequent volleys had in fact the most consistent and reproducible amplitudes among all evoked potential components collected in the control animals, and thus these responses were leveraged to monitor the injury progression (Figure 6.14-16). The onset latency of this volley is slightly larger compared to the earlier reports. This may be explained by the stimulation paradigm, i.e. the location of the peripheral stimulation and the type of the stimulus. For instance, PC response latencies can increase from 6-8 ms to 7-10 ms by using tactile stimulation on the periphery instead of electrical stimulation of afferents (Bower and Woolston, 1983a).

Conversely, CF-mediated potentials resembled late onset latencies (≥ 15 ms) in our results, which agreed with the previous reports. Pioneering studies on this subject showed that the CF activity arrives with ≥ 13 ms onset latencies in surface recordings (Eccles et al., 1966b;Armstrong and Drew, 1980). The delay varied between 13-19 ms in the contralateral hemisphere and between 16-22 ms in the contralateral vermis (Armstrong and Drew, 1980). Armstrong et al. also found evidence for increased PC activity with CF activation with 12-18 ms latencies compared to 4-10 ms latencies mediated by the MFs. More recently, Apps et al. demonstrated that CF response latencies to ipsilateral arm stimulation in anesthetized rats can vary between 16-26 ms when recorded from area 3 of the PML surface (Atkins and Apps, 1997a). In addition to onset latencies, the CF-mediated responses can be identified by their amplitude and polarity. They are the largest positive deflections in the signals recorded from the cerebellar surface (Oscarsson, 1968;Armstrong et al., 1973) and distinguished by a refractory period up to 40 ms proceeding from the positive deflections (Armstrong and Harvey, 1968). Based on these features, it was concluded that the latest volley in our recordings, which was detected at 15-20 ms in response to hand stimulation, was mediated

through CF activation. The onset latency of the deflection was not the only evidence to support CF identification. The wave also resembled a strong and slow nature that succeeded a long-lasting (> 50ms) refractory period. Although the magnitude of this potential was the greatest in most of the trials, this deflection wasn't included in the amplitude analysis due to high variability across animals and trials. All evoked recordings presented in this particular work were obtained in anesthetized animals to avoid variations in the evoked responses due to changes in the cerebellar excitability across different awake states.

Stability of evoked potential amplitudes in the control animals clearly demonstrated that the tissue responses did not compromise the electrode array's ability to measure reproducibility of signals during 3-week implant period (Figure 6.15). Pre-injury recordings in the FPI animals also served as an additional confirmation on the feasibility of this recording method of evoked potentials (Figure 6.15A). The depth of ketamine-xylazine anesthesia may alter the evoked potential amplitudes (Bengtsson and Jörntell, 2007;Ordek et al., 2012). Jorntell et al. showed the anesthesia effects on both MF- and CF-mediated responses at varying doses of ketamine/xylazine injections (Bengtsson and Jörntell, 2007). In order to minimize the effect of anesthesia depth, the timing and duration of the recording sessions from the injection of anesthesia were carefully controlled (see methods). After testing various peripheral sites (whisker, forelimb, hindlimb) of stimulation, it was concluded that the late MF-related response to (ipsilateral) dorsal hand mechanical stimulation was the most reproducible as a pattern in the recordings of the investigated PML region.

The fluid percussion injury (FPI) model implemented in the current study produces a combination of focal and diffuse damages, and it is widely used as an animal model of TBI (Thompson et al., 2005). It was documented that FPI can induce structural and functional

changes in the cerebellar cortex even at remote locations (Ai et al., 2007). This allowed us to apply the injury at a different location from the site of electrode implant without disturbing the electrode-tissue interface. Immunohistochemical analysis further verified that the injury was spread to remote locations within the ipsilateral cerebellum.

To investigate the relation between electrophysiological signals and the cerebellar insults, it was demonstrated that the EPA changes as early as 5 min post-injury to one week in anesthetized rats, following fluid percussion injury. Immediate recordings after trauma indicated substantial depression of the EP pattern as a whole; an effect that must be directly linked to initial impact of injury, e.g. tissue and/or blood vessel damage, and intracranial pressure elevation (Gaetz, 2004;Cernak, 2005). Interestingly, early arriving volley (<5 ms), presumably the direct MF activation, starts to increase in magnitude during the post-injury phase, which may be explained by hyper excitability of MFs as reported earlier (Ai and Baker, 2004). Monitoring the progression of injury-related changes at such detail can provide further insights about the course of the injury progression, which has been reported to present two main phases; primary and delayed-mechanisms (Doppenberg et al., 2004;Andriessen et al., 2010).

Progressive PC losses were documented in short (hours) as well as longitudinal (days - weeks) studies of immunohistology (Fukuda et al., 1996;Mautes et al., 1996). In support of this finding, mossy and climbing fiber mediated EPAs of this study monotonously decreased in the post-injury period (Figure 6.17). At a closer evaluation, the EPA alteration was quantified in the late MF-mediated responses by analyzing in two separate volleys; a-b and b-c. Alterations in both volley amplitudes were found to be very similar but not identical.

Current study determined that the largest drops were observed in the acute period for both amplitude measures between immediately after injuries to day-1, wherein the EPA drop was most significant (-40%, a-c volley). The second most drastic drop was noted from day-3 to day-7(-36%, a-c volley), which was termed as the delayed injury period by the earlier reports (Sato et al., 2001). The two phases with distinct characteristics suggest two different injury mechanisms involved. Baker and colleagues concluded that day-3 is a critical time point in the course of injury (Ai and Baker, 2004;Ai et al., 2007). They found majority of cell deaths within the next 24 hours after FPI, and the second wave of injury effect was delayed until day-3 (Ai et al., 2007).

Anesthesia regimen, ketamine/xylazine cocktail in the current study, was one of the co-variables in the injury context. Ketamine is a well-known NMDA antagonist that induced substantial depressions in the glutamate oriented excitations (MFs-GCs and PFs -PCs) of the cerebellar circuitry. Considering the delayed injury mechanism of the cerebellar insult, which triggers a glutamate associated hyperexcitation in the injured area, inhibition of this mechanism by the anesthesia may have altered the injury impacts in the observed results. Choice of another anesthesia regimen such as barbiturates may increase the injury progression in the disinhibited glutamate network.

Fluid percussion injury induces a combination of focal and diffuse type of injuries (Potts et al., 2009). It was found that the spatially varying degrees of EPA reduction across the PML surface covered by the electrode array (Figure 6.24). Somatotopy of the PML in the rat cerebellum was investigated in several reports including ours (Bower and Woolston, 1983b;Atkins and Apps, 1997b;Ordek et al., 2012), though there is no consensus regarding a single somatotopy in the cerebellum. In the animal shown in Figure 6.24 (blue traces) the EP

responses collected from the lateral side of the PML were relatively larger. Following FPI induction, EPAs were affected differentially across the PML surface without a certain directional preference. Interestingly, the smallest amplitude changes were observed on the most rostral contacts of the MEA closest to the injury site. This spatial differentiation supports our premise that the evoked amplitude changes are not due to some mechanical perturbation of the MEA by the fluid pressure wave at the time of impact, but because of damage to the underlying neural structures.

Local field potentials reflect the summation of synchronized activity from the local synapses and the cells underneath the electrode contacts (Buzsaki and Draguhn, 2004), (Roberts, 1968). There are two most salient factors, the spatial alignment and temporal synchrony that contribute to the extracellular field strength in a homogeneous structure, such as the cerebellum. Although this particular relation may not be entirely inter-dependent, indicating alterations in synchronous activity was plausible, where the structural deficits were occurred. The cerebellum was proposed to contain more than one type of organizational zone (see review (Apps and Hawkes, 2009)), most commonly known as microzones (Andersson and Oscarsson, 1978). Each microzone in the cerebellar cortex is organized into sagittally oriented smaller zones that are defined by a climbing fiber - PC innervation. There are nearly 1000 Purkinje cells lined up 200-300 μm below the cerebellar surface in the rat (Hillman and Chen, 1981). Our MEA covered about $2mm^2$ area on the PML surface with an inter-contact distance of 300 μm. Thus, it was anticipated to see differential effects in the synchronous activities collected by individual and/or clusters of electrode contacts.

Local field potentials emerge from the synchrony of a large population of neural components underneath the electrode contacts. Synchrony is observed at multiple levels of

cerebellar cortex at various frequency bands. Low-frequency band (1-4Hz) oscillations in the molecular layer were proposed to originate from the inferior olive and modulate the PC activity via the CF afferents (Lang et al., 2006). Whereas, theta and beta band oscillations are generated in the granular layer by MF activations (Hartmann and Bower, 1998;D'Angelo et al., 2001). In contrast to the deeper layers, the neurons in the molecular layer of the cerebellar cortex are capable of oscillating at higher frequencies, for instance at 30-80Hz due to the interneuronal feedback mechanism in the molecular layer (Middleton et al., 2008a) and 160-260Hz in the Purkinje layer via axon collaterals (de Solages et al., 2008a). Presumably, these oscillations originate from different neural structures, which have specific spatial alignments in the cerebellar cortex. For instance, it is possible to record sagittal synchrony in lower frequencies (1-4Hz) that is mediated by the CFs (Lang et al., 2006), while the interneurons in the ML exhibit higher frequency oscillations (30-80Hz) in the transverse plane (Middleton et al., 2008b).Considering that the surface recordings with ball electrodes are able to detect even the deep MF related potentials, the subdural MEAs should be able to detect synchronous activities from various layers of the cerebellar cortex.

Although the synchrony in cerebellar cortex has been investigated for decades, there are just a few reports on the spatial aspect of these events. De. Zeeuw et al. reviewed the spatiotemporal aspects of cerebellar oscillations in a recent report. They commented that the synchrony in the cerebellar cortex can demonstrate the diverse spatial patterns over large distances in the different lobules. They stated that complex spike synchrony, which can be detected in the low-frequency bands (2-4Hz or 6-9Hz), can be observed between PCs that are separated up to ~500 μm in the parasagittal zones. In contrast, simple spike synchrony did not indicate any particular directionality.

De Solages et al. (2008) reported that the high-frequency oscillations (~200Hz) could be observed in all the layers of the cerebellar cortex. They also showed that this synchrony horizontally extends as far as 375 μm. Furthermore, their report suggested that there was a correlation between the oscillations obtained from different layers of cerebellar cortex, where molecular and Purkinje layer recordings displayed peak coherences. Similarly, Cheron et al. (2005) reported a large-scale (up to ~1mm) PC synchrony in the anesthetized cerebellar ataxia mice model. These reports support the spatial synchrony that was observed in our recordings, although the area covered by our MEA was unprecedented in size (300 μm- 2100 μm).

Despite the fact all anesthesia regimens will affect the spontaneous and evoked potentials in the cerebellum, a dramatic reduction in the field potentials does not necessarily imply that peripheral responsiveness is completely removed, as stated by (Bengtsson and Jörntell, 2007). Recording synchronous LFPs in the cerebellar cortex was documented in earlier reports in awake as well as anesthetized rats (de Solages et al., 2008b;Courtemanche et al., 2013;Ordek et al., 2013). Even though the anesthesia regimen depresses the cerebellar synchrony (Joynt, 1958;Ordek et al., 2013), local field potentials have sufficient amplitudes to characterize the signals, particularly in low frequencies.

The effect of anesthesia on spontaneous recordings as well as evoked potentials is a concern raised by a number of investigators in the past. Cheron et al. (Servais and Cheron, 2005) compared the differential effects of two different anesthesia regimens (ketamine and pentobarbitone) on local field potentials. They found that ketamine, an NMDA antagonist, depresses the LFP oscillations with PC desynchronization, while pentobarbitone, which targets the GABAa receptors, caused slight changes in PC synchrony. In the cerebellum,

excitatory networks such as the MF-GC-PFs pathway use the NMDA receptors, whereas inhibitory signaling is mediated by GABAa receptors through the PCs and molecular layer interneurons. Therefore, using different anesthesia regimens could have different effects on the neural activity by selectively targeting different synaptic mechanisms. Another critical factor in anesthesia is the time delay allowed before data collection. Jorntell et al. (Bengtsson and Jörntell, 2007) reported that ketamine-xylazine (20:1) depressed both MF and CF responses significantly for 10 minutes after the injection. Similarly, LFP oscillations in the cerebellum exhibited sustained depressions for 5-10 minutes after anesthetic injection (Servais and Cheron, 2005). Although the recovery time was dose dependent, the delay allowed between the injection and recordings can be used to control the anesthesia level in a reproducible manner, and thus obtain stable recordings.

Current findings suggested that there was a significant correlation loss in all electrode groups starting day-1 of injury. The correlation test applied to the EEG signals after head injuries is a diagnostic technique that has been used over decades. Thatcher et al. reported coherence changes across short-distance in different frequency bands after mild injuries (Thatcher et al., 1989). Our findings indicated progressive reductions in correlation values during spontaneous as well stimulated periods (Figure 6.23, 23-24). Interestingly, correlation loss paralleled the decline in the EPAs. Both measures exhibited similar trends, i.e., greater losses at day-1 and then from day-5 to day- 7, but only subtle changes from day-1 to day-3. This suggests that the injury did not only affect the number of PCs that are firing in synch through MF or CF activations, hence the EPA loss, but also the connectivity between spatially distant zones (within $2mm^2$) was disrupted.

Immunohistological analysis also was included into this study primarily for two reasons; first, to verify that an injury-related neuronal degeneration was produced by direct-FPI to the cerebellum. Double immunostaining; CalbindinD28k and Fluoro-Jade C were used to determine the neuronal subtype that was injured. Fluoro-Jade markings showed irreversible cell deaths as delayed as one month of injury induction (molecular layer neurons and PCs) in the cerebellum by earlier reports (Sato et al., 2001). Hallam et al. also showed Fluoro-Jade C positive degenerating neurons at different time points (24h, 48h and 7-days) of the FPI in the rat cerebellum, which was correlated with motor behavioral deficits (Hallam et al., 2004). The second aim was to evaluate the sensitivity of the electrophysiological parameters to detect neural damage due to FPI compared to immunostaining. The results indicated that the subdural MEA recordings were able to glean valuable information about the injury at peak pressures as mild as 15 psi, an injury pressure that resulted in milder neuronal degeneration by immunohistology (Figure 6.30D-F) and no observable behavioral deficits.

Temporal pattern of PC loss was reported by the earlier researchers. Significant PC loss was indicated as early as within the first 24h of FPI induction (Baker et al., 2007), while the degeneration was also observed in the following 7 days of FPI (Ai et al., 2002; Baker et al., 2007; Fukuda et al.,1996; Mautes et al., 1996). Current study proposed the 7 day experimental survival period in order to monitor the injury progression with electrophysiological assessment. To this purpose, immunohistological analysis demonstrated only the 7 day injury consequences. However, findings in the electrophysiological results suggested that there was likely to observe PC loss in the earlier period of survival period.

This study presented data showing the feasibility of monitoring injury related changes in the cerebellar cortex using evoked potentials recorded with subdurally implanted multi-electrode arrays. Changes in peripherally evoked signal amplitudes were detected by 5-min post-injury recordings, and monitored periodically in the following seven days. The results also presented evidences showing that the decline of inter-contact correlations followed a similar trend to the evoked amplitudes in the one week post-injury period. Immunohistological results confirmed the cellular degenerations in the targeted cerebellar area as a result of injury. Overall, electrophysiological monitoring using MEAs is a promising technique to study the progression of neuronal degeneration in animal models of injury without the need of terminating experimental subjects at various time points in the study.

CHAPTER 8

CORRELATION OF FUNCTIONAL DEFICITS AND ELECTROPHYSIOLOGICAL ALTERATIONS

8.1 Motor Function Impairment after Cerebellar Injury

Cerebellar injury will not be detectable at the behavioral level before the injury reaches to a certain level of severity and scale. It should be determined when and to what degree the cerebellar injury becomes observable in the animal's behavior as assessed by the implemented electrophysiological method. The cerebellum is well-known associated with the motor outputs such as locomotion, motor learning and coordination [66-69]. Damage to cerebellum leads to impairment in the motor functions [70-74]. This will provide us with a simple and reproducible test paradigm to quantify the level of injury in a behavioral context. The experiments of this aim will reveal the electrophysiological correlates of the deficits observed in the animal's behavior, e.g., mossy and climbing fiber activity and network synchronization. This information cannot be obtained with histological techniques.

8.1.1 Experimental Design

The severity and scale of cerebellar injury has to reach a significant level before it can impair a skilled motor function such as a ladder crossing. Disruption in the network synchrony of cerebellar circuitry will be linked to the functional deficits manifested in the trained animals at a higher degree of injury. In contrast, electrophysiological method can be much more sensitive than the behavioral markers of the cerebellar injury in the milder cases.

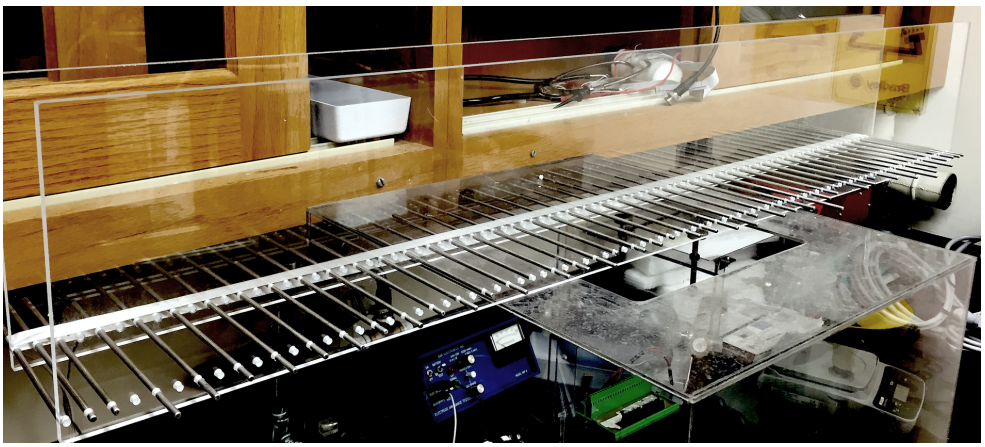

Figure 8.1 Horizontal ladder rung test. Animals were pre-trained 3-7 days before the injury induction with simultaneous camera capturing.

The horizontal ladder rung test apparatus was built in the investigator's laboratory with similar references as described earlier [62]. The ladder was constructed by using two Plexiglas side walls (each 3 feet long) connecting metal rungs in Figure 8.1. The ladder setup was heightened to 20-25cm from the ground during the training sessions. The regular pattern of the rungs was only used, where the metal rods are placed at equal distances (1cm) from each other. The task evaluated the animal's motor performances as they learn the pattern of the rungs on the horizontal plane and perform the ladder crossing over repeated trials.

Animals were subjected to one-week training sessions in the pre-injury period. A high-speed camera (Basler AG) was positioned to ladder setup recording close captions (one foot) as well as from a distance (3-4 feet) in order to record continuous steps and each step success on the rungs during training and injury recordings. The video recordings were analyzed using frame-by-frame analysis at 50 f/sec.

8.1.2 Preliminary Results during the Foot Placement

Behavioral analyses of motor functions after FPI induction was first evaluated via capturing the foot placement errors on the horizontal ladder paradigm in pre-trained four rats (Figure 8.2). Mean scores of forepaw placement on the rungs were ranked 4 to 6 (7-category scale) for trained animals in the pre-injury day trials. 7-category scale rated the paw placement success/failure rate by evaluating the position of grasping (fore and hind limbs).

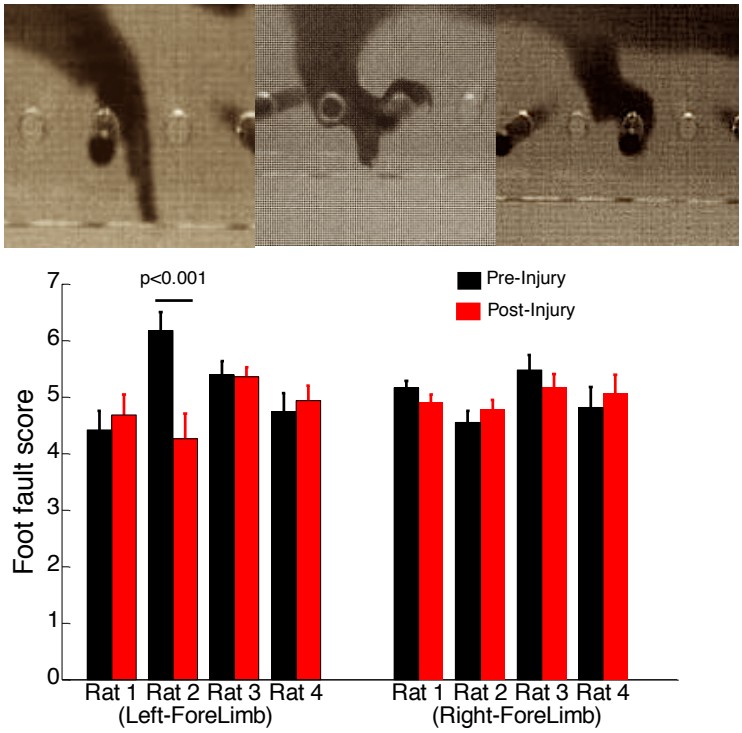

Figure 8.2 Forelimb placements on the ladder rungs were evaluated using a foot fault scoring system for bi-lateral performances across four injured rats. Example of three ranks for total miss (1), finger placement (3), and accurate grasping (7) are shown (Top). In only one rat, performance was degraded for the contralateral forehand placement after the injury induction (paired t-test, $p<0.001$).

Except in one case (Rat 2, Left forelimb; $P>0.001$), there was no measurable differences detected in the post-injury foot placement performances by using foot fault score system across all experimented rats ($N = 4$ rats; paired t-test, $P>0.05$). It was determined that

the foot fault scoring may not be suitable to assess the functional impairments in the walking test.

8.1.3 Impairments of the Walking Pattern in the Trained Animals

Next, the duration (blue) and length (red) of the steps in the forelimb protrusion was analyzed and compared for the pre- and post-injury values (Figure 8.3).

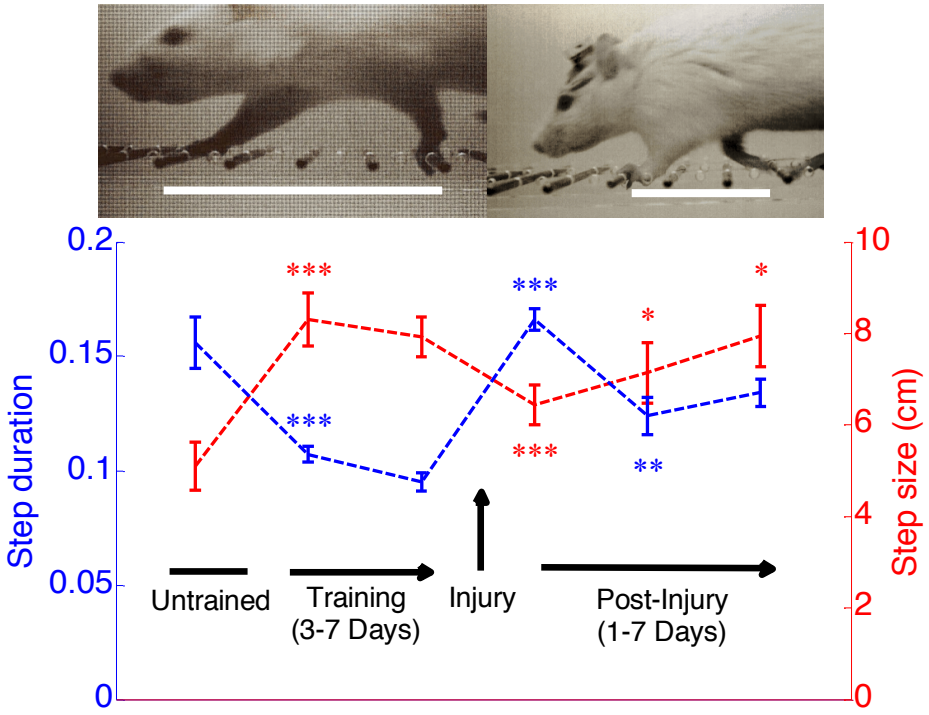

Figure 8.3 Behavioral analysis was further investigated for two additional tests, step size and step duration. Pre-injury vs. post-injury performances compared in mean ± s.d. for the experimented four rats including training improvements. Both step performances showed improvement during training period and diminishment after the FPI induction (P<0.001). Mean step size and duration values calculated and 'p' values indicate the pair data comparison for subsequent day performances. ***, P<0.001; **,P<0.005; *,P<0.05; (N=4 rats, 10 trials, paired t-test).

There were four noticeable trend windows in both analyses. Initial period was the training period where the animals preferred to perform the walking paradigm on the ladder in slower (0.16±0.08s) and smaller steps (5.23±0.45cm).

During one week training period, there were significant improvements in their step performances (N=4 rats, 10 trials; $P<0.001$). While step size was extended to 7.89±0.54cm (5.67±0.66cm, pre-training; $P<0.001$), injury shortened the step size to 6.15±0.26cm (Day 1). Similarly, animal's step duration increased to 0.17±0.13s from 0.11±0.05s at day-1 of FPI (Pre-Injury vs. Day-1 of Injury; $P<0.001$). In the next days (Day 3 - Day 7), injured animals demonstrated measurable improvements in their step performances. At the end of survival periods, the mean step size was 7.86cm and mean step duration was 0.13s, which resembled the trained performances in the pre-injury period. Trained animals tended to increase their stride length, while this declines after the injury. Lack of coordination and posture in the walking pattern was also noted in the injured animals.

8.1.4 Discussion

The cerebellum is involved in fine and skilled movements to generate motor outputs. According to the existing theory, damage to the cerebellum does not lead to absolute functional losses, but rather impair the motor activity such as inability in coordination. Therefore, identifying the cerebellar associated functional deficits in rats can be challenging in mild injuries. The behavioral results in the preliminary study were obtained from animals at a higher degree of injury (> 20psi). As the FPI severity was lowered, it was expected to observe that the behavioral threshold would be much higher than the electrophysiological threshold of detecting the injury.

This study hypothesized the sensitivity of the electrophysiological measurements would be more detailed to identify the brain injuries, particularly in the mild cases. In order to induce the detectable motor impairments in the trained animals, higher severity models of FPI was implemented. To correlate the behavioral deficits to electrophysiological changes in the cerebellar network, higher graded injuries that induces clear functional deficits, would be performed and correlated with the altered electrophysiology in the MEA implanted and trained animals.

Once the relationship had been identified, the severity of the injury was lowered to the electrophysiology threshold; 5psi. It was expected to observe similar changes in the electrophysiological recordings, while there would be no measurable impairments in the motor functions. In order to quantify these with repeated measures, one may need a larger number of experimental groups while extending the post-injury period from one week to one month.

CHAPTER 9

LIMITATIONS OF THE STUDY

One of the biggest issues in this study was encountered regarding the direct injury on the cerebellum, which may compromise the electrophysiological recordings obtained via the MEAs. The cerebellar structure is located beneath the occipital lobe lying on the brain stem, which makes a challenging site for the surgical implantations. This study introduced the subdural electrophysiology in the chronically implanted animals on the pia surface of the cerebellum. Two different incisions within the millimeter required an extreme delicacy of the surgical method. In order to provide the baseline recordings in the un-injured animals, first the MEA had to be implanted and made available for electrophysiological recordings. Though the evoked potentials of the cerebellar LFPs demonstrated very reliable results, which also reported in our initial assessments, the baseline recordings of the matching animal was essential for this study. This problem was addressed by several supporting methodologies in the experimental procedures. Firstly, both craniotomies were performed at the same surgery session, to avoid another mechanical disturbance that may have been introduced by the second injury. Secondly, cerebellar recordings were compared immediately before and after the injury application that could be the first indicator of possible electrode damage. Finally, the FPI control group was implemented, where the animals were exposed to the injury first and then followed by the electrode implantation. These results also supported the main hypothesis.

Another challenge was finding the relationship between the cerebellar neural mechanisms damaged by the injury and the altered electrophysiology. Cerebellar evoked potentials were well characterized by the earlier researchers; however most of them used

penetrating electrodes where the electrical activity could be explained by the activity of a single or several neurons. Designation of the evoked deflections in response to the same peripheral stimulations may introduce additional variables in the surface recordings. Thus, the current study tackled with this issue by setting a large group size and ensuring the reproducibility of the evoked responses in multiple animals.

Also, a typical problem in FPI experiments is the reproducibility of the pressure transfer from the device to the brain tissue. This induces much variability in the results. The thickness of the dura and the amount of the connective tissue around the injury port is probably the primary cause of this variability. In order to minimize these issues, young animals (less connective tissue) all at the same age (4-6 weeks old, similar dura thickness) were used in the current study. Dura was intact under the cranial hole for the FPI induction in order to keep our results comparable to other labs (most research labs apply the FPI epidurally). The FPI device measures the pressure waveform as it is applied to the animal at the point near the skull opening. By cleaning the skull port with sterile saline before each application and making sure that the animal is positioned the same way each time, the pressure variation were minimized.

Another challenge was the fact that the cerebellum is highly active during wakefulness even in resting state. The amplitude of high frequency oscillations also depend on the mental state of the animal in our observations (attentive vs. quietly resting). It was expected that the injury would induce a stronger effect on the cerebellar synchrony than the state of the animal so that the results were clearly distinguishable as they were in the preliminary data.

CHAPTER 10

CONCLUSIONS AND FUTURE WORK

To this day, brain injuries have not been investigated with electrophysiological techniques in this detail utilizing continuous or repetitive measurements in the living animals. Direct FPI on the cerebellum surface was used to demonstrate the alterations in the electrical activity of the cerebellum after the injury. Current study aimed to make a contribution to clinical electrophysiology by providing characterizing the evoked potentials and their high-frequency contents. Electrophysiological findings were compared with the immunohistological results where the structural degenerations supported the changes in the cerebellar circuitry. Finally, the role of the cerebellum in motor functions was shown to correlate with the electrophysiological alterations. Combination of three different techniques in one study to assess the brain injury in the cerebellum was a first to our knowledge.

Repetitive measurements via intact electrodes in the traumatized animals can be very powerful tool to identify the underlying mechanisms of the injury progression. For instance, one of the well-reported theories regarding the molecular mechanisms of brain injury is the hyperexcitation of the neurons, which ultimately would alter the electrophysiological properties of the damaged neural network. Similarly, the results in the current study proposed differential changes in the evoked potentials, which are associated with the different neural structures such as mossy fibers and climbing fibers. This particular finding was significant within the cerebellum where there are only two input pathways within the internal circuitry, despite the abundant number of the nerve cells and their connections.

Mild brain injuries are the most commonly experienced injury type, and yet it is hardest to diagnose. Current study aimed the lowest severity with ~5 psi fluid percussion

pressure on the dura surface of the cerebellum. At this severity, we were able to detect changes in the electrophysiological recordings with repetitive measurements in the seven-day survival animals. In contrast, the injury was not clear to make a conclusion neither in histological results nor by the behavioral paradigms at matching injury levels.

Future studies may involve pinpointing the neural mechanisms from the electrophysiological findings then linking them to functional impairments in the motor learning, where the cerebellum plays an important role. Another novel feature of the study was the temporal measurements in the post-injury period where the secondary injury mechanism was involved. Immediate measurements in the acute period combined with the seven-day monitoring highlighted the injury progression in the living animals. However, the concussion type injury produces symptoms in the longer periods such as weeks to months. Monitoring the electrophysiology of the injured animals in the broader time window may extract the additional features of the trauma. Nevertheless, the challenges of the neural recordings with chronically implanted electrodes will be needed to improve in this context.

Only few studies focused on the cerebellum in the context of TBI or mTBI, perhaps because the cerebellum related deficits are not very common clinical symptoms observed in TBI patients. However, recent research has shown that cerebellum has been involved not only in motor coordination and learning but also in cognitive functions, balance, and others as well. Thus, subtle effects of mild TBI may not be obvious in many cases and hence underdiagnosed. The cerebellum is a unique brain site because more than half of the cells in the brain are to be found in the cerebellum and if the results of TBI on one aspect of the cerebellar function is understood, this could be generalized to other brain functions that the

cerebellum plays a role because of the stereotypical structure of the neural connections across the cerebellar cortex.

Current study addressed the TBI phenomena in the animal model by characterizing the electrophysiological changes combined with the immunohistological verification and the behavioral evaluation following a direct insult on the cerebellum. To our knowledge, no other researchers to this date have investigated the combination of these three principal methods for assessment of a brain injury. Findings were not only valuable to provide a comparison across fundamental methods of TBI detection, but also demonstrate the sensitivity of each of these techniques in a reproducible model.

Finally, assessment of the brain injury mechanism with implanted MEA in the living animals will allow development of animal models where the temporal progression of neural damage and the associated behavioral changes can be investigated without the need to terminate the animals at various time points, and therefore enable development of much more accurate behavioral markers for specific local injuries in the cerebellum as well as in the other areas of the brain.

APPENDIX

MATLAB CODE

All the analyses and illustrations were performed using the combined code is shown at below.

```
for x = 1:length(functions_to_run)
   if functions_to_run(x) == 0.001

       frame_Size = 1;

       implay(['videos/trial' num2str(trial) '.avi'],frame_Size)

   end
 end

 for x = 1:length(functions_to_run)
   if functions_to_run(x) == 0.03

unfiltered_data_mean = mean(unfiltered_data(:,1:31)');
%
[coef, score, latent]=princomp(unfiltered_data(:,1:31));
score1=score(:,1);
coef(:,1)=zeros(number_channels,1);
unfiltered_data=score*coef';
% unfiltered_data = unfiltered_data';


%
 for i=1:31
%      unfiltered_data(:,i) = unfiltered_data(:,i) - unfiltered_data_mean';
        unfiltered_data(:,i) = unfiltered_data(:,i) - score(:,2);

 end

 figure;plot(unfiltered_data_mean)

   end
 end


for x = 1:length(functions_to_run)
   if functions_to_run(x) == 0.02
```

```
%           number_channels=31;

        bad_channel = find(var(unfiltered_data(:,1:number_channels)) >=
max(var(unfiltered_data(:,1:number_channels))));

        meanbar = mean(var(unfiltered_data(:,1:number_channels)));
        stdbar= std(var(unfiltered_data(:,1:number_channels)));

        outliers = find(abs(var(unfiltered_data(:,1:number_channels))-meanbar) >
2*stdbar)

        figure;stem(var(unfiltered_data(:,1:number_channels)))
        unfiltered_data = unfiltered_data(:,1:number_channels);
        unfiltered_data(:,outliers)=[];
         signal_length = min(size(unfiltered_data));
        number_channels = signal_length;

   end

end

for x = 1:length(functions_to_run)
   if functions_to_run(x) == 0.01
%        unfiltered_data=unfiltered_data(:,1:signal_length);

duration = 20;
LOOP = 20;
Fs = sampling_rate;
DURATION=duration/LOOP;
N=2048;

%% Taking the Power spectrum first for each period then average it.

% for ii=1:LOOP
%
% [Pww(:,ii), F] = pwelch(detrend(unfiltered_data((ii-
1)*DURATION*Fs+1:ii*DURATION*Fs,:)),hanning(N),N/2,N,sampling_rate);
% Pww(:,ii)  = 5*log10(Pww(:,ii).^2);
% end
%
% averaged_Pww = sum(Pww(:,1:20)',1)/20;
% averaged_Pww = averaged_Pww';

% figure;plot(F,averaged_Pww)
% Apparently it does not make any difference taking the power spect from
```

```
% the averaged DATA
 %% Averaging the data

tt=1/Fs:1/Fs:duration;

DATA = zeros(min(size(unfiltered_data)), Fs*DURATION);
% DATA2 = zeros(min(size(unfiltered_data_mean)), Fs*DURATION);

unfiltered_data = unfiltered_data';
% unfiltered_data_mean_averaged = unfiltered_data_mean';

for Y=1:LOOP,

   DATA = DATA+unfiltered_data(:,(Y-1)*DURATION*Fs+1:Y*DURATION*Fs);
%     DATA2 = DATA2+unfiltered_data_mean(:,(Y-
1)*DURATION*Fs+1:Y*DURATION*Fs);


end

DATA=DATA'/LOOP;
% DATA2=DATA2'/LOOP;

% unfiltered_data = unfiltered_data';

unfiltered_data = DATA;

%% Break each Evoked Signals into segments


% for i=1:32
% for p=1:LOOP
% DATA_Segments(:,p,i) = unfiltered_data((p-1)*Fs+1:p*Fs,i);
% end
% end


   end
end


for x = 1:length(functions_to_run)
   if functions_to_run(x) == 0.04
N=2048*4;
% hold on;
```

```
[Pww_cer, F] =
pwelch(LFP_data_sorted(:,1:number_channels),hanning(N/2),N/4,N/2,sampling_r
ate); % Cerebellum Power Spectrum
% [Pww_cor, F] =
pwelch(unfiltered_data(:,32:62),hanning(N),N/2,N,sampling_rate); % Cerebellum
Power Spectrum

cc = hsv(50);


Pww_cer = 10*log10(Pww_cer);
% Pww_cor = 10*log10(Pww_cor);

hold on;
figure(1);
plot(F,Pww_cer,'color',cc(trial,:));axis([0 1000 -180 -90])
% whitebg('k')


% hold on;plot(F,Pww_cor,'y');grid;legend('Cerebellum Quiet','Cerebrum Quiet')

% figure;plot(F,Pww_cer);hold on
% [Pww_mean, F] = pwelch(detrend(D ATA2),hanning(N),N/2,N,sampling_rate);
% Pww_mean = 5*log10(Pww_mean.^2);
% plot(F,Pww_mean,'c');legend('Cerebellum Mean Out','Cerebellum  Mean
DATA')

   end
end


clear raw_data
for x = 1:length(functions_to_run)
   if functions_to_run(x) == 0.1

row1=[zeros(size(unfiltered_data(:,14)))'; unfiltered_data(:,14)';
unfiltered_data(:,11)'; unfiltered_data(:,22)'; unfiltered_data(:,19)';
zeros(size(unfiltered_data(:,14)))'];
row2=[unfiltered_data(:,31)'; unfiltered_data(:,30)'; unfiltered_data(:,27)';
unfiltered_data(:,6)'; unfiltered_data(:,3)'; unfiltered_data(:,2)'];
row3=[unfiltered_data(:,15)'; unfiltered_data(:,28)'; unfiltered_data(:,10)';
unfiltered_data(:,23)'; unfiltered_data(:,5)'; unfiltered_data(:,18)'];
row4=[unfiltered_data(:,32)'; unfiltered_data(:,12)'; unfiltered_data(:,25)';
unfiltered_data(:,8)'; unfiltered_data(:,21)'; unfiltered_data(:,1)'];
row5=[unfiltered_data(:,16)'; unfiltered_data(:,29)'; unfiltered_data(:,9)';
unfiltered_data(:,24)'; unfiltered_data(:,4)'; unfiltered_data(:,17)'];
```

```
row6=[zeros(size(unfiltered_data(:,14)))'; unfiltered_data(:,13)';
unfiltered_data(:,26)'; unfiltered_data(:,7)'; unfiltered_data(:,20)';
zeros(size(unfiltered_data(:,14)))'];
%rows=[row1; row2; row3; row4; row5; row6];

s=zeros(150150,3);

  signaldif1(:,1)=row1(3,:)'-row1(2,:)';
  signaldif1(:,2)=row1(5,:)'-row1(4,:)';

  s=zeros(150150,3);

signaldif=s;

   for j=1:3
      i=j*2;
      signaldif2(:,j)=row2(i,:)'-row2(i-1,:)';
   end

   s=zeros(150150,3);

signaldif=s;

   for j=1:3
      i=j*2;
      signaldif3(:,j)=row3(i,:)'-row3(i-1,:)';
   end

   s=zeros(150150,3);

signaldif=s;

   for j=1:3
      i=j*2;
      signaldif4(:,j)=row4(i,:)'-row4(i-1,:)';
   end

   s=zeros(150150,3);

signaldif=s;

   for j=1:3
      i=j*2;
      signaldif5(:,j)=row5(i,:)'-row5(i-1,:)';
   end
```

```
    s=zeros(150150,3);

signaldif=s;

  signaldif6(:,1)=row6(3,:)'-row6(2,:)';
   signaldif6(:,2)=row6(5,:)'-row6(4,:)';

    signaldif=[signaldif1 signaldif2 signaldif3 signaldif4 signaldif5 signaldif6];
    unfiltered_data=signaldif;
    number_channels = 16;
    end
end
%csvwrite(unfiltered_data_name, unfiltered_data);
% unfiltered_data = csvread(unfiltered_data_name);
% filtered_data = csvread(filtered_data_name);
% envelope_data = csvread(envelope_name);

scale = 'uV';

if strcmp(scale, 'uV')
    scale_value = 1000000;
elseif strcmp(scale, 'mV')
    scale_value = 1000;
elseif strcmp(scale, 'V')
    scale_value = 1;
end

for x = 1:length(functions_to_run)
    if functions_to_run(x) == 0.5

for i=1:16
%i=500;
Signal=unfiltered_data(:,i);
Signal=Signal-mean(Signal);
Signal=detrend(Signal);
%Signal=Design;
%Signal=scores(:,5);
%Signal=hrf(1:72);

fs = 30000;
Ts = 1/fs;
 x = [0:1/fs:length(Signal)*Ts];
 N = length(Signal);
 index = 0:N-1;
```

```
%h0 = [1/sqrt(2) 1/sqrt(2)];
% Daubechies - 4
h0 = [0.4830 0.8365 0.2241 -0.1294];
% Daubechies - 10
%h0 = [0.32580343 1.01094572 0.8922014 -0.03957503 -0.26450717
0.0436163 0.0465036 -0.01498699];
%Daubechies - 2
%h0 = [0.3415    0.5915    0.1585   -0.0915];
%h0 = [0.5000    0.5000];
NSteps = log2(N);
coefs = (2^(-NSteps/2)).*Signal;

j = 1;
[LP1 HP1] = waveanalysis(coefs, h0);
% The output is the low and high pass bands of the signal.
%
% Plot the signal bands.
index = 0:2^(NSteps-j)-1;
time = index.*Ts*2^j;
% figure(1)
% subplot(121)
% plot(time,LP1)
% subplot(122)
% plot(time,HP1)

% This is the second pass. Here the LP range is investigated.
j = 2;
[LP2 HP2] = waveanalysis(LP1, h0);
index2 = 0:2^(NSteps-j)-1;
time = index2.*Ts*2^j;
 %Plot the signal bands.
 %figure(2)
 %subplot(121)
 %plot(time,LP2)
 %subplot(122)
 %plot(time,HP2)

% This is the second pass. Here the LP range is investigated.
j = 3;
[LP3 HP3] = waveanalysis(LP2, h0);
index3 = 0:2^(NSteps-j)-1;
time = index3.*Ts*2^j;
 %Plot the signal bands.
 %figure(3)
 %subplot(121)
 %plot(time,LP3)
```

```
 %subplot(122)
 %plot(time,HP3)



 % This is the second pass. Here the LP range is investigated.
j = 4;
[LP4 HP4] = waveanalysis(LP3, h0);
index4 = 0:2^(NSteps-j);
time = index4.*Ts*2^j;
 %Plot the signal bands.
 %figure(4)
 %subplot(121)
 %plot(time,LP4)
 %subplot(122)
 %plot(time,HP4)
 j = 5;
[LP5 HP5] = waveanalysis(LP4, h0);
index4 = 0:2^(NSteps-j);
time = index4.*Ts*2^j;


 j = 6;
[LP6 HP6] = waveanalysis(LP5, h0);
index4 = 0:2^(NSteps-j);
time = index4.*Ts*2^j;

 j = 7;
[LP7 HP7] = waveanalysis(LP6, h0);
index4 = 0:2^(NSteps-j);
time = index4.*Ts*2^j;

  j = 8;
[LP8 HP8] = waveanalysis(LP7, h0);
index4 = 0:2^(NSteps-j);
time = index4.*Ts*2^j;

  j = 9;
[LP9 HP9] = waveanalysis(LP8, h0);
index4 = 0:2^(NSteps-j);
time = index4.*Ts*2^j;


  j = 10;
[LP10 HP10] = waveanalysis(LP9, h0);
index4 = 0:2^(NSteps-j);
```

```
time = index4.*Ts*2^j;


 sigma1=mad(HP1)/0.6745;
 sigma2=mad(HP2)/0.6745;
 sigma3=mad(HP3)/0.6745;
 sigma4=mad(HP4)/0.6745;
 sigma5=mad(HP5)/0.6745;
 sigma6=mad(HP6)/0.6745;
 sigma7=mad(HP7)/0.6745;
 sigma8=mad(HP8)/0.6745;
 sigma9=mad(HP9)/0.6745;
 lHP1=length(HP1);
 lHP2=length(HP2);
 lHP3=length(HP3);
 lHP4=length(HP4);
 lHP5=length(HP5);
 lHP6=length(HP6);
 lHP7=length(HP7);
 lHP8=length(HP8);
 lHP9=length(HP9);
tHP1=sigma1.*sqrt(2.*log(lHP1));
tHP2=sigma2.*sqrt(2.*log(lHP2));
tHP3=sigma3.*sqrt(2.*log(lHP3));
tHP4=sigma4.*sqrt(2.*log(lHP4));
tHP5=sigma5.*sqrt(2.*log(lHP5));
tHP6=sigma6.*sqrt(2.*log(lHP6));
tHP7=sigma7.*sqrt(2.*log(lHP7));
tHP8=sigma8.*sqrt(2.*log(lHP8));
tHP9=sigma9.*sqrt(2.*log(lHP9));
for k=1:lHP1
    sig=HP1(k);
    sng=sign(sig);
    thresh=abs(sig)-tHP1;
    if thresh < 0
        rep=0;
    else
        rep=thresh;
    end
    dHP1(k)=sng*rep;
end

for k=1:lHP2
    sig=HP2(k);
    sng=sign(sig);
    thresh=abs(sig)-tHP2;
```

```
    if thresh < 0
        rep=0;
    else
        rep=thresh;
    end
    dHP2(k)=sng*rep;
end

for k=1:lHP3
    sig=HP3(k);
    sng=sign(sig);
    thresh=abs(sig)-tHP3;
    if thresh < 0
        rep=0;
    else
        rep=thresh;
    end
    dHP3(k)=sng*rep;
end

for k=1:lHP4
    sig=HP4(k);
    sng=sign(sig);
    thresh=abs(sig)-tHP4;
    if thresh < 0
        rep=0;
    else
        rep=thresh;
    end
    dHP4(k)=sng*rep;
end

for k=1:lHP5
    sig=HP5(k);
    sng=sign(sig);
    thresh=abs(sig)-tHP5;
    if thresh < 0
        rep=0;
    else
        rep=thresh;
    end
    dHP5(k)=sng*rep;
end

for k=1:lHP6
    sig=HP6(k);
```

```
    sng=sign(sig);
    thresh=abs(sig)-tHP6;
    if thresh < 0
        rep=0;
    else
        rep=thresh;
    end
    dHP6(k)=sng*rep;
end

for k=1:lHP7
    sig=HP7(k);
    sng=sign(sig);
    thresh=abs(sig)-tHP7;
    if thresh < 0
        rep=0;
    else
        rep=thresh;
    end
    dHP7(k)=sng*rep;
end

for k=1:lHP8
    sig=HP8(k);
    sng=sign(sig);
    thresh=abs(sig)-tHP8;
    if thresh < 0
        rep=0;
    else
        rep=thresh;
    end
    dHP8(k)=sng*rep;
end

for k=1:lHP9
    sig=HP9(k);
    sng=sign(sig);
    thresh=abs(sig)-tHP9;
    if thresh < 0
        rep=0;
    else
        rep=thresh;
    end
    dHP9(k)=sng*rep;
end
```

```
rLP8 = dewaveanalysis(dHP9',LP9, h0);
rLP7 = dewaveanalysis(dHP8',rLP8(4:end), h0);
rLP6 = dewaveanalysis(dHP7',rLP7(5:end), h0);
rLP5 = dewaveanalysis(dHP6',rLP6(4:end), h0);
rLP4 = dewaveanalysis(dHP5',rLP5(5:end), h0);
rLP3 = dewaveanalysis(dHP4',rLP4(5:end), h0);
%L=length(rLP3)-lHP3;

%rLP2 = dewaveanalysis(dHP3',rLP3(L:length(rLP3)-1)*20, h0);
rLP2 = dewaveanalysis(dHP3',rLP3(4:end), h0);
L=length(rLP2)-lHP2;
%rLP1 = dewaveanalysis(dHP2',rLP2(L+1:length(rLP2))*1, h0);
rLP1 = dewaveanalysis(dHP2',rLP2(4:end), h0);
rrcomp = dewaveanalysis(dHP1',rLP1(1:25000), h0); %%(L+1:length(rLP1))
%size(rrcomp)
 processedsignal(:,i)=rrcomp;
end
size(processedsignal)
unfiltered_data=processedsignal;
   end
end

%%%%%%%%%%%%%%%%%%%%%%%%%%%%%%%%%%%%%%%%
%%%%%%%%%%
% Create arrays to be used for x-data in future plots. These include time,
% frequency, and video frame number.

number_data_points = length(unfiltered_data);
time = (1:number_data_points)/sampling_rate;
freq = (1:number_data_points)*sampling_rate/number_data_points;
video = (1:number_data_points)*video_frame_rate/sampling_rate;

% 1) Plot unfiltered data
%
% This function plots the unfiltered gain-compensated, scaled data versus
% either a time scale, sample scale, or video frame scale. Specify x_data
% according to which scale is appropriate (time, sample, or video). Also,
% set the appropriate minimum and maximum x and y values to plot.


for x = 1:length(functions_to_run)
   if functions_to_run(x) == 1

      x_data = time;
```

```
        x_min = 0;
        x_max = max(x_data);

        y_min = min(unfiltered_data*scale_value);
        y_max = max(unfiltered_data*scale_value);

        x_label = 'Time (s)';
%         x_label = 'Video Frame';
%         x_label = 'Sample Number';
%         y_label = {'Unfiltered Signal'; ['(' scale ')']};
        y_label = ['Unfiltered Signal (' scale ')'];

        run sp_mfiles/plot_unfiltered_data
%     run sp_mfiles\plot_unfiltered_data_quadrant
    end
end


% 2) Plot frequency response (FFT)
%
% This function computes and plots the fast fourier transform (FFT) of the
% unfiltered gain-compensated data versus the frequency.


for x = 1:length(functions_to_run)
    if functions_to_run(x) == 2
number_of_data_points=25000
        unfiltered_fft = abs(fft(detrend(unfiltered_data)));

        x_data = freq;

        x_min = 0;
        x_max = sampling_rate/2;

        y_min = 0;
%         y_max = max(unfiltered_fft);
        for y = 1:number_channels
            y_max(y) = 0.05;
%mean(unfiltered_fft(round(number_data_points/3):round(number_data_points/2
),y))+25*std(unfiltered_fft(round(number_data_points/3):round(number_data_poin
ts/2),y));
        end

        x_label = 'Frequency (Hz)';
        y_label = 'FFT Magnitude';
```

```
        run sp_mfiles\plot_fft

    end
end


% 3) Filter data (Bandpass FIR) for population activity
%
% This function constructs a bandpass FIR filter and filters the
% gain-compensated data accordingly. Filtered data is saved into a
% pre-specified dat file. Filter parameters (number of coefficients, low
% cutoff, and high cutoff) are specified prior to calling the function.

for x = 1:length(functions_to_run)
    if functions_to_run(x) == 3

        filter_order = 1000;
        low_cut =200;           % freq in Hz
        high_cut = 600;         % freq in Hz

        high_pass_norm = high_cut/(sampling_rate/2);
         low_pass_norm = low_cut/(sampling_rate/2);

        b_filt_band = fir1(filter_order, [ low_pass_norm high_pass_norm  ]);
        a_filt_band=1;
        filtered_data = filtfilt(b_filt_band, a_filt_band, unfiltered_data);

%         csvwrite(filtered_data_name, filtered_data);

    end
end


% 4) Plot filter
%
% This function plots the frequency response of the filter being used. Set
% the appropriate minimum and maximum x and y values to plot.


for x = 1:length(functions_to_run)
    if functions_to_run(x) == 4

        x_data = freq;

        x_min = 0;
        x_max = sampling_rate/2;
```

```
        y_min = 0;
        y_max = 1.1;

        run sp_mfiles\plot_filter

    end
end


% 5) Plot filtered data
%
% This function plots the filtered gain-compensated, scaled data versus
% either a time scale, sample scale, or video frame scale. Specify x_data
% according to which scale is appropriate (time, sample, or video). Also,
% set the appropriate minimum and maximum x and y values to plot.


for x = 1:length(functions_to_run)
    if functions_to_run(x) == 5

        x_data = time;

        x_min = 0;
        x_max =max(x_data);

        y_min = -70*ones(1,68); %min(filtered_data*scale_value);
        y_max = 70*ones(1,68); % max(filtered_data*scale_value);

        x_label = 'Time (s)';
%         x_label = 'Video Frame';
%         x_label = 'Sample Number';
%         y_label = {'Filtered Signal'; ['(' scale ')']};
        y_label = ['Filtered Signal for population activity (' scale ')'];

        run sp_mfiles\plot_filtered_data

    end
end


% 6) Calculates and plots signal envelope (rectified moving avg of filtered data)
%
% This function calculates the signal envelope by rectifying and then
% performing a moving average calculation on the filtered data. Set the
% appropriate bin length for calculating the moving average in seconds.
```

```
for x = 1:length(functions_to_run)
   if functions_to_run(x) == 6

      bin_length = 0.05;     % in sec

     run sp_mfiles\calculate_envelope

%        csvwrite(envelope_name, envelope_data);

      x_data = time;

      x_min = 0;
      x_max = max(time); % max(x_data);

      y_min = 5e-6; % ones(1,32)* min(min(envelope_data*scale_value));
     y_max = ones(1,32)*40;
      %y_max = ones(1,32)*max(max(envelope_data*scale_value));

      x_label = 'Time (s)';
%        x_label = 'Video Frame';
%        x_label = 'Sample Number';
%        y_label = {'Signal Envelope'; ['(' scale ')']};
      y_label = ['Signal Envelope (' scale ')'];

      run sp_mfiles\plot_envelope
   end
end


% 7) Filter data (Bandpass FIR) for LFP
%
% This function constructs a bandpass FIR filter and filters the
% gain-compensated data accordingly. Filtered data is saved into a
% pre-specified dat file. Filter parameters (number of coefficients, low
% cutoff, and high cutoff) are specified prior to calling the function.

for x = 1:length(functions_to_run)
   if functions_to_run(x) == 7


         L=length(unfiltered_data);
         T=1000/sampling_rate;
         % design a low - pass
```

```
fch=20;
fcl=800;


fn2=2*fcl/(sampling_rate);
fn1=2*fch/(sampling_rate);


[b,a]=butter(5,fn1,'high');

LFP_data=filtfilt(b,a,unfiltered_data);

%        LFP_data=filtfilt(b,a,DATA);
[b,a]=butter(5,fn2,'low');

LFP_data=filtfilt(b,a,LFP_data);

%        LFP_data2=filtfilt(b,a,LFP_data2);


fc1=5;
fc2=30;
fc3=30;
fc4=80;
fc5=80;
fc6=160;
fc7=160;
fc8=250;


  fn1=2*fc1/(sampling_rate);
fn2=2*fc2/(sampling_rate);

 [b,a]=butter(5,fn2,'low');
LFP_data1=filtfilt(b,a,raw_dataA);
[b,a]=butter(5,fn1,'high');
LFP_data1=filtfilt(b,a,LFP_data1);


fn4=2*fc4/(sampling_rate);
fn3=2*fc3/(sampling_rate);
%        fn2=[fn3 fn4];
[b,a]=butter(5,fn4,'low');
LFP_data2=filtfilt(b,a,raw_dataA);
[b,a]=butter(5,fn3,'high');
LFP_data2=filtfilt(b,a,LFP_data2);
```

```
%
          fn6=2*fc6/(sampling_rate);
         fn5=2*fc5/(sampling_rate);
         [b,a]=butter(5,fn6,'low');
         LFP_data3=filtfilt(b,a,raw_dataA);
         [b,a]=butter(5,fn5,'high');
         LFP_data3=filtfilt(b,a,LFP_data3);
%



          fn7=2*fc7/(sampling_rate);
         fn8=2*fc8/(sampling_rate);
         [b,a]=butter(5,fn8,'low');
         LFP_data4=filtfilt(b,a,raw_dataA);
         [b,a]=butter(5,fn7,'high');
         LFP_data4=filtfilt(b,a,LFP_data4);

         % plot the filter amplitude and phase
%           [h,w] = freqz(b,a,10000); % this calculates the transfer function at N
different points of digital frequency; h is the transfer function at w frequencies
%           f=w/(2*pi*T);              % convert the digital frequency array to analog
frequency in KHz
%           figure;
%           subplot(211);
%           plot(f,abs(h));          % amplitide
%           grid
%           subplot(212)
%          % plot(f,angle(h));    % phase
%           grid
%           xlabel('frequency (kHz)');

LFP_data_cer =LFP_data(:,1:number_channels);
% LFP_data_cor = LFP_data(:,number_channels+1:2*number_channels);

unfiltered_data_cer = unfiltered_data(:,1:number_channels);
% unfiltered_data_cor =
unfiltered_data(:,number_channels:2*number_channels);

for p = 1:number_channels
LFP_data_sorted(:,p) = LFP_data_cer(:,positions_sorted(p));
unfiltered_DATA(:,p) = unfiltered_data(:,positions_sorted(p));

end
% for p = 1:number_channels
```

```
% LFP_data_sorted(:,p+number_channels) =
LFP_data_cor(:,positions_sorted(p));
% unfiltered_DATA(:,p+number_channels) =
unfiltered_data_cor(:,positions_sorted(p));
% end
% end
%  end



for x = 1:length(functions_to_run)
   if functions_to_run(x) == 200

       per = sampling_rate/1000*100;    % Define your temporal window in ms
       figure;
       i=per*3;
 for kkk=1:31
%  subplot(4,8,kkk);
% figure(kkk);
% for i=per*2:per:length(LFP_data)-6*per
for ii=1:31

% clf;
% subplot(1,2,1)
% surface(corrcoef(unfiltered_data(i:i+per,1:number_channels)));caxis([-1 1])
% y_start = num2str(i,'%d');
% title(y_start)
% subplot(1,2,2)
% plot(LFP_data(i:i+per,1:number_channels))
% y_start = num2str(i,'%d');
% title(y_start)


[r,lags]=xcorr(LFP_data_sorted(4800:6500,ii),LFP_data_sorted(4800:6500,kkk),'c
oeff');

% [r,lags]=xcorr(LFP_data_sorted(i:i+per,ii),LFP_data_sorted(i:i+per,kkk),'coeff');
win_gauss = gausswin(length(r));
az = find(r==max(r));
kk = i/per;
zz(kkk,ii) = lags(az)
win_gauss = gausswin(length(r));
yy = r.*win_gauss;      % Gauss windowing
%
figure(132);clf;subplot(2,1,1);plot(1e6*LFP_data_sorted(5900:6500,[ii kkk]));
y_start = num2str(kkk,'%d');title(y_start)
```

```
subplot(2,1,2); plot(lags,r,'color',cc(4*kk,:));
% pause(.5);

% figure(103);hold on

end
%  end
%  pause;
 %        mean(zz)        % average of lagging or leading across time.
%   figure;plot(zz(kkk,:),'color',cc(4*kk,:))

 end
 figure;stem(zz)

%  for kkk=1:31
%  subplot(4,8,kkk);plot(zz(kkk,:));end
   end
end


for x = 1:length(functions_to_run)
   if functions_to_run(x) == 201
%       LFP_data = LFP_data2;
for i=EPs1 - marg:1:EPs1 + marg
   for k=1:32

  if (LFP_data(i,k)>0)

     LFP_rectify_exc(i,k)=LFP_data(i,k);
  else

     LFP_rectify_inh(i,k) = -LFP_data(i,k);

      end
   end
end

for i=EPs2 - marg:1:EPs2 + marg
   for k=1:32

  if (LFP_data(i,k)>0)

     LFP_rectify_exc2(i,k)=LFP_data(i,k);
  else

     LFP_rectify_inh2(i,k) = -LFP_data(i,k);
```

```
      end
   end
end

figure;plot(LFP_rectify_exc)
figure;plot(LFP_rectify_exc2)
% figure;plot(LFP_rectify_inh)
% LFP_rectify_exc = LFP_rectify_exc(:,[2:16,19:30]); % Discard the
unresponsive channels
LFP_rectify_exc =LFP_rectify_inh;
LFP_rectify_exc2 =LFP_rectify_inh2;

figure;for p = 1:number_channels
subplot(4,8,positions(p));

r= randi(32,32,1);
r=r(1);

maxresp = find(LFP_rectify_exc(:,r) == max(max(LFP_rectify_exc(:,r))));

% maxresp2 = find(LFP_rectify_inh(:,r) == max(max(LFP_rectify_inh(:,r))));

imagesc(LFP_rectify_exc(maxresp,p)');
colormap(gray);caxis([min(min(LFP_rectify_exc(maxresp,1:32)))
max(max(LFP_rectify_exc(maxresp,1:32)))])

% imagesc(LFP_rectify_inh(maxresp2,p)');
colormap(jet);caxis([min(min(LFP_rectify_inh(maxresp2,[1:32])))
max(max(LFP_rectify_inh(maxresp2,1:32)))])


yhead_start = num2str(i,'%d');
yhead_end = num2str(i+1,'% d');
title([yhead_start])
head=num2str(p,'%d');
ylabel(head)

end

% figure
% for k=5000:16:7000;
%
% clf
% for p = 1:32
% subplot(4,8,positions(p));
```

```
% imagesc(LFP_rectify_exc(k:k+10,p)'); colormap(jet);caxis([0
max(max(LFP_rectify_exc))])
% yhead_start = num2str(i,'%d');
% yhead_end = num2str(i+1,'% d');
% title([yhead_start])
% head=num2str(p,'%d');
% ylabel(head)
%
% end
% pause(.1)
% for p = 1:number_channels
% unfiltered_data_cere_electrode(:,p) = unfiltered_data(:,positions_sorted(p));
% end
%
% unfiltered_data_cortex = unfiltered_data(:,33:64);
% for p = 1:32
% unfiltered_data_cor_electrode(:,p) =
unfiltered_data_cortex(:,positions_sorted(p));
% end


figure;subplot(2,1,1);
imagesc(corrcoef(unfiltered_DATA(:,1:number_channels)));axis tight

[Corr_Cerebellum,p] = corrcoef(unfiltered_DATA(:,1:number_channels)) ;

% Corr_Cerebellum = Corr_Cerebellum(1,:);
subplot(2,1,2)
imagesc(corrcoef(unfiltered_DATA(:,number_channels:number_channels*2)));axi
s tight
[Corr_Cortex,p] =
corrcoef(unfiltered_DATA(:,number_channels:number_channels*2)) ;



Correlation_Unfiltered_data_cere = zeros(31,31);
Correlation_Unfiltered_data_cor = zeros(31,31);

for i=1:number_channels

Correlation_Unfiltered_data_cere(i,i:31) = Corr_Cerebellum(i,i:31);
Correlation_Unfiltered_data_cor(i,i:31) = Corr_Cortex(i,i:31);

end
figure;surface(Correlation_Unfiltered_data_cere) ; caxis([0 1]);axis tight
figure;surface(Correlation_Unfiltered_data_cor) ; caxis([0 1]);axis tight
```

```
   end
end



for x = 1:length(functions_to_run)
   if functions_to_run(x) == 206

      LFP_data_sorted = LFP_data_sorted(4900:5500,1:32);

% X = input('desired channel')      % to process distinct channel manually

figure;surface(corrcoef(LFP_data_sorted)); % Open the Surface plot to double
check


for X = 1:min(size(LFP_data_sorted))

row1 = [1:8]; row2 = [9:16]; row3 = [17:24]; row4=[25:32]; % Divide into row
vectors

X

if (find(row1 ==X))

medial = find(row1<X)
lateral = find(row1>X)         %% Look for medial-lateral direction

rost_caud = [X+8 X+16 X+24]     % Assign the rost-caudal position
row = row1;
y_row = 300;
y_row2 = y_row-20;

x_row = mod(X-1,8)*55;
end

if (find(row2 ==X))

medial = find(row2<X)
lateral = find(row2>X)         % 2.row

rost_caud = [X-8 X+8 X+16]      % Intersected Rost-caudal contacts
row = row2;
medial = medial+max(row1);      %% NEEDED for plotting
```

```
lateral = lateral+max(row1);
y_row = 225;
y_row2 = y_row-20;

x_row = mod(X-1,8)*55;

end

if (find(row3 ==X))

medial = find(row3<X)
lateral = find(row3>X)

rost_caud = [X-16 X-8 X+8]
row = row3;                    %3.row
medial = medial+max(row2);
lateral = lateral+max(row2);
y_row = 125;
y_row2 = y_row-20;

x_row = mod(X-1,8)*55;

end

if (find(row4 ==X))

medial = find(row4<X);
lateral = find(row4>X);
                               %4.row
rost_caud = [X-8 X-16 X-24]
row = row4;
medial = medial+max(row3);
lateral = lateral+max(row3);
y_row=50;
y_row2 = y_row-20;

x_row = mod(X-1,8)*55;

end

R=ones(8,1)                    % Autocorrelation Coeff is defined as '1'.

for i=1:length(medial)
   r = corrcoef(LFP_data_sorted(:,X),LFP_data_sorted(:,medial(i)));
   R(i) = r(2,1) ;
end
```

```
for ii=1:length(lateral)
   r = corrcoef(LFP_data_sorted(:,X),LFP_data_sorted(:,lateral(ii)));
   R(length(medial)+1+ii) = r(2,1);

end


for k=1:length(rost_caud)

   r = corrcoef(LFP_data_sorted(:,X),LFP_data_sorted(:,rost_caud(k)))
   Rc(k) = r(2,1) ;
end

electrode=zeros(8,4);
electrode(row) = R;
electrode(rost_caud) = Rc;
figure(100);clf;imagesc(electrode')

Rmean = mean(R);
Rcmean =mean(Rc);
A = num2str(Rmean);
B = num2str(Rcmean);
text('units','pixels','position',[x_row y_row],'fontsize',12,'string',A)
text('units','pixels','position',[x_row y_row2],'fontsize',12,'string',B)

pause(1);

end

   end
end

for x = 1:length(functions_to_run)
   if functions_to_run(x) == 207
  unfiltered_data=unfiltered_data(:,1:signal_length);

duration = 20;
LOOP = 20;
Fs = sampling_rate;
DURATION=duration/LOOP;
% use it for quite data

%
% Ns * Ts = Ncycles * Trej
%
```

```
% Ts = 1/sampling_rate;
% Ncycles = # of cycles will be each averaged data
% Tnoise = 1/60 (60Hz elimination)

Trej = 1/60;
Ncycles = 100; % for 16kHz sampling rate
Ts = 1/sampling_rate;
Ns = Ncycles*Trej/Ts;


duration = 1;
LOOP = 20;
Fs = sampling_rate;
DURATION=duration/LOOP;
N=2048;

%% Taking the Power spectrum first for each period then average it.

% for ii=1:LOOP
%
% [Pww(:,ii), F] = pwelch(detrend(unfiltered_data((ii-
1)*DURATION*Fs+1:ii*DURATION*Fs,:)),hanning(N),N/2,N,sampling_rate);
% Pww(:,ii)  = 5*log10(Pww(:,ii).^2);
% end
%
% averaged_Pww = sum(Pww(:,1:20)',1)/20;
% averaged_Pww = averaged_Pww';

% figure;plot(F,averaged_Pww)
% Apparently it does not make any difference taking the power spect from
% the averaged DATA

%% Averaging the data

tt=1/Fs:1/Fs:duration;

DATA = zeros(min(size(unfiltered_data)), Fs*DURATION);
unfiltered_data = unfiltered_data';

for Y=1:LOOP,

   DATA = DATA+unfiltered_data(:,(Y-1)*DURATION*Fs+1:Y*DURATION*Fs);
end

DATA=DATA'/LOOP;
```

```
unfiltered_data = unfiltered_data';

   end
end


 for x = 1:length(functions_to_run)
   if functions_to_run(x) == 210

%        unfiltered_DATA = LFP_data4(:,1:31);

       unfiltered_DATA(:,32) = mean(unfiltered_DATA(:,1:31)');
       unfiltered_data(:,32) = mean(unfiltered_data(:,1:31)');
       N=2048;

%        unfiltered_DATA = LFP_data_sorted;
%       I = input('Like to return desired channels (1) or Electrode Organization (0)
or Random (any)');
        I=0;

     if (I == 1)
        ch1 = input('1.pair channel 1 ');
        ch2 = input('1.pair channel 2 ');
        ch3 = input('2.pair channel 1 ');
        ch4 = input('2.pair channel 2 ');
        ch5 = input('3.pair channel 1 ');
        ch6 = input('3.pair channel 2 ');
        ch7 = input('4.pair channel 1 ');
        ch8 = input('4.pair channel 2 ');

     elseif (I == 0 )

        RC1 = randi(8);
        RC2 = randi(16);            % Define your preference whether in Rostro-
Caudal (RC) or Medio-Lateral (ML) direction
        RC3 = 24;
        ML1  = 3;
        ML2 = 7 ;


        ch1 = randi(8);
        ch2 = ch1+RC1;

        ch3 = randi([8 16]);
        ch4 = ch3+RC2;
```

```
        ch5 = randi([16 24]);
        ch6 = ch5+RC1 ;

        ch7 = randi([24 31]);

       ch8 = ch7 - ceil(mod(ch7,24)/2);

    else

ch1 = randi(number_channels);
ch2 = randi(number_channels);

ch3 = randi(number_channels);
ch4 = randi(number_channels);

ch5 = randi(number_channels);
ch6 = randi(number_channels);

ch7 = randi(number_channels);
ch8 = randi(number_channels);
    end

%%



%       Windowing and Video segments start here
%       Playing video file simultaneously with temporal coherence analysis
%       Video_data max is taken as 5 sec

%       video_data = VideoReader(['videos/trial' num2str(trial) '.avi']);
%       all_frames = read(video_data);
%
%       clear i
%       Dur = length(unfiltered_DATA)/sampling_rate;            % recalculating the
duration of data for temp coherence
%
%       II = input('Would you like the movie file to be played? (1/0)');  % Run the
video file/NOt
%
%  for i=1:1:Dur;                                  % 1 sec window spacing
%       i;
%
%     if (II ==1)
%       if (i<=5)                                 % limit the video file with 5 sec
```

```
%       l =  i*video_frame_rate;                        %% Synch frame video file  to
data file
%       for ll = (l-video_frame_rate) +1 : l
%
%         figure(112);clf;imagesc(all_frames(:,:,:,ll));colormap(gray);
%         t1 = num2str((i-1),'% d'); t2 = num2str(i,'% d');
%         title([t1,'s - ',t2,'s'])
%         pause(0.1)
%
%       end
%       end
%  end
%
% N=1024;
% unfiltered_DATA = unfiltered_data(((i-1)*sampling_rate+1):i*sampling_rate,:);

%%

[COHERE,f] =mscohere(unfiltered_DATA(:,ch1),
unfiltered_DATA(:,ch2),hanning(N/4) ,N/8 ,N/2 ,sampling_rate);
[COHERE2,f] =mscohere(unfiltered_DATA(:,ch3),
unfiltered_DATA(:,ch4),hanning(N/4) ,N/8 ,N/2 ,sampling_rate);
[COHERE3,f] =mscohere(unfiltered_DATA(:,ch5),
unfiltered_DATA(:,ch6),hanning(N/4) ,N/8 ,N/2 ,sampling_rate);
[COHERE4,f] =mscohere(unfiltered_DATA(:,ch7),
unfiltered_DATA(:,ch8),hanning(N/4) ,N/8 ,N/2 ,sampling_rate);

figure;
hold on; subplot(2,1,1);
plot(f,COHERE);hold on
plot(f,COHERE2,'r');plot(f,COHERE3,'g');plot(f,COHERE4,'k');
axis([ 0 2000 0 1])
COH1 = num2str([ ch1 ch2 ],'% d');
COH2= num2str([ ch3 ch4 ],'% d');
COH3 = num2str([ ch5 ch6 ],'% d');
COH4 = num2str([ ch7 ch8 ],'% d');
legend(COH1,COH2,COH3,COH4)
t1 = num2str((i-1),'% d'); t2 = num2str(i,'% d');
title([t1,'s - ',t2,'s'])



%% LOAD electode image into matlab

a=imread('electrode_contacts_numbered.png','png');
subplot(2,1,2)
```

```
image(a);
hold on

% Specifiy the contact coordinates on the image

refx1 = mod(ch1,8);
if(refx1 == 0);
   refx1 = 8;
end
X_ch1 = 140+((refx1-1) * 50);
Y_ch1 = (ceil(ch1/8) * 50);
plot(X_ch1,Y_ch1,'--bs','LineWidth',10) ;       % 1. pairs

refx2 = mod(ch2,8);
if(refx2 == 0);
   refx2 = 8;
end


X_ch2 = 140+((refx2-1) * 50);
Y_ch2 = (ceil(ch2/8) * 50);
plot(X_ch2,Y_ch2,'--bs','LineWidth',10)   ;

refx3 = mod(ch3,8);
if(refx3 == 0);
   refx3 = 8;
end
X_ch3 = 140+((refx3-1) * 50);
Y_ch3 = (ceil(ch3/8) * 50);
plot(X_ch3,Y_ch3,'--rs','LineWidth',10)     %2.pairs
refx6 = mod(ch6,8);
if(refx6 == 0);
   refx6 = 8;
end
X_ch6 = 140+((refx6-1) * 50);
Y_ch6 = (ceil(ch6/8) * 50);
plot(X_ch6,Y_ch6,'--gs','LineWidth',10)

refx7 = mod(ch7,8);                         % 4.pairs
if(refx7 == 0);
   refx7 = 8;
end
X_ch7 = 140+((refx7-1) * 50);
Y_ch7 = (ceil(ch7/8) * 50);
plot(X_ch7,Y_ch7,'--ks','LineWidth',10)
```

```
refx8 = mod(ch8,8);
if(refx8 == 0);
   refx8 = 8;
end
X_ch8 = 140+((refx8-1) * 50);
Y_ch8 = (ceil(ch8/8) * 50);
plot(X_ch8,Y_ch8,'--ks','LineWidth',10)



% N=2048;
% [Pww_cer, F] =
pwelch(unfiltered_DATA(:,1:number_channels),hanning(N),N/2,N,sampling_rate);
% Cerebellum Power Spectrum
% % [Pww_cor, F] =
pwelch(unfiltered_data(:,32:62),hanning(N),N/2,N,sampling_rate); % Cerebellum
Power Spectrum
%
% cc = hsv(50);
%
%
% Pww_cer = 10*log10(Pww_cer);
% % Pww_cor = 10*log10(Pww_cor);
%
% figure(11);clf;plot(F,Pww_cer,'color',cc(trial,:));axis([0 1000 -140 -90])
% pause(3)

%        end
   end
 end

 % check the rostro-caudal cross-corr spectrum estimation
 % Enter the desired channels



  for x = 1:length(functions_to_run)
    if functions_to_run(x) == 211

 for i=1:6

base_ch1(i) = input('enter first one:'); % enter the desired line starting from first
contact
    base_ch2(i) = input('enter second one:');
```

REFERENCES

Abdul-Wahab R, S.B., Mina S, Sampath S, Santhakumar V, Pfister Bj (2011). "Precisely controllable traumatic brain injury devices for rodent models. ", in: Bioengineering Conference (NEBEC), 2011 IEEE 37th Annual Northeast, 1-2.).

Adrian, E.D. (1944). Localization in Cerebrum and Cerebellum. Br Med J 2**,** 137-140.

Ai, J., and Baker, A. (2002). Presynaptic hyperexcitability at cerebellar synapses in traumatic injury rat. Neuroscience letters 332**,** 155-158. doi: 10.1016/S0304-3940(02)00945-X.

Ai, J., and Baker, A. (2004). Presynaptic excitability as a potential target for the treatment of the traumatic cerebellum. Pharmacology 71**,** 192-198. doi: 10.1159/000078085.

Ai, J., Liu, E., Park, E., and Baker, A. (2007). Structural and functional alterations of cerebellum following fluid percussion injury in rats. Experimental brain research. Experimentelle Hirnforschung. Expérimentation cérébrale 177**,** 95-112. doi: 10.1007/s00221-006-0654-9.

Alavi, A., Mirot, A., Newberg, A., Alves, W., Gosfield, T., Berlin, J., Reivich, M., and Gennarelli, T. (1997). Fluorine-18-FDG evaluation of crossed cerebellar diaschisis in head injury. J Nucl Med 38**,** 1717-1720.

Anis, N.A., Berry, S.C., Burton, N.R., and Lodge, D. (1983). The dissociative anaesthetics, ketamine and phencyclidine, selectively reduce excitation of central mammalian neurones by N-methyl-aspartate. British Journal of Pharmacology 79**,** 565-575.

Armstrong, D., and Drew, T. (1980). Responses in the posterior lobe of the rat cerebellum to electrical stimulation of cutaneous afferents to the snout. Journal of Physiology, 309**,** 357-374.

Armstrong, D.M., and Harvey, R.J. (1968). Responses to a spino-olivo-cerebellar pathway in the cat. Journal of Physiology 194**,** 147-168.

Armstrong, D.M., and Rawson, J.A. (1979). Activity patterns of cerebellar cortical neurones and climbing fibre afferents in the awake cat. Journal of Physiology VOL 289**,** 425-448.

Atkins, M., and Apps, R. (1997a). Somatotopical organisation within the climbing fibre projection to the paramedian lobule and copula pyramidis of the rat cerebellum. The Journal of comparative neurology 389**,** 249-263. doi: 10.1002/(SICI)1096-9861(19971215)389:2<249::AID-CNE5>3.0.CO;2-1.

Atkins, M.J., and Apps, R. (1997b). Somatotopical organisation within the climbing fibre projection to the paramedian lobule and copula pyramidis of the rat cerebellum. J Comp Neurol 389**,** 249-263.

Axmacher, N., Elger, C.E., and Fell, J. (2008). Ripples in the medial temporal lobe are relevant for human memory consolidation. Brain 131**,** 1806-1817. doi: 10.1093/brain/awn103.

Baker, M.R., Javid, M., and Edgley, S.A. (2001). Activation of cerebellar climbing fibres to rat cerebellar posterior lobe from motor cortical output pathways. Journal of Physiology, 536**,** 825-839.

Basford, J.R., Chou, L.-S.S., Kaufman, K.R., Brey, R.H., Walker, A., Malec, J.F., Moessner, A.M., and Brown, A.W. (2003). An assessment of gait and balance deficits after traumatic brain injury. Archives of physical medicine and rehabilitation 84**,** 343-349. doi: 10.1053/apmr.2003.50034.

Bazhenov, M., Lonjers, P., Skorheim, S., Bedard, C., and Dstexhe, A. (2011). Non-homogeneous extracellular resistivity affects the current-source density profiles of up-down state oscillations. Philos Trans A Math Phys Eng Sci 369**,** 3802-3819. doi: 10.1098/rsta.2011.0119.

Bengtsson, F., and Jörntell, H. (2007). Ketamine and xylazine depress sensory-evoked parallel fiber and climbing fiber responses. Journal of neurophysiology 98**,** 1697-1705. doi: 10.1152/jn.00057.2007.

Benzinger, T.L., Brody, D., Cardin, S., Curley, K.C., Mintun, M.A., Mun, S.K., Wong, K.H., and Wrathall, J.R. (2009). Blast-related brain injury: imaging for clinical and research applications: report of the 2008 st. Louis workshop. Journal of neurotrauma 26**,** 2127-2144. doi: 10.1089/neu.2009-0885.

Bosman, L., Koekkoek, S., Shapiro, J., Rijken, B., Zandstra, F., Van Der Ende, B., Owens, C., Potters, J.-W., De Gruijl, J., Ruigrok, T., and De Zeeuw, C. (2010). Encoding of whisker input by cerebellar Purkinje cells. Journal of Physiology 588**,** 3757-3783. doi: 10.1113/jphysiol.2010.195180.

Bower, J., and Woolston, D. (1983). Congruence of spatial organization of tactile projections to granule cell and Purkinje cell layers of cerebellar hemispheres of the albino rat: vertical organization of cerebellar cortex. Journal of neurophysiology 49**,** 745-766.

Braga, L.W., Souza, L.N., Najjar, Y.J., and Dellatolas, G. (2007a). Magnetic resonance imaging (MRI) findings and neuropsychological sequelae in children after severe traumatic brain injury: the role of cerebellar lesion. Journal of child neurology 22**,** 1084-1089. doi: 10.1177/0883073807306246.

Braga, L.W., Souza, L.N., Najjar, Y.J., and Dellatolas, G. (2007b). Magnetic resonance imaging (MRI) findings and neuropsychological sequelae in children after severe

traumatic brain injury: the role of cerebellar lesion. J Child Neurol 22**,** 1084-1089. doi: 22/9/1084 [pii].

Bramlett, H.M., and Dietrich, W.D. (2007). Progressive damage after brain and spinal cord injury: pathomechanisms and treatment strategies. Prog Brain Res 161**,** 125-141. doi: 10.1016/S0079-6123(06)61009-1.

Brice, J., Mclellan, D.L., and Wright, G.D. (1983). Epilepsy, the cerebellum, and cerebellar stimulation. Lancet 2**,** 1500.

Bruns, J., Jr., and Hauser, W.A. (2003). The epidemiology of traumatic brain injury: a review. Epilepsia 44 Suppl 10**,** 2-10.

Buzsáki, G., Anastassiou, C., and Koch, C. (2012). The origin of extracellular fields and currents--EEG, ECoG, LFP and spikes. Nature reviews. Neuroscience 13**,** 407-420. doi: 10.1038/nrn3241.

Cerminara, N.L., Apps, R., and Marple-Horvat, D.E. (2009). An internal model of a moving visual target in the lateral cerebellum. Journal of Physiology 587**,** 429-442.

Cernak, I. (2005). Animal models of head trauma. NeuroRx : the journal of the American Society for Experimental NeuroTherapeutics 2**,** 410-422. doi: 10.1602/neurorx.2.3.410.

Chae, J.H., Kim, S.K., Wang, K.C., Kim, K.J., Hwang, Y.S., and Cho, B.K. (2001). Hemifacial seizure of cerebellar ganglioglioma origin: seizure control by tumor resection. Epilepsia 42**,** 1204-1207.

Chen, S., and Aston-Jones, G. (1994). Cerebellar injury induces NADPH diaphorase in Purkinje and inferior olivary neurons in the rat. Experimental neurology 126**,** 270-276. doi: 10.1006/exnr.1994.1064.

Cohen, A.S., Pfister, B.J., Schwarzbach, E., Sean Grady, M., Goforth, P.B., and Satin, L.S. (2007). Injury-induced alterations in CNS electrophysiology. Prog Brain Res 161**,** 143-169.

Connolly, J.F., and D'arcy, R.C. (2000). Innovations in neuropsychological assessment using event-related brain potentials. Int J Psychophysiol 37**,** 31-47.

Conti, A., Raghupathi, R., Trojanowski, J., and Mcintosh, T. (1998). Experimental brain injury induces regionally distinct apoptosis during the acute and delayed post-traumatic period. The Journal of neuroscience : the official journal of the Society for Neuroscience 18**,** 5663-5672.

Courjon J, S.E. (1972). Handbook of electroencephalography and clinical neurophysiology. . Clinical EEG IV Traumatic disorders 14B. Amsterdam: E**,** p. 1–104.

Courtemanche, R., Robinson, J.C., and Aponte, D.I. (2013). Linking oscillations in cerebellar circuits. Front Neural Circuits 7**,** 125. doi: 10.3389/fncir.2013.00125.

De Solages, C., Szapiro, G., Brunel, N., Hakim, V., Isope, P., Buisseret, P., Rousseau, C., Barbour, B., and Lena, C. (2008a). High-frequency organization and synchrony of activity in the purkinje cell layer of the cerebellum. Neuron 58**,** 775-788. doi: 10.1016/j.neuron.2008.05.008.

De Solages, C., Szapiro, G., Brunel, N., Hakim, V., Isope, P., Buisseret, P., Rousseau, C., Barbour, B., and Léna, C. (2008b). High-frequency organization and synchrony of activity in the purkinje cell layer of the cerebellum. Neuron 58**,** 775-788. doi: 10.1016/j.neuron.2008.05.008.

De Zeeuw, C.I., Hoebeek, F.E., Bosman, L.W.J., Schonewille, M., Witter, L., and Koekkoek, S.K. (2011). Spatiotemporal firing patterns in the cerebellum. Nature Reviews Neuroscience 12**,** 327-344.

Delande, O., Rodriguez, D., Chiron, C., and Fohlen, M. (2001). Successful surgical relief of seizures associated with hamartoma of the floor of the fourth ventricle in children: report of two cases. Neurosurgery 49**,** 726-730; discussion 730-721.

Ding, Y., Yao, B., Lai, Q., and Mcallister, J.P. (2000). Impaired motor learning and diffuse axonal damage in motor and visual systems of the rat following traumatic brain injury. Neurological research 23**,** 193-202. doi: 10.1179/016164101101198334.

Diwakar, S., Lombardo, P., Solinas, S., Naldi, G., and D'angelo, E. (2011). Local field potential modeling predicts dense activation in cerebellar granule cells clusters under LTP and LTD control. PLoS One 6**,** e21928. doi: 10.1371/journal.pone.0021928.

Dixon, C.E., Lyeth, B.G., Povlishock, J.T., Findling, R.L., Hamm, R.J., Marmarou, A., Young, H.F., and Hayes, R.L. (1987a). A fluid percussion model of experimental brain injury in the rat. J Neurosurg 67**,** 110-119. doi: 10.3171/jns.1987.67.1.0110.

Dixon, C.E., Lyeth, B.G., Povlishock, J.T., Findling, R.L., Hamm, R.J., Marmarou, A., Young, H.F., and Hayes, R.L. (1987b). A fluid percussion model of experimental brain injury in the rat. Journal of neurosurgery 67**,** 110-119. doi: 10.3171/jns.1987.67.1.0110.

Dow, R.S. (1938). The electrical activity of the cerebellum and its functional significance. J Physiol 94**,** 67-86.

Ebner, T.J., Hewitt, A.L., and Popa, L.S. (2011). What features of limb movements are encoded in the discharge of cerebellar neurons? Cerebellum 10**,** 683-693.

Eccles, J., Sasaki, K., and Strata, P. (1967). Interpretation of the potential fields generated in the cerebellar cortex by a mossy fibre volley. Experimental brain research. Experimentelle Hirnforschung. Expérimentation cérébrale 3**,** 58-80. doi: 10.1007/BF00234470.

Eccles, J.C., Llinas, R., and Sasaki, K. (1966). Intracellularly recorded responses of the cerebellar Purkinje cells. Exp Brain Res 1**,** 161-183.

Fatemi, S.H., Aldinger, K.A., Ashwood, P., Bauman, M.L., Blaha, C.D., Blatt, G.J., Chauhan, A., Chauhan, V., Dager, S.R., Dickson, P.E., Estes, A.M., Goldowitz, D., Heck, D.H., Kemper, T.L., King, B.H., Martin, L.A., Millen, K.J., Mittleman, G., Mosconi, M.W., Persico, A.M., Sweeney, J.A., Webb, S.J., and Welsh, J.P. (2012). Consensus Paper: Pathological Role of the Cerebellum in Autism. Cerebellum**,** 1-31.

Floyd, C.L., Golden, K.M., Black, R.T., Hamm, R.J., and Lyeth, B.G. (2002). Craniectomy position affects morris water maze performance and hippocampal cell loss after parasagittal fluid percussion. Journal of neurotrauma 19**,** 303-316. doi: 10.1089/089771502753594873.

Foerster, O., Altenburger, H. (1935). Elektrobiologische Vorgänge an der menschlichen Hirnrinde. . Deutsche Zeitschrift für Nervenheilkunde 135.

Freed, S., and Hellerstein, L.F. (1997). Visual electrodiagnostic findings in mild traumatic brain injury. Brain Inj 11**,** 25-36.

Fukuda, K., Aihara, N., Sagar, S., Sharp, F., Pitts, L., Honkaniemi, J., and Noble, L. (1996). Purkinje cell vulnerability to mild traumatic brain injury. Journal of neurotrauma 13**,** 255-266. doi: 10.1089/neu.1996.13.255.

Gale, S.D., Baxter, L., Roundy, N., and Johnson, S.C. (2005a). Traumatic brain injury and grey matter concentration: a preliminary voxel based morphometry study. J Neurol Neurosurg Psychiatry 76**,** 984-988. doi: 76/7/984 [pii]10.1136/jnnp.2004.036210.

Gale, S.D., Baxter, L., Roundy, N., and Johnson, S.C. (2005b). Traumatic brain injury and grey matter concentration: a preliminary voxel based morphometry study. Journal of neurology, neurosurgery, and psychiatry 76**,** 984-988. doi: 10.1136/jnnp.2004.036210.

Gao, J.H., Parsons, L.M., Bower, J.M., Xiong, J., Li, J., and Fox, P.T. (1996). Cerebellum implicated in sensory acquisition and discrimination rather than motor control. Science 272**,** 545-547.

Geraud, J., Rascol, A., and Benazet-Favarel, A.M. (1965). [The tremor of cerebellar diseases and multiple sclerosis]. Rev Prat 15**,** 4201-4208.

Goodman, J.C., Cherian, L., Bryan, R.M., and Robertson, C.S. (1994). Lateral cortical impact injury in rats: pathologic effects of varying cortical compression and impact velocity. Journal of neurotrauma 11**,** 587-597.

Gupta, N.K., Verma, N.P., Guidice, M.A., and Kooi, K.A. (1986). Visual evoked response in head trauma: pattern-shift stimulus. Neurology 36**,** 578-581.

Hallam, T.M., Floyd, C.L., Folkerts, M.M., Lee, L.L., Gong, Q.Z.Z., Lyeth, B.G., Muizelaar, J.P., and Berman, R.F. (2004). Comparison of behavioral deficits and acute neuronal degeneration in rat lateral fluid percussion and weight-drop brain injury models. Journal of neurotrauma 21**,** 521-539. doi: 10.1089/089771504774129865.

Hamm, R.J. (2001). Neurobehavioral assessment of outcome following traumatic brain injury in rats: an evaluation of selected measures. Journal of neurotrauma 18**,** 1207-1216. doi: 10.1089/089771501317095241.

Hamm, R.J., Temple, M.D., Pike, B.R., O'dell, D.M., Buck, D.L., and Lyeth, B.G. (1996). Working memory deficits following traumatic brain injury in the rat. J Neurotrauma 13**,** 317-323.

Hart, H. (2011). The cerebellum, cognition, and behaviour. Developmental Medicine and Child Neurology 53**,** 1069-1070.

Hattori, N., Huang, S.C., Wu, H.M., Yeh, E., Glenn, T.C., Vespa, P.M., Mcarthur, D., Phelps, M.E., Hovda, D.A., and Bergsneider, M. (2003). Correlation of regional metabolic rates of glucose with glasgow coma scale after traumatic brain injury. J Nucl Med 44**,** 1709-1716.

Hayes, R.L., Jenkins, L.W., Lyeth, B.G., Balster, R.L., Robinson, S.E., Clifton, G.L., Stubbins, J.F., and Young, H.F. (1988). Pretreatment with phencyclidine, an N-methyl-D-aspartate antagonist, attenuates long-term behavioral deficits in the rat produced by traumatic brain injury. J Neurotrauma 5**,** 259-274.

Herculano-Houzel, S. (2010). Coordinated scaling of cortical and cerebellar numbers of neurons. Frontiers in neuroanatomy 4**,** 12. doi: 10.3389/fnana.2010.00012.

Herculano-Houzel, S., Mota, B., and Lent, R. (2006). Cellular scaling rules for rodent brains. Proceedings of the National Academy of Sciences of the United States of America 103**,** 12138-12143. doi: 10.1073/pnas.0604911103.

Hewitt, A.L., Popa, L.S., Pasalar, S., Hendrix, C.M., and Ebner, T.J. (2011). Representation of limb kinematics in Purkinje cell simple spike discharge is conserved across multiple tasks. Journal of Neurophysiology 106**,** 2232-2247.

Hill, N.J., Gupta, D., Brunner, P., Gunduz, A., Adamo, M.A., Ritaccio, A., and Schalk, G. (2012). Recording human electrocorticographic (ECoG) signals for neuroscientific research and real-time functional cortical mapping. J Vis Exp. doi: 10.3791/3993.

Hoshino, S., Kobayashi, S., Furukawa, T., Asakura, T., and Teramoto, A. (2003). Multiple immunostaining methods to detect traumatic axonal injury in the rat fluid-percussion brain injury model. Neurologia medico-chirurgica 43**,** 165-174.

Hustveit, O., Maurset, A., and Oye, I. (1995). Interaction of the chiral forms of ketamine with opioid, phencyclidine, σ and muscarinic receptors. Pharmacology and Toxicology 77**,** 355-359.

Iwadate, Y., Saeki, N., Namba, H., Odaki, M., Oka, N., and Yamaura, A. (1989). Post-traumatic intention tremor--clinical features and CT findings. Neurosurg Rev 12 Suppl 1**,** 500-507.

Jeret, J.S., Mandell, M., Anziska, B., Lipitz, M., Vilceus, A.P., Ware, J.A., and Zesiewicz, T.A. (1993). Clinical predictors of abnormality disclosed by computed tomography after mild head trauma. Neurosurgery 32**,** 9-15; discussion 15-16.

Joynt, R.J. (1958). Micro-electrode studies of cerebellar electrical activity in the frog. J Physiol 144**,** 23-37.

Katayama, Y., Young, H.F., Dunbar, J.G., and Hayes, R.L. (1988). Coma associated with flaccidity produced by fluid-percussion concussion in the cat. II: Contribution of activity in the pontine inhibitory system. Brain Inj 2**,** 51-66.

Kelly, J.P., and Rosenberg, J.H. (1997). Diagnosis and management of concussion in sports. Neurology 48**,** 575-580.

Kelly, P.J. (1980). Microelectrode recording for the somatotopic placement of stereotactic thalamic lesions in the treatment of parkinsonian and cerebellar intention tremor. Appl Neurophysiol 43**,** 262-266.

Knuepffer, C., Murdoch, B.E., Lloyd, D., Lewis, F.M., and Hinchliffe, F.J. (2012). Reduced N400 semantic priming effects in adult survivors of paediatric and

adolescent traumatic brain injury. Brain Lang 123**,** 52-63. doi: 10.1016/j.bandl.2012.06.009.

Kushner, M., Tobin, M., Alavi, A., Chawluk, J., Rosen, M., Fazekas, F., Alavi, J., and Reivich, M. (1987). Cerebellar glucose consumption in normal and pathologic states using fluorine-FDG and PET. J Nucl Med 28**,** 1667-1670.

Lalo, E., Thobois, S., Sharott, A., Polo, G., Mertens, P., Pogosyan, A., and Brown, P. (2008). Patterns of bidirectional communication between cortex and basal ganglia during movement in patients with Parkinson disease. J Neurosci 28**,** 3008-3016. doi: 10.1523/JNEUROSCI.5295-07.2008.

Langlois, J.A., Rutland-Brown, W., and Wald, M.M. (2006). The epidemiology and impact of traumatic brain injury: a brief overview. J Head Trauma Rehabil 21**,** 375-378.

Larson, B., Miller, S., and Oscarsson, O. (1969). Termination and functional organization of the dorsolateral spino-olivocerebellar path. The Journal of physiology 203**,** 611-640.

Larsson, L.E., Melin, K.A., Nordstrom-Ohrberg, G., Silfverskiold, B.P., and Ohrberg, K. (1954). Acute head injuries in boxers; clinical and electroencephalographic studies. Acta Psychiatr Neurol Scand Suppl 95**,** 2-42.

Leblanc, K.E. (1999). Concussion in sport: diagnosis, management, return to competition. Compr Ther 25**,** 39-44; discussion 45.

Lehew, G., and Nicolelis, M.a.L. (2008). "State-of-the-Art Microwire Array Design for Chronic Neural Recordings in Behaving Animals," in Methods for Neural Ensemble Recordings, ed. M.a.L. Nicolelis. 2nd ed (Boca Raton (FL)).

Leuthardt, E.C., Schalk, G., Roland, J., Rouse, A., and Moran, D.W. (2009). Evolution of brain-computer interfaces: going beyond classic motor physiology. Neurosurg Focus 27**,** E4. doi: 10.3171/2009.4.FOCUS0979.

Levin, H.S., and Eisenberg, H.M. (1978). Neuropsychological outcome of closed head injury in children and adolescents. Child's brain 5**,** 281-292.

Louis, E.D., Lynch, T., Ford, B., Greene, P., Bressman, S.B., and Fahn, S. (1996a). Delayed-onset cerebellar syndrome. Archives of neurology 53**,** 450-454.

Louis, E.D., Lynch, T., Ford, B., Greene, P., Bressman, S.B., and Fahn, S. (1996b). Delayed-onset cerebellar syndrome. Arch Neurol 53**,** 450-454.

Ludwig, K.A., Langhals, N.B., Joseph, M.D., Richardson-Burns, S.M., Hendricks, J.L., and Kipke, D.R. (2011). Poly(3,4-ethylenedioxythiophene) (PEDOT) polymer

coatings facilitate smaller neural recording electrodes. J Neural Eng 8**,** 014001. doi: 10.1088/1741-2560/8/1/014001.

Marklund, N., Bakshi, A., Castelbuono, D.J., Conte, V., and Mcintosh, T.K. (2006). Evaluation of pharmacological treatment strategies in traumatic brain injury. Curr Pharm Des 12**,** 1645-1680.

Matschke, J., Laas, R., and Schulz, F. (2006). Cerebellar atrophy following mild head injury in a 4-year-old girl. Pediatric neurosurgery 43**,** 330-333. doi: 10.1159/000103317.

Matschke, J., Laas, R., and Schulz, F. (2007). Cerebellar atrophy following mild head injury in a 4-year-old girl. Pediatr Neurosurg 43**,** 330-333. doi: 000103317 [pii] 10.1159/000103317.

Matthews, M., Carey, M., Soblosky, J., Davidson, J., and Tabor, S. (1998). Focal brain injury and its effects on cerebral mantle, neurons, and fiber tracks. Brain research 794**,** 1-18. doi: 10.1016/S0006-8993(98)00107-3.

Mautes, A., Fukuda, K., and Noble, L. (1996). Cellular response in the cerebellum after midline traumatic brain injury in the rat. Neuroscience letters 214**,** 95-98. doi: 10.1016/0304-3940(96)12916-5.

Mcintosh, T.K., Vink, R., Noble, L., Yamakami, I., Fernyak, S., Soares, H., and Faden, A.L. (1989). Traumatic brain injury in the rat: characterization of a lateral fluid-percussion model. Neuroscience 28**,** 233-244.

Mesiwala, A.H., Kuratani, J.D., Avellino, A.M., Roberts, T.S., Sotero, M.A., and Ellenbogen, R.G. (2002). Focal motor seizures with secondary generalization arising in the cerebellum. Case report and review of the literature. J Neurosurg 97**,** 190-196. doi: 10.3171/jns.2002.97.1.0190.

Meyer, J.S., Kondo, A., Nomura, F., Sakamoto, K., and Teraura, T. (1970). Cerebral hemodynamics and metabolism following experimental head injury. J Neurosurg 32**,** 304-319. doi: 10.3171/jns.1970.32.3.0304.

Middleton, S., Racca, C., Cunningham, M., Traub, R., Monyer, H., Knöpfel, T., Schofield, I., Jenkins, A., and Whittington, M. (2008). High-frequency network oscillations in cerebellar cortex. Neuron 58**,** 763-774. doi: 10.1016/j.neuron.2008.03.030.

Morales, D.M., Marklund, N., Lebold, D., Thompson, H.J., Pitkanen, A., Maxwell, W.L., Longhi, L., Laurer, H., Maegele, M., Neugebauer, E., Graham, D.I., Stocchetti, N., and Mcintosh, T.K. (2004). Experimental models of traumatic brain injury: do we really need to build a better mousetrap? Neuroscience 136**,** 971-989. doi: 10.1016/j.neuroscience.2005.08.030.

Mukawa, J. (1985). [the cerebellum and epilepsy]. No Shinkei Geka 13**,** 7-14.

Newberg, A.B., Alavi, A., and Alavi, J. (2000). Contralateral cortical diaschisis in a patient with cerebellar astrocytoma after radiation therapy. Clin Nucl Med 25**,** 431-433.

Nicolelis, M.A., Dimitrov, D., Carmena, J.M., Crist, R., Lehew, G., Kralik, J.D., and Wise, S.P. (2003). Chronic, multisite, multielectrode recordings in macaque monkeys. Proc Natl Acad Sci U S A 100**,** 11041-11046. doi: 10.1073/pnas.1934665100.

Niimura, K., Chugani, D.C., Muzik, O., and Chugani, H.T. (1999). Cerebellar reorganization following cortical injury in humans: effects of lesion size and age. Neurology 52**,** 792-797.

Nilsson, P., Ronne-Engström, E., Flink, R., Ungerstedt, U., Carlson, H., and Hillered, L. (1994). Epileptic seizure activity in the acute phase following cortical impact trauma in rat. Brain Research 637**,** 227-232. doi: http://dx.doi.org/10.1016/0006-8993(94)91237-8.

O'hearn, E., and Molliver, M.E. (1997). The olivocerebellar projection mediates ibogaine-induced degeneration of Purkinje cells: a model of indirect, trans-synaptic excitotoxicity. The Journal of neuroscience : the official journal of the Society for Neuroscience 17**,** 8828-8841.

Ordek, G., Groth, J., and Sahin, M. (2013). Differential effects of ketamine/xylazine anesthesia on the cerebral and cerebellar cortical activities in the rat. Journal of neurophysiology 109**,** 1435-1443. doi: 10.1152/jn.00455.2012.

Oscarsson, O. (1968). Termination and functional organization of the ventral spino-olivocerebellar path. J Physiol 196**,** 453-478.

Pampus, F., and Grote, W. (1956). Elektrencephalographische und klinische Befunde bei Boxern und ihre Bedeutung für die Pathophysiologie der traumatischen Hirnschädigung. Archiv für Psychiatrie und Nervenkrankheiten 194**,** 152-178. doi: 10.1007/BF00342839.

Park, E., Mcknight, S., Ai, J., and Baker, A. (2006). Purkinje cell vulnerability to mild and severe forebrain head trauma. Journal of neuropathology and experimental neurology 65**,** 226-234. doi: 10.1097/01.jnen.0000202888.29705.93.

Pellerin, J.P., and Lamarre, Y. (1997). Local field potential oscillations in primate cerebellar cortex during voluntary movement. J Neurophysiol 78**,** 3502-3507.

Potts, M.B., Adwanikar, H., and Noble-Haeusslein, L.J. (2009). Models of traumatic cerebellar injury. Cerebellum 8**,** 211-221. doi: 10.1007/s12311-009-0114-8.

Prasad, A., and Sanchez, J.C. (2012). Quantifying long-term microelectrode array functionality using chronic in vivo impedance testing. J Neural Eng 9**,** 026028. doi: 10.1088/1741-2560/9/2/026028.

R., J. (1950). Die praktische Anwendung des Elektroencephalogramms in Neurologie und Psychiatrie. Ein Uberblick uber 12 Jahre EEG und Klinik 9**,** 66.

Reeves, T.M., Kao, C.Q., Phillips, L.L., Bullock, M.R., and Povlishock, J.T. (2000). Presynaptic excitability changes following traumatic brain injury in the rat. J Neurosci Res 60**,** 370-379.

Roggeri, L., Rivieccio, B., Rossi, P., and D'angelo, E. (2008). Tactile stimulation evokes long-term synaptic plasticity in the granular layer of cerebellum. The Journal of neuroscience : the official journal of the Society for Neuroscience 28**,** 6354-6359. doi: 10.1523/JNEUROSCI.5709-07.2008.

Rosenthal, J.A., Foraker, R.E., Collins, C.L., and Comstock, R.D. (2014). National High School Athlete Concussion Rates From 2005-2006 to 2011-2012. Am J Sports Med. doi: 10.1177/0363546514530091.

Rubovitch, V., Ten-Bosch, M., Zohar, O., Harrison, C.R., Tempel-Brami, C., Stein, E., Hoffer, B.J., Balaban, C.D., Schreiber, S., Chiu, W.T., and Pick, C.G. (2011). A mouse model of blast-induced mild traumatic brain injury. Exp Neurol 232**,** 280-289. doi: 10.1016/j.expneurol.2011.09.018.

Sarna, J.R., and Hawkes, R. (2003). Patterned Purkinje cell death in the cerebellum. Progress in neurobiology 70**,** 473-507. doi: 10.1016/S0301-0082(03)00114-X.

Sato, M., Chang, E., Igarashi, T., and Noble, L. (2001a). Neuronal injury and loss after traumatic brain injury: time course and regional variability. Brain research 917**,** 45-54. doi: 10.1016/S0006-8993(01)02905-5.

Sato, M., Chang, E., Igarashi, T., and Noble, L.J. (2001b). Neuronal injury and loss after traumatic brain injury: time course and regional variability. Brain Res 917**,** 45-54. doi: S0006-8993(01)02905-5 [pii].

Sato, M., Chang, E., Igarashi, T., and Noble, L.J. (2001c). Neuronal injury and loss after traumatic brain injury: time course and regional variability. Brain research 917**,** 45-54.

Scheller, M., Bufler, J., Hertle, I., Schneck, H.J., Franke, C., and Kochs, E. (1996). Ketamine blocks currents through mammalian nicotinic acetylcholine receptor

channels by interaction with both the open and the closed state. Anesthesia and Analgesia 83**,** 830-836.

Schmued, L.C., Albertson, C., and Slikker, W., Jr. (1997). Fluoro-Jade: a novel fluorochrome for the sensitive and reliable histochemical localization of neuronal degeneration. Brain Res 751**,** 37-46.

Schneider E, H.H. (1962). Das EEG der traumatischen Psychosen. Dtsch Z Nervenheilk 183**,** 27.

Schnoebel, R., Wolff, M., Peters, S.C., Bräu, M.E., Scholz, A., Hempelmann, G., Olschewski, H., and Olschewski, A. (2005). Ketamine impairs excitability in superficial dorsal horn neurones by blocking sodium and voltage-gated potassium currents. British Journal of Pharmacology 146**,** 826-833.

Schwarzbach, E., Bonislawski, D.P., Xiong, G., and Cohen, A.S. (2006). Mechanisms underlying the inability to induce area CA1 LTP in the mouse after traumatic brain injury. Hippocampus 16**,** 541-550.

Servais, L., Bearzatto, B., Delvaux, V., Noel, E., Leach, R., Brasseur, M., Schiffmann, S.N., and Guy, C. (2005). Effect of chronic ethanol ingestion on Purkinje and Golgi cell firing in vivo and on motor coordination in mice. Brain Res 1055**,** 171-179. doi: 10.1016/j.brainres.2005.07.026.

Servais, L., and Cheron, G. (2005). Purkinje cell rhythmicity and synchronicity during modulation of fast cerebellar oscillation. Neuroscience 134**,** 1247-1259. doi: 10.1016/j.neuroscience.2005.06.001.

Slemmer, J.E., De Zeeuw, C.I., and Weber, J.T. (2004). Don't get too excited: mechanisms of glutamate-mediated Purkinje cell death. Progress in brain research 148**,** 367-390. doi: 10.1016/S0079-6123(04)48029-7.

Smith, D.J., Bouchal, R.L., Desanctis, C.A., Monroe, P.J., Amedro, J.B., Perrotti, J.M., and Crisp, T. (1987). Properties of the interaction between ketamine and opiate binding sites in vivo and in vitro. Neuropharmacology 26**,** 1253-1260.

Soto-Ares, G., Vinchon, M., Delmaire, C., Abecidan, E., Dhellemes, P., and Pruvo, J.P. (2001). Cerebellar atrophy after severe traumatic head injury in children. Childs Nerv Syst 17**,** 263-269.

Spanos, G.K., Wilde, E.A., Bigler, E.D., Cleavinger, H.B., Fearing, M.A., Levin, H.S., Li, X., and Hunter, J.V. (2007). cerebellar atrophy after moderate-to-severe pediatric traumatic brain injury. AJNR Am J Neuroradiol 28**,** 537-542. doi: 28/3/537 [pii].

Strahlendorf, J.C., Brandon, T., Miles, R., and Strahlendorf, H.K. (1998). AMPA receptor-mediated alterations of intracellular calcium homeostasis in rat cerebellar Purkinje cells in vitro: correlates to dark cell degeneration. Neurochemical research 23**,** 1355-1362.

Stuart, D., Ott, K., and Eldred, E. (1965). Effects of cerebellar lesions and stimulation on the shivering tremor. Am J Physiol 209**,** 1261-1266.

Teune, T.M., Van Der Burg, J., De Zeeuw, C.I., Voogd, J., and Ruigrok, T.J. (1998). Single Purkinje cell can innervate multiple classes of projection neurons in the cerebellar nuclei of the rat: a light microscopic and ultrastructural triple-tracer study in the rat. J Comp Neurol 392**,** 164-178.

Thach, W.T. (1968). Discharge of Purkinje and cerebellar nuclear neurons during rapidly alternating arm movements in the monkey. Journal of Neurophysiology 31**,** 785-797.

Thompson, H.J., Lifshitz, J., Marklund, N., Grady, M.S., Graham, D.I., Hovda, D.A., and Mcintosh, T.K. (2005). Lateral fluid percussion brain injury: a 15-year review and evaluation. J Neurotrauma 22**,** 42-75. doi: 10.1089/neu.2005.22.42.

Tolbert, D.L., Ewald, M., Gutting, J., and La Regina, M.C. (1995). Spatial and temporal pattern of Purkinje cell degeneration in shaker mutant rats with hereditary cerebellar ataxia. J Comp Neurol 355**,** 490-507. doi: 10.1002/cne.903550403.

Tolosa De Talamoni, N., Smith, C.A., Wasserman, R.H., Beltramino, C., Fullmer, C.S., and Penniston, J.T. (1993). Immunocytochemical localization of the plasma membrane calcium pump, calbindin-D28k, and parvalbumin in Purkinje cells of avian and mammalian cerebellum. Proceedings of the National Academy of Sciences of the United States of America 90**,** 11949-11953.

Tsai, F., Teal, J., Itabashi, H., Huprich, J., Hieshima, G., and Segall, H. (1980a). Computed tomography of posterior fossa trauma. Journal of computer assisted tomography 4**,** 291-305.

Tsai, F.Y., Teal, J.S., Itabashi, H.H., Huprich, J.E., Hieshima, G.B., and Segall, H.D. (1980b). Computed tomography of posterior fossa trauma. J Comput Assist Tomogr 4**,** 291-305.

Villanueva, R. (2012). The cerebellum and neuropsychiatric disorders. Psychiatry Research.

Voogd, J., and Glickstein, M. (1998). The anatomy of the cerebellum. Trends in Cognitive Sciences 2**,** 307-313.

Walker, A.E. (1994). The physiological basis of concussion: 50 years later. J Neurosurg 81**,** 493-494. doi: 10.3171/jns.1994.81.3.0493.

Williams, J.C., Rennaker, R.L., and Kipke, D.R. (1999). Long-term neural recording characteristics of wire microelectrode arrays implanted in cerebral cortex. Brain Res Brain Res Protoc 4**,** 303-313.

Wise, A.K., Cerminara, N.L., Marple-Horvat, D.E., and Apps, R. (2010). Mechanisms of synchronous activity in cerebellar Purkinje cells. Journal of Physiology 588**,** 2373-2390.

Xiong, Y., Mahmood, A., and Chopp, M. (2013). Animal models of traumatic brain injury. Nature reviews. Neuroscience 14**,** 128-142. doi: 10.1038/nrn3407.

Yamamura, T., Harada, K., Okamura, A., and Kemmotsu, O. (1990). Is the site of action of ketamine anesthesia the N-methyl-D-aspartate receptor? Anesthesiology 72**,** 704-710.

Yeager, J.D., Phillips, D.J., Rector, D.M., and Bahr, D.F. (2008). Characterization of flexible ECoG electrode arrays for chronic recording in awake rats. J Neurosci Methods 173**,** 279-285. doi: 10.1016/j.jneumeth.2008.06.024.

Young, R.J., and Destian, S. (2002). Imaging of traumatic intracranial hemorrhage. Neuroimaging Clin N Am 12**,** 189-204.